China's 10-year progress in DC gas-insulated equipment: From basic research to industry perspective

Chuanyang Li[1], Changhong Zhang[2], Jinzhuang Lv[3], Fangwei Liang[1], Zuodong Liang[1], Xianhao Fan[1], Uwe Riechert[4], Zhen Li[5], Peng Liu[6], Jianyi Xue[7], Cheng Pan[8], Geng Chen[9], Lei Zhang[10], Zheming Wang[10], Wu Lu[10], Hucheng Liang[11], Zijun Pan[8], Weijian Zhuang[1], Giovanni Mazzanti[12], Davide Fabiani[12], Bo Liu[13], Shaohua Cao[13], Jianying Zhong[14], Yuan Deng[14], Zhenle Nan[15], Jingen Tang[16] and Jinliang He[1] ✉

ABSTRACT

The construction of the future energy structure of China under the 2050 carbon-neutral vision requires compact direct current (DC) gas-insulation equipment as important nodes and solutions to support electric power transmission and distribution of long-distance and large-capacity. This paper reviews China's 10-year progress in DC gas-insulated equipment. Important progresses in basic research and industry perspective are presented, with related scientific issues and technical bottlenecks being discussed. The progress in DC gas-insulated equipment worldwide (Europe, Japan, America) is also reported briefly.

KEYWORDS

DC gas-insulated switchgear (GIS), DC gas-insulated power transmission line (GIL), surface charge, flashover, metal particle, offshore projects.

The competition of electric power transmission with direct current (DC) or alternating current (AC) continuously existed until the end of the 19th century. Power transmission using alternating current won because AC voltage can be transformed flexibly, and long-distance power transmission can be realized at high voltage with less power loss. Entering the 21st century, the electric power structure will undoubtedly be developed from a coal-dominated one to a diversified and co-progressive one with rapidly grown renewable energy. From this stand, the traditional AC transmission solutions reach their limit when greater capacities have to be transmitted over a long distance.

The 14th Five-Year Plan (2021–2025) for the National Economic and Social Development of China takes the development of deep/far-sea offshore wind power as an essential strategy for future energy structure construction. It is estimated that from 2022 to 2025, newly installed offshore wind power capacity will be more than 300 GW. Reducing the volume and weight of the offshore platform dramatically reduces the investment cost of the platform, which is the key to developing large-scale offshore wind power in the future. Apart from that, as a Chinese national major project, the clean energy transmission from southeastern Tibet to the Greater Bay Area (±800 kV DC power transmission project) faces

harsh natural environments such as snow-capped mountains and uninhabited areas. These complex scenarios bring severe challenges in constructing future energy structures in China.

A possible solution to these problems is to use DC electric power transmission and distribution equipment with more compact, lightweight, and high current carrying capacity. The gas-insulated equipment, i.e., gas-insulated switchgear (GIS) and gas-insulated power transmission line (GIL), offers a solution.

Figure 1 shows a possible scenario of power transmission and distribution in the future of China, as well as critical components inside gas-insulated equipment. The electric power generated by the offshore wind turbine is collected, boosted, and rectified at the offshore platform, and is transported back to the mainland using the DC submarine cable with its termination connected to the DC GIS at the offshore platform. Another special scenario falls into the bulk power transmission through harsh natural regions. As shown in Figure 1, the electric energy in the primary energy-rich areas in the southwest region adopts the form of ultra-high voltage (UHV) DC transmission, combined with a direct buried GIL to realize the electric energy transmission across the snow-capped mountains and unmanned areas.

In China, the research of DC GIS/GIL has been carried out for

[1]State Key Laboratory of Power Systems, Department of Electrical Engineering, Tsinghua University, Beijing 100084, China; [2]Maintenance & Test Center of EHV Power Transmission Company China Southern Power Grid, Guangzhou 510663, China; [3]EHV Power Transmission Company China Southern Power Grid, Guangzhou 510663, China; [4]Hitachi Energy Switzerland Ltd, Zürich, Switzerland; [5]Key Laboratory of Engineering Dielectrics and Its Application, Ministry of Education, Harbin University of Science and Technology, Harbin 150080, China; [6]State Key Laboratory of Electrical Insulation and Power Equipment, Xi'an Jiaotong University, Xi'an 710049, China; [7]School of Electrical Engineering and Automation, Hefei University of Technology, Hefei 230009, China; [8]School of Electrical Engineering and Automation, Wuhan University, Wuhan 430072, China; [9]Key Laboratory of Alternate Electrical Power System with Renewable Energy Sources, North China Electric Power University, Beijing 102206, China; [10]Department of Electrical Engineering, Shanghai University of Electric Power, Shanghai 200090, China; [11]School of Electrical and Information Engineering, Tianjin University, Tianjin 300072, China; [12]Department of Electrical, Electronic and Information Engineering, University of Bologna, Bologna 40136, Italy; [13]Shandong Taikai Electrical Insulation Co., Ltd., Tai'an 271000, China; [14]PingGao Group CO., Ltd., Pingdingshan 467001, China; [15]China XD Group Co., Ltd., Xi'an 710075, China; [16]Jiangsu Jinxin Electric Appliance Co., Ltd., Yangzhou 225202, China

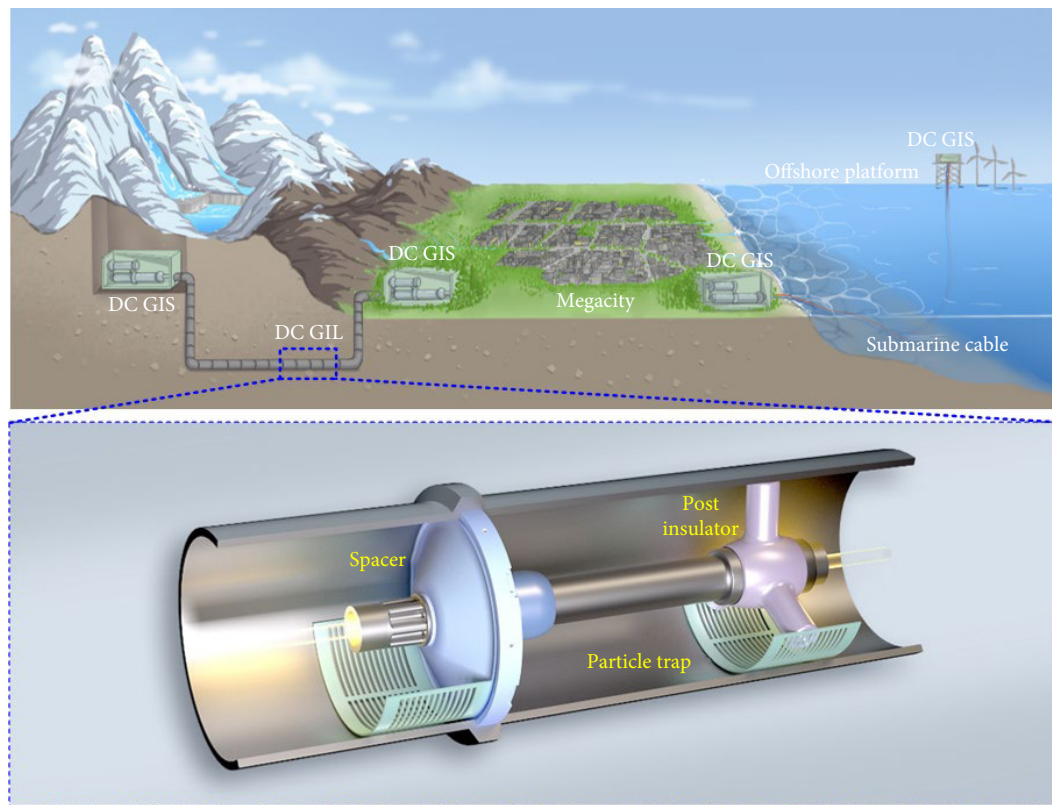Address correspondence to Jinliang He, hejl@tsinghua.edu.cn

Fig. 1   A possible scenario of power transmission and distribution in the future of China, and the critical components inside the gas-insulated equipment.

more than ten years. In terms of theoretical research, universities in China have obtained rich experience. In terms of products, some progress has also been achieved, led by State Grid, China Southern Power Grid, and high voltage (HV) equipment manufacturers. However, at present, there is still no report on commercial GIS/GIL products with voltage levels of ±500 kV and above in China. On the one hand, the reason for the lag in product development is that some basic theories are not yet mature, and industrialization faces some technical bottlenecks. In addition to the lack of basic theory and technical bottlenecks, on the other hand, policy orientation and project demand are also key factors that affect product development. With the proposal of China's ambitious goal in carbon neutrality[1], the construction of a new type of power system will, to a great extent, provide thrust pushing forward the development of DC gas-insulated equipment.

Therefore, at this important time node, this paper, written by experts from domestic universities, factories, grids, and foreign experts with rich experience in DC gas-insulation equipment, is prepared to review the past 10-years' progress in the field of DC gas-insulation equipment. We hope that with this paper we can see the technical gap between China and the world's leading group, and accelerate the research and development of DC gas-insulation equipment. Note that the content of this paper does not include basic theory of environmentally friendly gas, DC GIS/GIL transmission mechanism parts, online monitoring techniques, GIS /GIL termination, etc., although they are also of particular importance.

1   Progress in basic research and remaining issues

It has been mentioned that the immature basic theories and technical bottlenecks limit the development of DC gas-insulated

equipment. Here we listed the scientific issues and technical bottlenecks we need to tackle in the future in Table 1. Issues regarding integrated DC equipment are discussed in Section 2.3.

This section contains six parts, including insulator design principal, surface charge, charge suppression, flashover, metal particle, and conductor roughness.

1.1   Insulator design principal

Insulators, serving as electrical insulation and mechanical support of HV conductor, are critical components of DC gas-insulated equipment. The unreliable insulation performance of insulators under DC is one of the key issues preventing the development of DC gas-insulated equipment[2,3]. Under DC, the resistive electric field distribution inevitably leads to surface charge accumulation, which may cause electric field distortion, thus probably initiating surface flashover[4–6]. Therefore, DC insulator design is of cardinal significance for DC gas-insulated equipment. The ultimate goal of DC insulator design is to synthetically optimize the electrical and mechanical properties under various operating conditions. The existing DC insulator design principle is shown in Figure 2. The foundations of DC insulator design are design criteria and simulation analysis, based on which the design strategies are determined to design DC insulators.

At present, the DC insulator design criteria are ambiguous, and the only reference is the AC insulator design criteria listed in Table 2. The common principal to design DC insulator is minimizing the electric field strength in insulator and at gas–solid interface under DC stress when the design criteria for AC insulator are satisfied. However, the electrical properties of epoxy under DC stress are much different from those under AC stress[7–9]. The bulk electrical strength of epoxy under DC stress are usually higher than that under AC stress. The DC electrical trees are triggered at much higher voltage and grow slower than AC electrical trees in

Table 1 Scientific issues and technical bottlenecks limiting the development of DC gas-insulated equipment

Scientific issues
● Surface/bulk charge kinetics and charge accumulation mechanism of epoxy resins;
● Surface/bulk charge kinetics subjected to temperature gradient/temperature variation;
● Essence and method of surface charge dissipation/suppression of epoxy resin;
● Surface charge accumulation and charge-induced flashover/breakdown mechanism;
● Dynamics and hazard level of particles under DC electric field;
● Particle lifting and inhibition mechanism;
● Essence of particle-induced insulation surface charging and flashover/breakdown;
● Metal surface ionization and micro discharge theory at the mesoscopic scale.

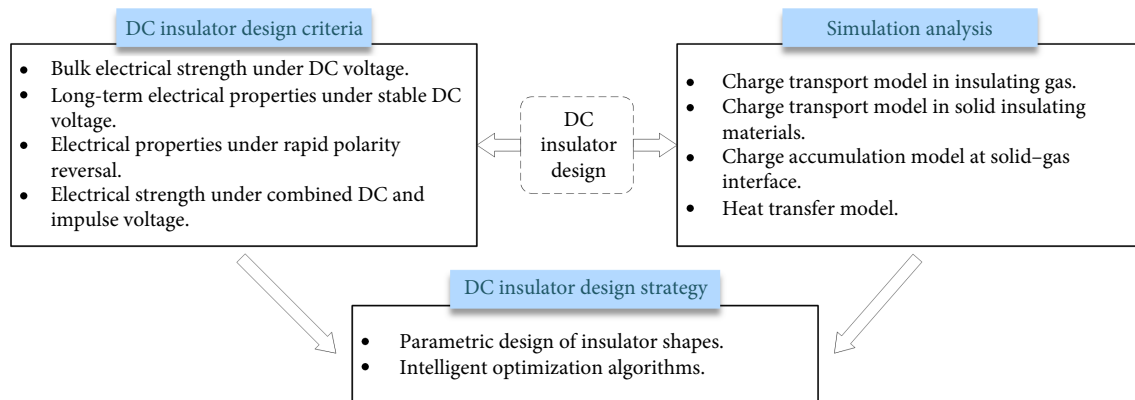| Technical bottlenecks |
| --- |
| (1) Solid insulating parts |
| ● Design principle of DC spacer with excellent electrical and mechanical properties and high reliability under different working conditions. What is the design margin? |
| ● Electric field increasing at the conductor–insulation interface of post-insulator, especially at higher voltages. |
| ● Is it scientific to use the design standard for AC insulators on DC? If not, how to set the field strength criteria for DC? |
| ● The feasibility of material modification technology in large-scale insulating parts. How to evaluate the long-term operation stability of insulating parts after material modification? |
| ● What is the future of 3D printing in the application of insulators for DC? |
| (2) Particle suppression |
| ● Particle traps for AC become invalid at DC, so how to limit the movement of particles under DC? |
| ● How to assess the efficiency for particle traps at DC? |
| ● Locally sharp particles easily induce arcs connecting the particles and conductors when they are close to high-voltage conductors. How to avoid this phenomenon? |
| ● How to suppress particles inside a vertically arranged GIL chamber? |
| (3) Conductor roughness |
| ● What is the permitted roughness level of DC GIS/GIL conductors? |
| ● How to control the roughness of large-sized GIS/GIL conductors? |
| (4) DC GIS/GIL assessment test |
| ● How to set a more scientific assessment standard for DC GIS/GIL testing? |
| ● Should the residual voltage of surge arrester be considered in combination with the actual situation in assessing super and ultra-high voltage DC superimposed impact? |
| (5) DC GIS/GIL online monitoring techniques |
| ● What monitoring solutions should be considered for DC GIS/GIL? |
| ● Can surface charge variation/distribution be monitored for spacers? |

Fig. 2 The existing DC insulator design principle.

epoxy. There is no consensus on the electrical field strength criteria of insulator design under special operating conditions such as rapid polarity reversal and combined DC and impulse voltage. The ambiguous insulator design criteria make it difficult to design DC insulators with excellent electrical and mechanical properties and high reliability under different operating conditions.

There are various methods to design DC insulators including parametric design and intelligent optimization algorithms[10, 11]. The design of DC basin and post insulators both encounter the difficulty that the electric field is distorted and the maximum electric field strength is increased sharply under temperature gradients[12–14]. Increasing insulation distance is an effective method to reduce electric field strength of DC basin and post insulators. However,

the size of gas-insulated equipment and the ratio of the conductor and enclosure diameters are limited with a certain range, so the insulation distance is also limited[15]. Another effective method of DC insulator design is the geometry shape optimization. For DC basin insulator, the tilt angles have a relatively large adjustment range, the method of geometry shape optimization can significantly reduce the maximum electric field strength under temperature gradients[16–18].

Nevertheless, the adjustment range of the geometry shape of DC post insulator is relatively small, and geometry shape optimization is not so effective for post insulator as basin insulator[19, 20]. Furthermore, the electric field strength increases sharply at the conductor–insulation interface of post insulator under DC

Table 2 Design criteria of electric field strength for AC insulator

Design criteria	Conditions
Permissible electric field strength of shielding cover in SF_6, $E_1 < 24$ kV/mm	Peak value under lighting impulse voltage
Permissible electric field strength on bus surface in SF_6, $E_2 < E_1 - 3$ kV/mm	Peak value under lighting impulse voltage
Permissible electric field strength in insulators, $E_3 < 3$ kV/mm	RMS at rated phase voltage
Permissible electric field strength on grounded enclosure surface, $E_4 < 14$ kV/mm	Peak value under lighting impulse voltage
Permissible tangential electric field strength on insulator surface, $E_5 < 0.5 \times E_1$	Peak value under lighting impulse voltage

stress, especially under temperature gradients. It is difficult to suppress the interface electric field using the mentioned methods.

1.2   Surface charge

Research on DC gas-insulated equipment initially focuses on surface charge measurement techniques. In this section, surface charge measurement, charge simulation and calculation, and charge pattern are briefly reviewed. The existing issues are also discussed.

1.2.1   Surface charge measurement

Three methods can generally be used to obtain surface charge distribution, e.g., dust figure technique, electrostatic probe, and linear electro-optic method[2, 21, 22]. Since the third method, also known as Pockels effect, is available only for thin and transparent/translucent insulating material, it is not suitable for the insulators in gas insulated equipment and will not be involved here.

It is convenient for dust figure technique to qualitatively obtain surface charge distribution. Chen et al.[23, 24] employed it to get residual charge distribution after positive and negative surface discharge at the interface between C_4F_7N/CO_2 and PMMA subjected to impulse voltages. In their experiments, very fine and detailed patterns of surface charge distribution corresponding to discharge channels were presented by a type of charged dust, i.e., printer toner, as shown in Figures 3(a) and 3(b). Considering that the high mass density of charged dust is not beneficial to measurement, Li et al.[3] used uncharged one with relatively low density so that charge clusters were observed before surface flashover, as shown in Figure 3(c). It is widely recognized that dust figure technique has the advantages of easy operation and low cost, but is an offline method. After dust particles are attracted to insulator's surface, the original charge distribution of surface charges may be altered, so the effectiveness of this method is questionable.
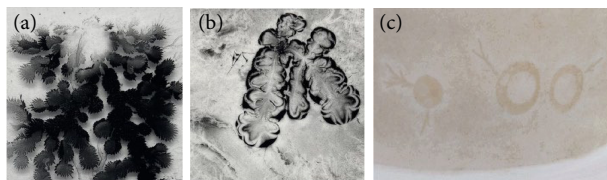

Fig. 3   Typical dust figures. (a) Positive surface discharge (reprinted with permission from ref. [23], © 2022 Author(s).); **(b)** negative surface discharge (reprinted with permission from ref. [24], © 2022 Author(s)); **(c)** charge cluster before surface flashover (reprinted with permission from ref. [3], © 2020 IOP Publishing Ltd).

The electrostatic probe method consists of passive one and active one. The passive electrostatic probe is designed according to electrostatic induction, and its output voltage linearly depends on surface charge density. The linear relationship, characterized by calibration coefficient, determines the sensitivity to surface charge density. Zhang et al.[25] developed a groove-shaped probe to increase the sensitivity, and Gao et al.[26] designed a hollow one so that the sensitivity can be up to 0.036 μC/(m²·mV). Since the mea-

surement by passive probe is easily interrupted, the active one attracts more attention. Based on commercial products, some researchers put forward to improvement methods. Li et al.[21] simulated the effect of active probe introduction on the measured surface charges, and concluded it can be neglected when the gap between probe and insulator surface was 2–3 mm. Wang et al.[27] pointed out that the effect should not be ignored for online measurement. In order to protect the probe during high voltage application, Fan et al.[28, 29] proposed that measured potentials on one side of a film (the thickness is less than 125 μm, the relative error will be less than 0.35%) were almost identical to the potentials induced by surface charges on the other side. Both passive and active probe methods require scanning points for 2D or 3D measurements, which takes a long time, typically several minutes, so electrostatic probe method cannot capture very transient surface charges. In addition, since surface charges and space charges just underneath the surface both contribute to surface potential, it is difficult to distinguish.

An inversion method is required to transfer measured surface potentials to surface charge distribution, i.e charge inversion algorithm. It is because that there is a certain difference between the measured potential and charge density. In early stage, Davis[30] proposed a linear scale method based on the hypothesis that the relationship between surface potential and charge density is linear. However, this hypothesis only fits the requirement of the sample with thickness less than 5 mm[31]. At present, there is a consensus that the measured potentials are determined by the all accumulated charges on insulator surface[31]. Moreover, there is a certain matrix relationship between the potential distribution and the surface charge accumulation. Therefore, the surface charge density can be calculated by combining the potential-charge transfer matrix and measured potentials[2]. The existing algorithms always set the dielectric parameters as constants, and carries out charge inversion by simple electric field calculation. With the development of inversion technology, it is necessary to take the influence of environmental factors on the dielectric parameters into account, bringing the relation equation between dielectric parameters and environmental factors into the calculation model, then the reliability and accuracy of the algorithm can be increased.

Based on electric field calculation, some typical algorithms have been proposed, such as λ function method[32], φ function method[33], and simulated charge method[34]. However, the application of above methods will be limited if the measured points N is large, the potential-charge matrix will be ill-conditioned due to the huge dimension. To solve this problem Zhang et al.[35] proposed an optimized algorithm based on Tikhonov regularization. This is a functional strategy for the "shift-variant system"[36], in which the insulator shapes are basin type, cone-type, etc. To improve the accuracy and efficiency of calculation, Luo[37] proposed an algorithm based on Lanczos bidiagonalization and Tikhonov regularization hybrid method. In detail, the potential-charge matrix is projected into a subspace with smaller dimensions through Lanczos bidiagonalization, Tikhonov regularization was applied to solve the pro-

jected least squares problem in subspace, which greatly reduces the computation cost. Meanwhile, an adaptive weighted generalized cross validation (A-WGCV) method was introduced to select regularization parameters for each iteration step. Considering the problem of interaction between surface charges on concave and convex sides of basin type insulator, Lin et al.[38] created an inversion

algorithm based on bilateral surface potential measurement, therefore, the testing systematic error is further reduced. Figure 4 shows the charge inversion results of several methods. Comparing with the dust figure, it seems that the hybrid Lanczos–Tikhonov algorithm presents the better ability of noise inhibition.
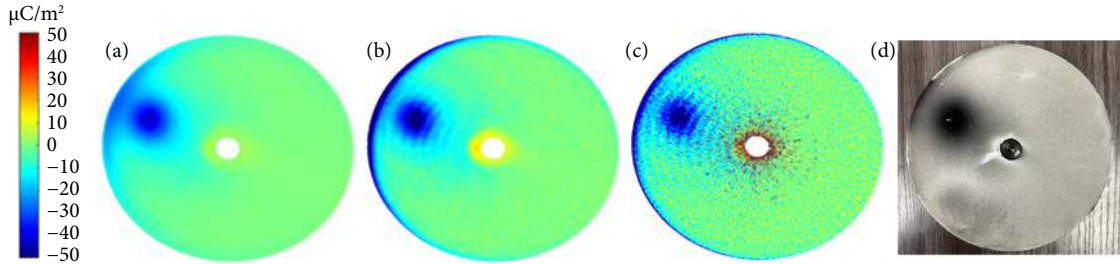

Fig. 4 Surface charge inversion results for shift-variant system. **(a)** Hybrid Lanczos–Tikhonov algorithm; **(b)** standard Tikhonov algorithm; **(c)** apparent charge method; **(d)** dust figure.

For "shift-invariant systems"[39], such as plate-shaped insulator, the digital image processing technology can be utilized. It is because that the induced potential is independent of the accumulated charge location on the insulator surface[35], hence the matrix equation can be expressed in convolution. Zhang et al.[35] and Deng et al.[40] conducted this method, the complicated matrix calculation can be posted into frequency domain by 2-D Fourier transform. This method eliminates the volume of numerical calculations, and suppresses noise by Wiener filter. However, the filter coefficient of Wiener filter is determined by the power spectrum ratio of noise image and original image, which are often difficult

to be measured in practical test. So the filter coefficient is always replaced by a constant k in calculation, then the optimal tradeoff between charge inversion and noise suppression can be obtained by artificially adjusting the value of k. To solve this problem, Pan et al.[41] designed an inversion algorithm based on constrained least square filter. The filter coefficient can be selected by iteration, and its calculation result was compared with the Wiener filter method and simulated charge method, as shown in Figure 5. As seen, the calculation accuracy is better than the Wiener filter method and simulated charge method, especially under high level noise interference.
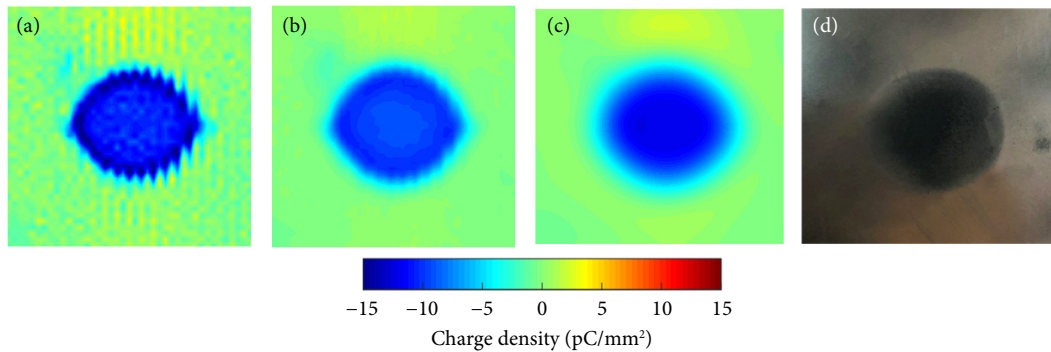

Fig. 5 Surface charge inversion results for shift-invariant system. **(a)** Simulated charge method; **(b)** Wiener filter method; **(c)** constrained least square filter method; **(d)** dust figure. Reprinted with permission from ref. [41], © 2021 IEEE.

There is a problem for surface charge inversion that how to check its validity. At present, it is verified by comparing it with dust figure. In this way the distributed pattern can only be checked, because the dust figure method is not able to qualitatively obtain the surface charge density. Therefore, a novel calibration method is required to develop.

1.2.2 Charge simulation and calculation

In recent 10 years, simulation and calculation on surface charge accumulation of DC gas-insulated equipment mainly includes three aspects: basic research, multi-physical field simulation, and 3D simulation technology, with their structure as shown in Figure 6.

For the basic research, the theoretical model of surface charge accumulation at the solid-gas interface was proposed[42, 43], which

was widely used in subsequent simulation studies. The gas conductance, volume conductance and surface conductance are comprehensively considered by this model, and the accumulation process of surface charge density at the solid–gas interface is characterized as Eq. (1):

$$\frac{\partial \rho_s}{\partial t} = \boldsymbol{n} \cdot \boldsymbol{J}_V - \boldsymbol{n} \cdot \boldsymbol{J}_G - div(\kappa_s \cdot \boldsymbol{E}_\tau) \tag{1}$$

where ρ_s is the surface charge density. $\boldsymbol{J}_V$ and $\boldsymbol{J}_G$ are the current density on the solid-side and gas-side of the interface, respectively. $\boldsymbol{n}$ is the unit normal vector with the direction from solid-side pointing to gas-side. κ_s is the surface conductivity of the insulator. $\boldsymbol{E}_\tau$ is the tangential component of the electric field on the interface.

The solid conduction current density in the insulator can be calculated by Ohm's law:
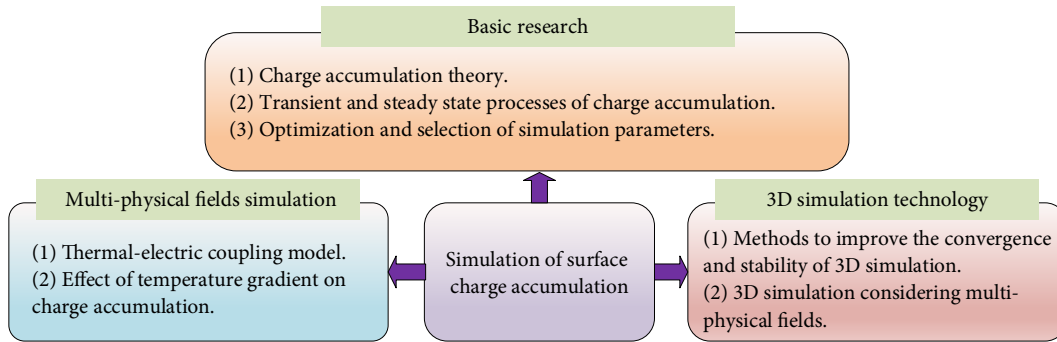
Basic research

(1) Charge accumulation theory.
(2) Transient and steady state processes of charge accumulation.
(3) Optimization and selection of simulation parameters.

Multi-physical fields simulation

(1) Thermal-electric coupling model.
(2) Effect of temperature gradient on charge accumulation.

Simulation of surface charge accumulation

3D simulation technology

(1) Methods to improve the convergence and stability of 3D simulation.
(2) 3D simulation considering multi-physical fields.

Fig. 6 The main research content of surface charge accumulation simulation.

$$J_V = \kappa_V \cdot E \qquad (2)$$

where κ_V is the volume conductivity of the insulator. E is the electric field.

The dynamic change of positive and negative ions density in gas-side can be described by the generation, recombination, drift and diffusion of carriers:

$$\frac{\partial n^+}{\partial t} = \frac{\partial n_{IP}}{\partial t} - k_r \cdot n^+ \cdot n^- - div(n^+ \cdot b^+ \cdot E) + D^+ \cdot \nabla^2 n^+ \qquad (3)$$

$$\frac{\partial n^-}{\partial t} = \frac{\partial n_{IP}}{\partial t} - k_r \cdot n^+ \cdot n^- + div(n^- \cdot b^- \cdot E) + D^- \cdot \nabla^2 n^- \qquad (4)$$

where n^+ and n^- are the positive and negative ions density, respectively. $\partial n_{IP}/\partial t$ is the ion pair generation rate due to the natural radiation ionization. k_r is the recombination coefficient. b^+ and b^- are the positive and negative ions mobility. D^+ and D^- are the positive and negative diffusion coefficient. Then, the current density J_G on the gas-side can be determined by the ion drift caused by the electric field and the diffusion caused by the local ion concentration difference:

$$J_G = e \cdot E \cdot (n^+ \cdot b^+ + n^- \cdot b^-) - e \cdot \nabla(D^+ \cdot n^+ - D^- \cdot n^-) \qquad (5)$$

Previous studies have shown that the electric field inside DC GIL will transition from the initial capacitive distribution to the steady-state resistive distribution[17,42]. During this process, surface charges will continuously accumulate and change the electric field distribution. Yan et al.[44] conducted a simulation study on the changes of surface charge density, electric field intensity, and current density in the transient process of surface charge accumulation, which found that the solid-side conductance plays a dominant role in the surface charge accumulation. The accumulated surface charge will continuously reduce the normal electric field and current density on the solid side until it reaches a balance with the current density on the gas-side. Li et al.[45] conducted a simulation study on the dynamic accumulation process of surface charge and the change of electric field line distribution under different solid conductivity (as shown in Figure 7), which further revealed the transport and accumulation mechanism of surface charge.

The selection and optimization of simulation parameters have been extensively studied[6,46,47], which mainly include solid conductivity, surface conductivity, and gas-side ion transport parameters. Ma et al.[46] carried out experimental measurements on the volume and surface conductivity of the Al$_2$O$_3$-filled insulator, and the measurement results were used in subsequent simulation studies. Chen et al.[6] studied the influence of different solid conductivity on surface charge accumulation. Zhang et al.[47] proposed the calculation method of ion mobility under different temperatures, gas pressure, and electric field. Xue et al.[48] optimized the surface con-

(a) Volume conductivity of the spacer is 2×10^{-18} S/m.

(b) Volume conductivity of the spacer is 9×10^{-18} S/m.

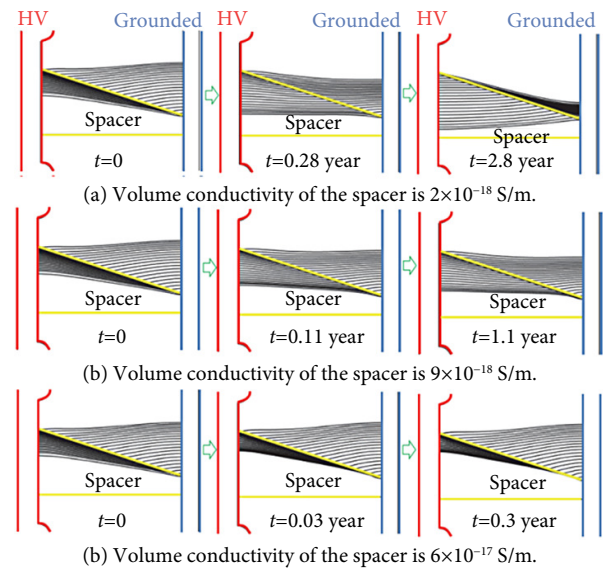(b) Volume conductivity of the spacer is 6×10^{-17} S/m.

Fig. 7 Variation of electric field line distribution on insulator surface during transient to steady state. Reprinted with permission from ref. [48], © 2023 The Authors.
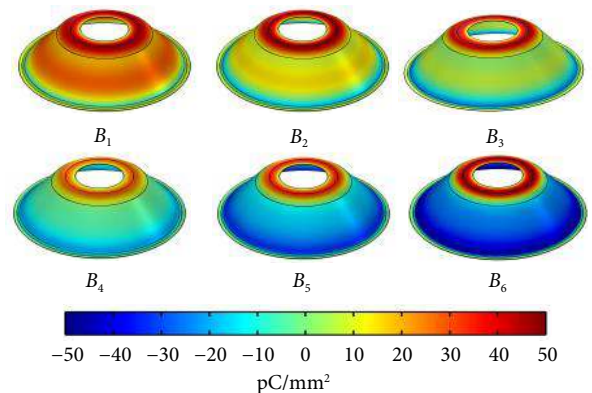

$-50 \quad -40 \quad -30 \quad -20 \quad -10 \quad 0 \quad 10 \quad 20 \quad 30 \quad 40 \quad 50$
pC/mm^2

Fig. 8 Surface charge density of coatings with different conductivity. Reprinted with permission from ref. [45], © 2019 IEEE.

ductivity of the temperature-adaptive coating by the simulation, and the optimal conductivity parameters to inhibit charge accumulation are obtained (as shown in Figure 8).

For the DC GIL in actual operation, the temperature of the center conductor will be increased significantly, resulting in a temperature gradient between the center conductor and the grounding enclosure. The temperature gradient will not only affect the volume conductivity of insulators, but also have a great impact on the migration, diffusion and recombination of ions in
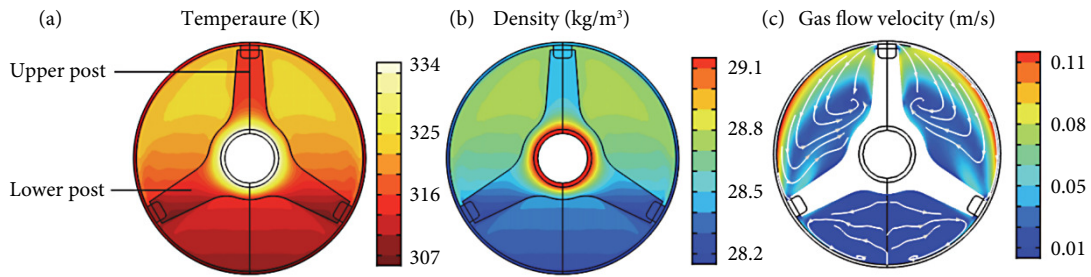
Fig. 9 Distribution of temperature, gas density and gas velocity inside GIL[49]. Reprinted with permission from ref. [52], © 2021 IEEE.
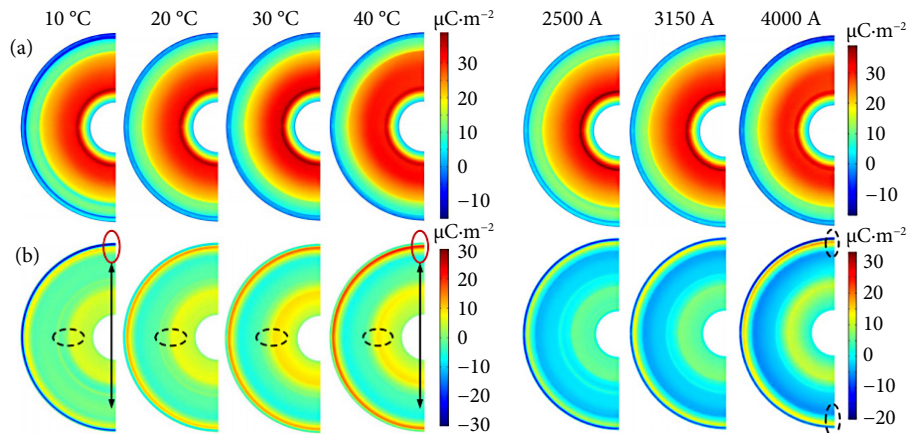

Fig. 10 Influence of ambient temperature and load current on surface charge density on (a) convex surface and (b) concave surface[53]. Reprinted with permission from ref. [53], © 2022 IEEE.

the gas[49–51]. Therefore, the surface charge accumulation in electric-thermal coupling field has been studied. Du et al.[52] comprehensively considered the heat transfer process in the DC ±800 kV GIL model, which includes thermal conduction, thermal convection and thermal radiation, and the temperature distribution inside GIL (as shown in Figure 9) and the surface charge density on the three pillar insulators were simulated. Li et al.[53] considered the influence of external ambient temperature, load current and gas pressure on surface charge accumulation of DC GIL insulators (as shown in Figure 10).

In order to simulate the actual geometric size and operating environment of DC GIL, researchers have carried out 3D simulation research of DC GIL in recent years to replace the traditional 2D axisymmetric model. For the 3D simulation of surface charge accumulation, how to balance the amount of calculation and the accuracy of the calculation result is an extremely important problem. Li et al.[54] adopted a weak form of ion transport equation, that is, transformed the original differential form into integral form by adding a test function, then the second partial derivative in the transport equation can be removed by partial integration equation, which greatly reduced the computation amount and improved the convergence rate. In our recent work, we carried out a 3D simulation by using the method of adding artificial diffusion term, it was proved that the calculation time was reduced by nearly 56% and the error is kept within 0.6%. Furthermore, the influence of temperature gradient on surface charge accumulation have been simulated by a 3D GIL model (as shown in Figure 11).

The existing simulation results show that volume conductance plays a dominant role in surface charge accumulation. However, the process of space charge injection, transport, trapping and detrapping inside the insulator has not been considered in the surface charge accumulation model. Meanwhile, possible gas discharges in GIL, such as corona discharge and micro-discharge etc., have not been considered in current simulation studies, which is
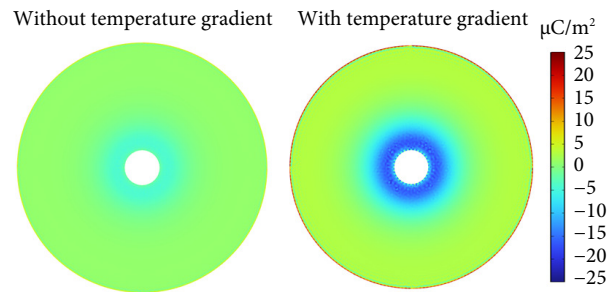

Fig. 11 Simulation results by using a 3D GIL model with slant plate insulator.

necessary for further study in the future. In addition, the influence of multiple factors such as temperature, humidity, external environment conditions and possible impulse voltage on surface charge accumulation is worth studying.

1.2.3 Surface charge pattern

Parsing surface charge patterns accurately is the basis of deeply understanding surface charge transport behaviors. Different understandings for experimental results lead to a disagreement of interpreting surface charge patterns. The surface charge pattern obeys the field-dependent theory[4], where the dominant ways of surface charging process transform from ohmic conductivity to gas conductivity as the raising of local electric field, as presented in Figure 12. At low electric field, the surface charge distribution shows a non-repetitive and irregular pattern since many factors could contribute to surface charge accumulation and not a single one is in domination. At high electric field, the surface charge patterns are in accordance with the distribution of normal component of surface electric field, which indicates that the gas ionization becomes the prominent factor for surface charge accumulation.
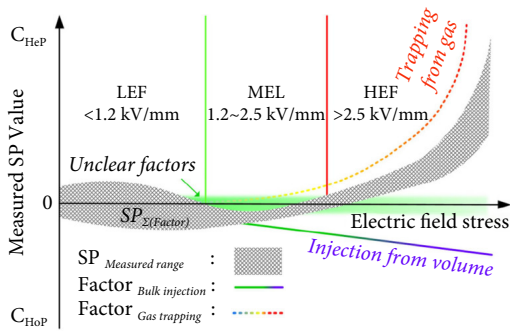
Fig. 12 Field-dependent surface charging theory[55]**. Reprinted with permission from ref. [4], © 2019 Author(s).**
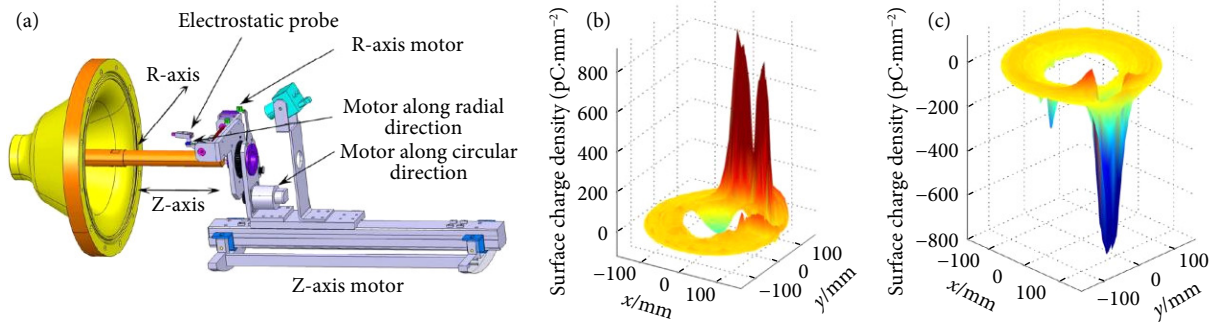
In this section, surface charge patterns obtained by previous researchers are discussed and related mechanism is illustrated.

Charging from single mechanism

The interpretation of surface charge pattern is influenced by lots of factors, such as surface charge inversion method, different electrode-insulation arrangements, different experimental conditions, etc. When surface charge accumulation is dominated by gas bulk conductivity, the charge patterns are mainly determined by the normal component of surface electric field E_n. If E_n points to spacer surface, charges are hetero-polarity. Otherwise, charges are homo-polarity. In most cases, they are random charge speckles. Wang et al.[55] found that the charge pattern on spacer concave surface had the same polarity as the applied DC voltage, as displayed in Figure 13.

Fig. 13 Charge patterns on concave surface. (a) Experimental spacer and measurement device; **(b)** surface charge patterns under +40 kV DC; **(c)** surface charge patterns under −40 kV DC. Reprinted with permission from ref. [56], © 2012 IEEE.

The distribution position of peak charge density was random. The charge quantity was closely dependent on the gas pressure, where the increased gas pressure brought about lower surface charges. They believed that the gas ionization induced by the rough surface of the electrodes was responsible for surface charge accumulation. After polishing the electrode surface, nearly no charges were observed, which verified the above analysis.

Plenty of researchers hold the same viewpoint according to their experiments. Pan et al.[56] believed that the charged particles produced by gas ionization were the main sources of surface charge accumulation. Qi et al.[7] thought that the gas conductivity model dominated surface charge accumulation. The factors that lead to gas ionization included the protrusion on the electrode surface, the impurity on spacer surface, the enhanced electric field at the triple junction near the high voltage (HV) electrode.

When solid bulk conductivity dominates surface charge accumulation, the charge patterns are also dependent on the normal

component of surface electric field E_n. If E_n points to spacer surface, charges are homo-polarity. Otherwise, charges are hetero-polarity. In most cases, they are uniform charge ring. Ma et al.[17] measured surface charge distribution on GIL spacer after DC charging, and found that the charge patterns were consistent with the normal component of surface electric field, as presented in Figure 14(a). Therefore they considered that the solid bulk conductivity played a leading role in surface charge accumulation. Wang et al.[58] measured the surface charge distribution patterns on a downsized GIL spacer after +20 kV/−20 kV DC charging, as presented in Figure 14(b). The accumulated charges were almost ring-shaped with the polarity was the same as that of DC excitation, which coincided with the normal component of surface electric field distribution. Thus they concluded that the surface charge accumulation process satisfied the solid bulk conductivity model.

When solid surface conductivity dominates surface charge accumulation, the charge patterns are dependent on the tangential
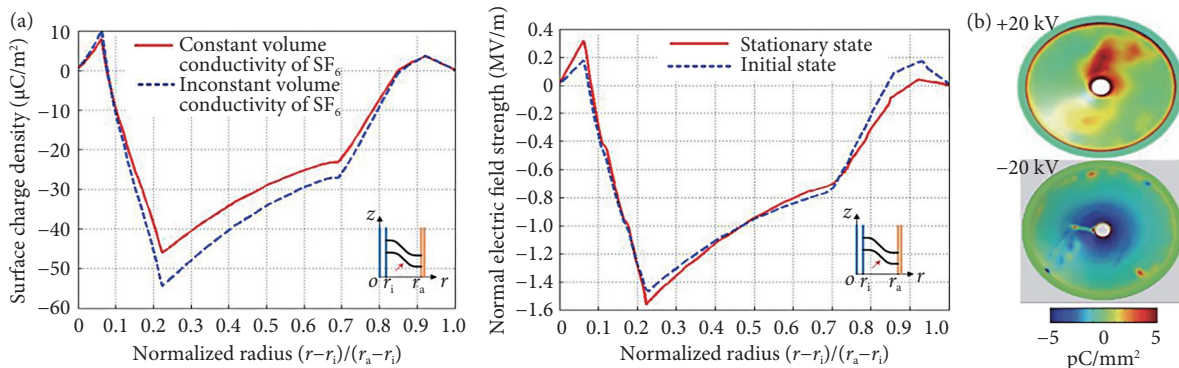

Fig. 14 Surface charge patterns and normal electric field profile. (a) Surface charge and normal electric field profile (reprinted with permission from ref. [17], © 2015 IEEE); **(b)** Surface charge patterns (reprinted with permission from ref. [59], © 2020 IOP Publishing Ltd).

component of surface electric field E_t. Charges can be hetero-polarity or homo-polarity, which is determined by the distribution of surface conductivity. They can be uniform charge ring or random charge speckles. Xue et al.[59] investigated the effects of non-uniform surface conductivity on gas–solid charge accumulation characteristics by spraying SiC/epoxy coatings on different locations of spacer surface, as is shown in Figure 15. They found that at the interface between high and low conductive area, bipolar charges were commonly observed. It was revealed from their study that the non-uniform surface conductivity was a non-negligible reason responsible for the randomly distributed bipolar charges.
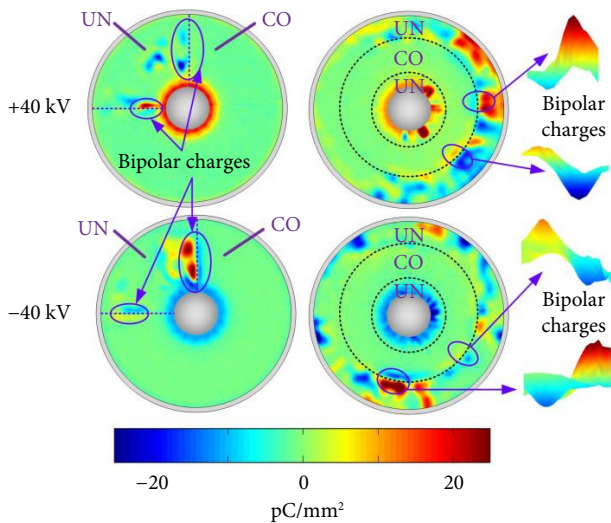

Fig. 15 Surface charge patterns and normal electric field profile. The label UN refers to untreated area (i.e., low conductive area) while the label CO refers to the SiC/epoxy coated area (i.e., high conductive area).

Charging from multiple mechanisms

When there exists local electric field enhancement in the GIL or the surface condition of the spacer is not clean enough, such as contaminated by tine metallic particles, with non-uniform surface conductivity during the curing process, different charge patterns can be obtained with advanced charge inversion algorithm. Zhang et al.[60] measured surface charge distribution on a downsized GIL spacer in atmospheric air after DC charging, and found that two patterns were coexisting on spacer, i.e.uniform charge pattern and charge speckles, as shown in Figure 16(a). Xue et al.[61] also found

the similar charge patterns in SF_6 gas atmosphere. Three kinds of charge patterns were classified including the centrosymmetric distribution with homo-polarity, spot-like distribution with random polarity and cloud-like distribution with mostly hetero-polarity as shown in Figure 16(b), where the electrode injection, the gas ionization induced by metallic particles and the random gas microdischarge played a dominant role respectively.

Zhou et al.[62] obtained the surface charge distribution patterns on a cone-type GIL spacer after −150 kV DC charging for 60 h, as shown in Figure 17. Charge ring patterns of both homo-polarity and hetero-polarity were observed on spacer surface. They judged from the electric field distribution that the ring-shaped charge with hetero-polarity was dominated by solid bulk conductivity while the solid surface conductivity dominated the ring-shaped charge of homo-polarity. Besides, the non-uniform charge patterns were mainly induced by the uneven distribution of the conductivity or surface traps of the spacer during the manufacturing process.

In sum, we collected previous obtained charge patterns on downsized spacers in different gas atmospheres including air, SF_6, 20% SF_6/80%N_2 mixtures, and the results are displayed in Figure 18(a). It can be seen that no matter involved in what gas atmosphere, primarily two patterns coexist on spacer surface, charge ring with homo-polarity near HV electrode and charge speckles with random polarity located between the ring-shaped charges and the grounded (GND) electrode. The experimental results are repeatable, where the location of charge ring is almost stable while that of charge speckles is random. According to the polarity and location of the accumulated charges, the correlation between the charge distributed location and the dominant mechanism is established, as presented in Figure 18(b). As for the charge ring near HV electrode, the electrode injection into spacer surface and bulk becomes the main sources of surface charges.

The charges injected to spacer surface layer are captured by surface trap while charges injected to spacer bulk are driven by the normal component of surface electric field towards to spacer surface, forming the surface charges. Sometimes, the hetero-charge speckles can be observed near HV electrode, which mainly come from the gas ionization at the triple junction over there or is due to the back discharge during the withdraw of DC high voltage. As for the randomly distributed charge speckles, the sources are relatively more complicated. Generally, the defects of the spacer itself, such as tiny metallic particles, the non-uniform surface or bulk conductivity, can bring about these charge speckles. As for the
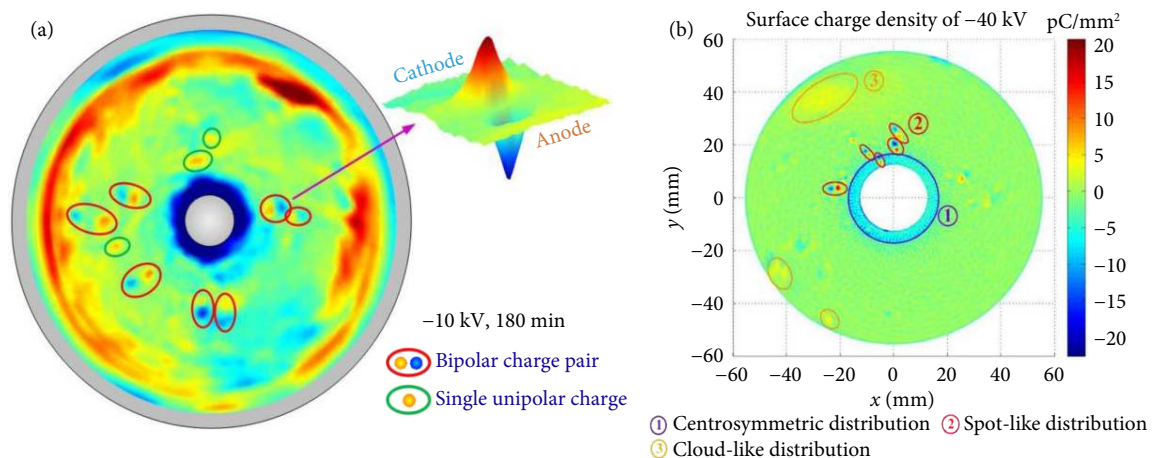

Fig. 16 The surface charge patterns in (a) atmospheric air (reprinted with permission from ref. [60], © 2017 IEEE) and (b) SF_6 gas (reprinted with permission from ref. [61], © 2018 The Institution of Engineering and Technology).
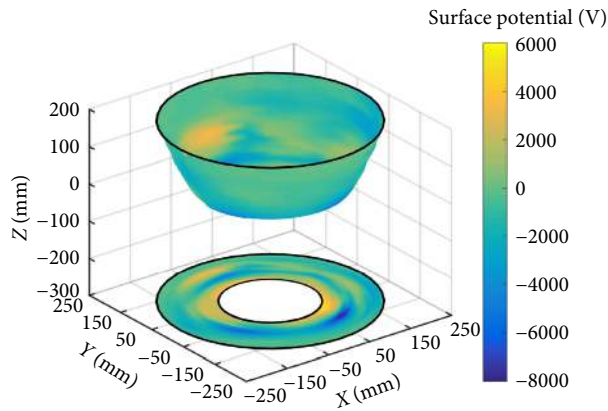
Fig. 17 The surface charge distribution patterns on a cone-type spacer after −150 kV for 60 h. Reprinted with permission from ref. [62], © 2018 IEEE.

hetero-charges near GND electrode, the electrode injection or the gas ionization at the triple junction over there can be responsible for this kind of charge pattern.

Charging from transformational mechanisms

When the experimental conditions change, the charge sources may also be altered. When the surface conductivity of the spacer increases, the surface charge distribution will turn into a different pattern, which indicates the dominant mechanism gets changed. Xue et al.[63] sprayed a partially high conductive coating on spacer surface, and found that the location of the partial coating dramatically affected surface charge patterns, as shown in Figure 19. They verified that the charges originated from surface leakage current on coated area whereas the bulk leakage current was the sources of charges on untreated area. Furthermore, they proposed that with the increase of surface conductivity, the surface charge dominant mechanism changed from bulk conductivity model to surface conductivity model.

Besides that, when the experimental or simulation conditions changes, surface charge dominant mechanism can be transformed among solid surface conductivity, solid bulk conductivity and gas conductivity[64], which can be judged from the charge polarity and location reflected by charge patterns. In consequence, the surface charge patterns are vital for accurately interpreting the surface charge accumulation process, furthermore contributing to the proposal of effective surface charge suppression methods.

1.3 Surface charge suppression

Generally, the presence of surface charges modifies local electric field and may greatly affects the insulation properties of the epoxy-based spacer[65]. The flashover voltage could be either improved or reduced, depending on the surface charge density, position, and polarity. In the past decade, much effort has been made on proposing effective charge regulation methods. However, due to the reason that the charge origin is not the same, different charge tailoring methods shall have different motivations. Li et al.[66] and Zhang et al.[67] proposed a Dam model in 2020, in which the typical surface charge tailoring methods can be sorted into four categories, i.e., charge spilling, charge restraining, charge dredging optimization, and comprehensive charging activity management. By referring to the Dam model, as shown in Figure 20, the corresponding charge tailoring orientations for surface charge suppression from the four categories are discussed with more details in the following sections.

1.3.1 Charge spilling methods

According to the Dam model, charge spilling could be achieved by applying charge tailoring techniques which can increase surface charge decay rate. Previous studies have proved that higher charge decaying rate can be achieved by increasing the surface conductivity. Common approaches for charge spilling include direct fluorination, plasma treatment, surface coatings, gamma-ray irradiation, and ozone treatment[68–75].

Surface fluorination

Du et al.[76–78] made fluorination treatment on variety of DC GIL spacers, such as epoxy, polypropylene, and polyimide types of spacers. By direct fluorination, the surface charge dissipation rates of spacer samples were found to be accelerated, which is due to the gradually increased surface conductivity with the increment of deep taps and reduction of shallow traps on the spacer. Que et al.[79] also apply direct fluorination on the cone-type spacer. The testing results indicate that the surface potential decay rate was increased and the flashover voltage was enhanced. Zhang et al.[80] divided the overall surface areas of the spacer into four regions artificially, and treated those regions by fluorination for 0, 15, 30, and 60 min, respectively. As shown in Figure 21, obvious surface charge accumulation with a random distribution pattern was found in the untreated region. For the fluorinated regions, the surface charge distributions were more uniform and the charge
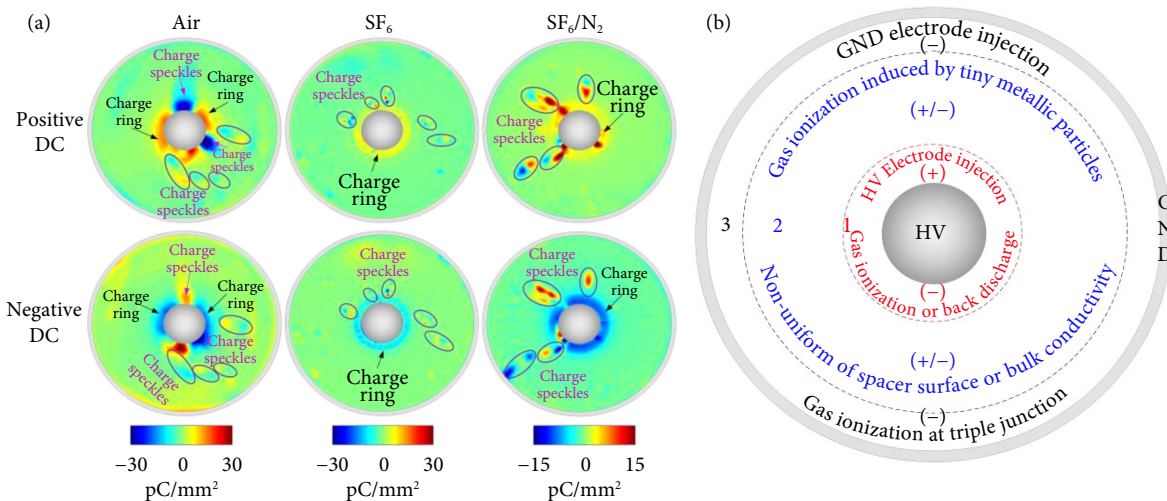

Fig. 18 (a) Surface charge patterns in air, SF$_6$, SF$_6$/N$_2$ mixtures and (b) the corresponding charge accumulation model.

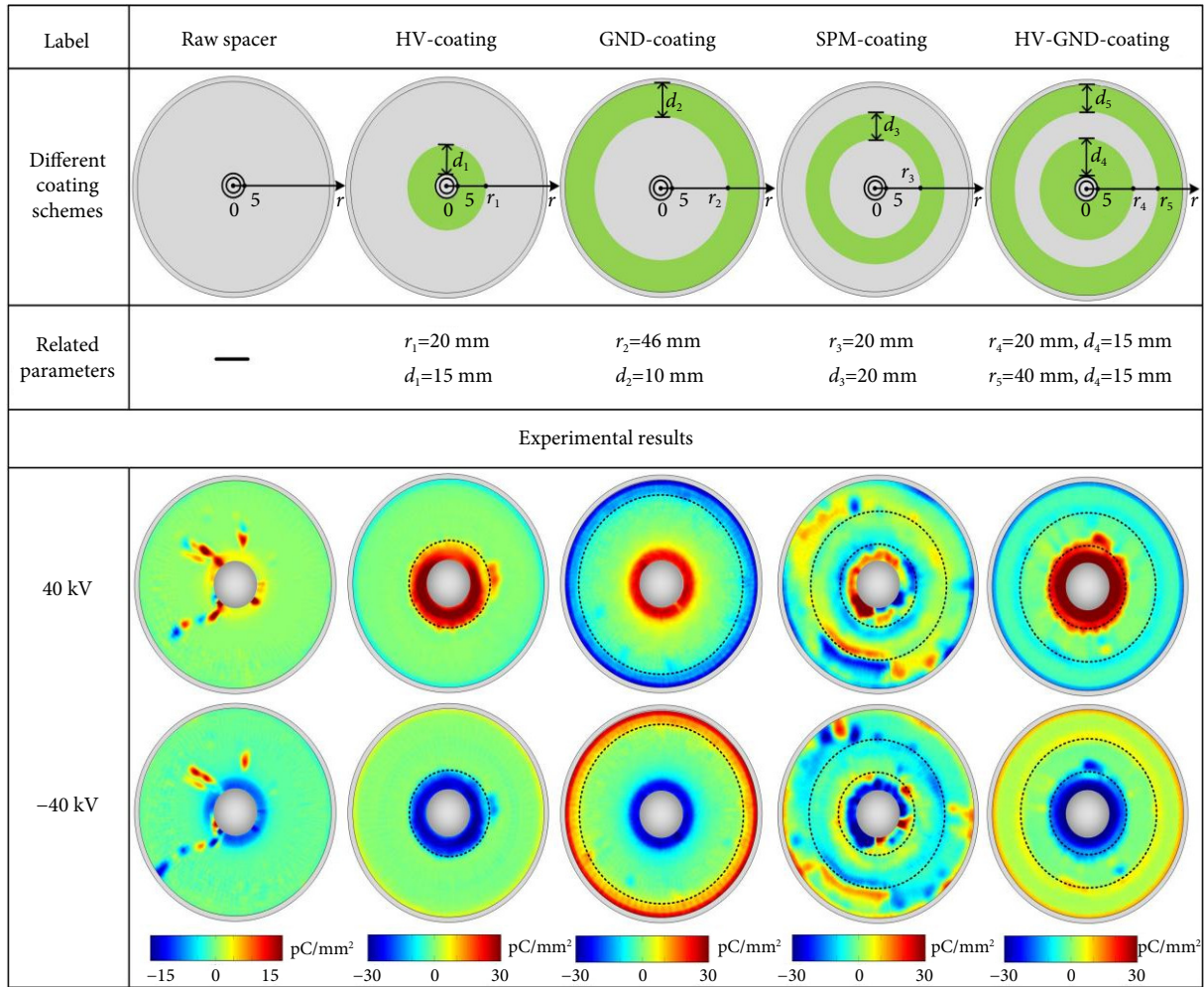| Label	Raw spacer	HV-coating	GND-coating	SPM-coating	HV-GND-coating
Different coating schemes					
Related parameters	—	r_1=20 mm d_1=15 mm	r_2=46 mm d_2=10 mm	r_3=20 mm d_3=20 mm	r_4=20 mm, d_4=15 mm r_5=40 mm, d_4=15 mm
Experimental results					
40 kV					
−40 kV					

Fig. 19   Surface charge patterns with partially high conductive coating on spacer. Reprinted with permission from ref. [63], © 2020 IOP Publishing Ltd.
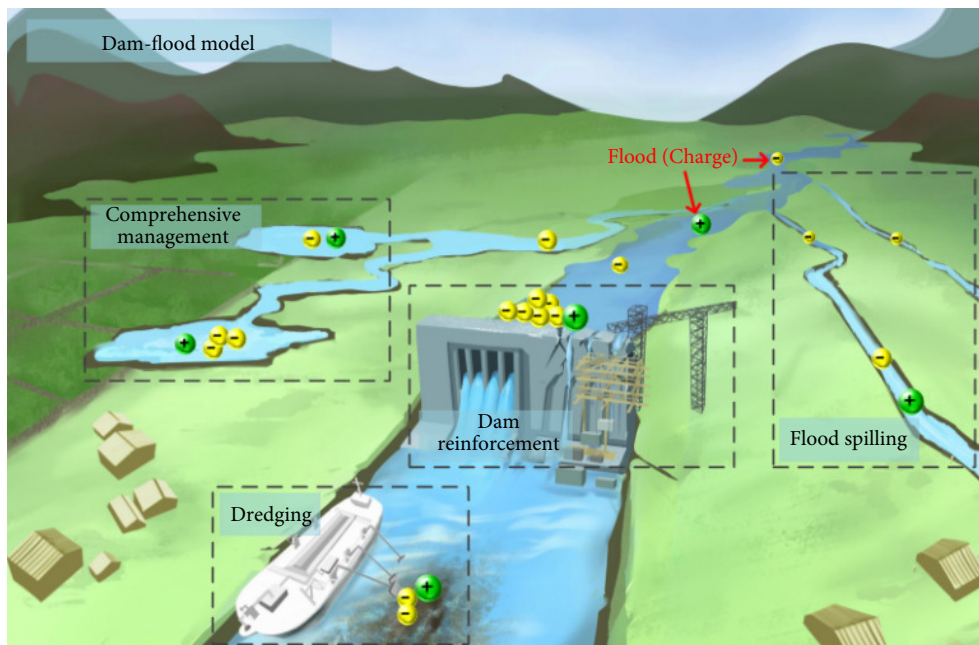

Fig. 20   Equivalent diagram of the Dam-flood model. Reprinted with permission from ref. [66], © 2022 IEEE.

densities were obviously reduced, due to the increased surface conductivities. Li et al.[81] made similar surface treatment research, indicating that fluorination treatment is an effective way for surface charge suppression.
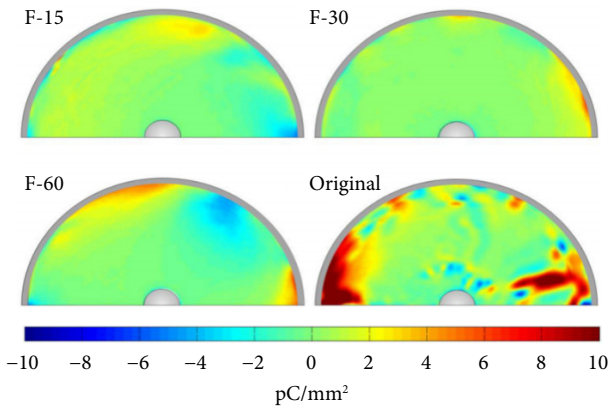
Fig. 21 Surface charge distributions of spacers fluorinated for 0, 15, 30, and 60 min. Reprinted with permission from ref. [80], © 2015 Author(s).

Plasma treatment

Plasma treatment is an effective way to modify the dielectric properties of spacer surface, such as the ratios between deep/shallow traps, carrier mobility, and surface conductivity[71, 82–84]. Shao et al.[82, 84] investigated the effect of plasma treatment on the insulation performance of epoxy-based polymers and found that the plasma treatment effectively increases the surface hydrophilicity of epoxy resin, which in turn attenuates surface charge decay rate. They found that the O radicals in plasma and the carbonyl groups formed on the surface create more shallow charge traps on the surface, increasing the surface conductivity and accelerating surface charge dissipation. Yue et al.[85] studied the effect of surface plasma treatment on the surface charge decay property of epoxy-based composite materials. After 3 minutes of treatment, the surface conductivity reaches 1.4×10^{-17} S/m, which is approximately 2 orders of magnitude higher than that of untreated samples.

Surface coating

Surface coating is another effective method to suppress charge injection by promoting charge dissipation process. Typical surface coating techniques include plasma deposition, magnetron sputtering coating, spray coating, and dipping.

Nano-TiO_2/EP coating method can increase the surface charge decay rate of epoxy resin, which was firstly developed by Tu et al.[86] When the weight content of nano-TiO_2 particles is in the range of 1% ~ 3%, surface charges mainly concentrated near the high-voltage electrode, whereas when weight content increase to the range of 5% ~ 7%, the surface charges mainly settle near the grounded electrode.

Further, Zhang et al.[87] proposed a nacre-mimetic coating method on epoxy-based spacers, which is achieved by using a facile flow induced co-assembly technique. By doing so, a faster charge dissipation and a higher surface flashover voltage were observed in Figure 22.

Other charge tailoring methods—Gamma-ray irradiation

Gao et al.[72] studied the effects of gamma-ray irradiation on the surface charge behaviors of polymer insulating materials. The results showed that oxidation was induced in the surface layer of the sample by the gamma-ray irradiation, leading to the increment of the surface conductivity with the total dose growth. Accordingly, the surface charge dissipation was enhanced.

Other charge tailoring methods—Surface roughness treatment

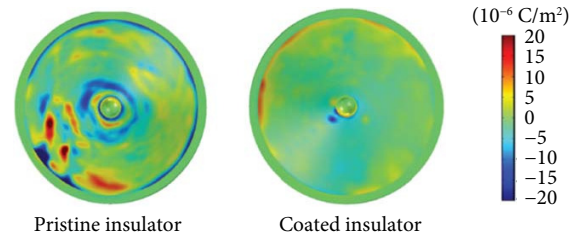Xue et al.[88] studied the surface charging behaviors of epoxy alumina

Fig. 22 Surface charge density distribution on cone-type insulators after application of a −20 kV DC voltage for 30 min. Reprinted with permission from ref. [87], © 2019 The Royal Society of Chemistry.

spacers with different surface roughness, and it was concluded that the surface roughness treatment introduced more deep traps and suppressed the surface charge accumulation.

Other charge tailoring methods—Ozone treatment

The effect of ozone treatment on the flashover strength of epoxy/Al_2O_3 composites was studied by Huang et al.[74] The results showed that the surface conductivity after 4 hours of ozone treatment increases by 2 orders of magnitude compared with the untreated sample, which is mainly due to the increments in both the charge carrier density and the surface charge dissipation rate.

Other charge tailoring methods—Radical scavenging

In 2013, Baytekin et al.[89] discovered that scavenging the free radicals from spacer surface could be a more efficient way to increase surface charge decay rate rather than tailoring the surface charging process itself. A series of charging tests were performed on untreated polymers as reference, and polymers doped with small amounts of chemical substances as radical scavenger, i.e., (T)-a-tocopherol (vitamin E), bis(1-octyloxy-2,2,6,6-tetramethyl-4-piperidyl) sebacate (HALS), 2,2-diphenyl-1-picry-lhydrazyl (DPPH) and 2,2-diphenyl-1-picryl hydrazine (DPPH-H). The results showed that the surface charge decay rates of the samples with radical scavengers are significantly higher than those of the reference, particularly in the case of DPPH as scavenger.

Other charge tailoring methods—X-ray irradiation

Wang et al.[73] proposed a novel surface charge suppression technique, namely X-ray based non-contact charge dissipation method (XNCDM). Surface charges on the spacer can be almost completely dissipated after a short-time of X-ray irradiation with enough dose, owing to the significant enhancement of electric conduction along the insulator surface and charge neutralization by gas ions near the gas-solid interface.

1.3.2   *Charge restraining methods*

According to the Dam model, charge restraining could be achieved by applying charge tailoring techniques which can inhibiting charge injection from volume or gas or retarding gas ionization. Common approaches for charge restraining include coating or doping on the conductor surface to decrease the conducting current from the volume, and reduce the roughness of conductor surface to decrease micro discharge and thereby limit charges incoming from gas ionization.

Suppressing charge from volume conduction

Li et al.[90,91] deposited Cr_2O_3 on the epoxy surface, found that deep traps were introduced and surface charge injection from the electrode was inhibited. He et al.[92] focused on restraining the charge transport inside the bulk by doping $K_2Ti_6O_{13}$ whiskers into epoxy-

based material. They took advantage of the thermal barrier effect of $K_2Ti_6O_{13}$ whiskers to suppress the transport of homo-polar charges in the bulk, and the result demonstrate that the introducing the $K_2Ti_6O_{13}$ whiskers can effectively restrain heat propagation due to its excellent thermal barrier property, which in turn limits charge transport effectively, especially when temperature gradient varies.

In recent years, it has been widely accepted that the basic distribution patterns of surface charges were dominated by the bulk conduction of spacers when there were no micro/partial discharges in the gas domain. In other words, most surface charges came from the solid-side charge injection. Therefore, the basic charge accumulation distribution is expected to be greatly reduced by reducing the insulator bulk conductivity. Doping nano-particles is one of the mostly used method to reduce the conductivity of polymers. Li et al.[93] modified epoxy resin with the doping of nano-

alumina (Al_2O_3) and nano-titanium dioxide (TiO_2) with different mass fractions. Results showed that the conductivity of the epoxy composite was reduced, due to the charge carrier restrain occurred in the interaction zone when nanoparticle was in an isolated dispersion. Chu et al.[94] modified epoxy resin with the doping of nano-SiO_2, where the bulk resistivity of the composite was increased by 27% when the mass fraction of SiO_2 is 1%. Du et al.[95] doped epoxy resin with nano-graphene. The optimized doping level is confirmed to be 0.1 wt.% epoxy/graphene composite, where the highest trap level can be reached and greatly reducing the conductivity of the epoxy composite. Zhang et al.[96] doped the basin-type spacer with a proper amount of nano-C_{60} for distorting the surface charge accumulation by reducing the bulk conductivity, as shown in Figure 23. It is concluded that the doping of 200 ppm fullerene C_{60} into epoxy resin can effectively suppress the surface charge accumulation.
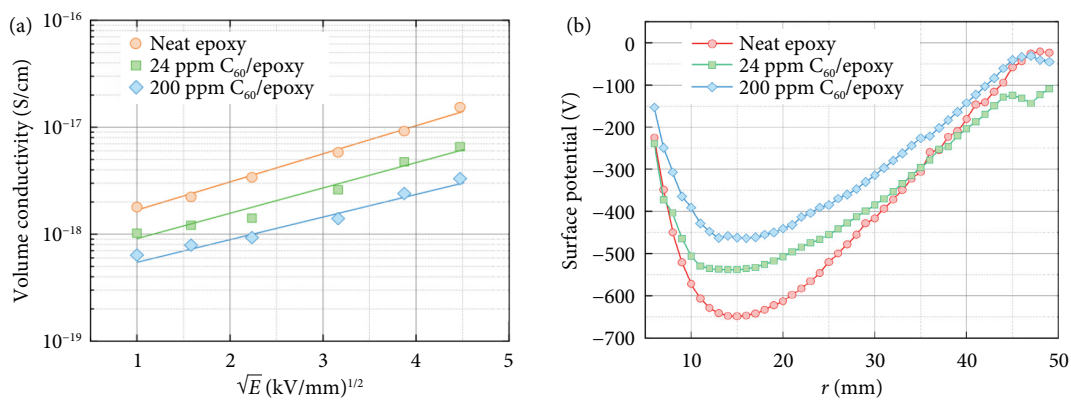

Fig. 23 Effects of C_{60} doping on the (a) volume conductivity and (b) surface charge accumulation. Reprinted with permission from ref. [96], © 2018 IEEE.

Suppressing charge from gas ionization

In practical, the electric field at the micro-protrusions on the rough electrode surface can be enhanced to a threshold level where micro-discharges could take place. Optimizing the surface roughness of electrodes can minimize the source of charge generated by the micro-discharge from the gas ionization[97–99].

1.3.3   Charge dredging optimization methods

According to the Dam model, charge dredging optimization could be achieved by applying charge tailoring techniques which can decay charges near high electric field zones. Common approaches such as applying nonlinear insulation materials and spacer shape modifications could optimize the local electric field and increase local surface charge dissipation.

Nonlinear insulation materials—Bulk doping

It is well known that the surface charge accumulation of the DC-GIL spacer is a result of the combined charging competition effects by gas conduction, surface conduction and bulk conduction. The competition process is very complex depending on various testing conditions such as temperature gradient, metal particle, and micro protrusion, leading to irregular surface charge distributions and unpredictable electric field distortions. The insulating materials with nonlinear conductivity can adaptively increase the volume conductivities of spacers along with the electric field enhancement. Therefore, such materials can be used to release the accumulated surface charges when the induced electric field distortion reaches the threshold values. In the past decade, polymers doped with micro-SiC or micro-ZnO particles are the most widely

used solutions for creating nonlinear conductivities. Liang et al. [100] studied the surface charge accumulation characteristics of the epoxy/SiC composites and found that the surface potential on the 14 vol% sample could be kept at a certain level with the increase of applied voltage, sine the excess surface charges were adaptively released.

Nonlinear insulation materials—Surface coating

The insulating materials with nonlinear conductivity can also be produced by proper surface coating[101, 102]. Although the insulating materials with nonlinear conductivity can adaptively release the accumulated surface charges, the high doping of semi-conductive particles into the spacer bulk may lead to a huge leakage current and reduce the breakdown strength of epoxy resin, leading to a questionable safety and reliability issue of such spacers. To solve this problem, Xue et al. and Liang et al. conducted an additional coating process on the GIL/GIS spacers with epoxy/SiC composites[59, 103]. Xue et al. sprayed epoxy/SiC coatings with different doping contents on half areas of the spacer surface. With the increase of SiC content, surface charges firstly increase to a certain level and then decrease gradually[102]. Liang et al.[103] coated the whole surface of the basin-type spacer with epoxy/SiC composites with different doping contents and thicknesses. As the coating thickness and the doping content increase, surface charges on the spacer surface firstly decrease to zero and then increase reversely, as shown in Figure 24. It is turned out that the insulating materials with nonlinear-conductivity can adaptively regulate the surface charge distribution rather than simply suppress the surface charge accumulation.
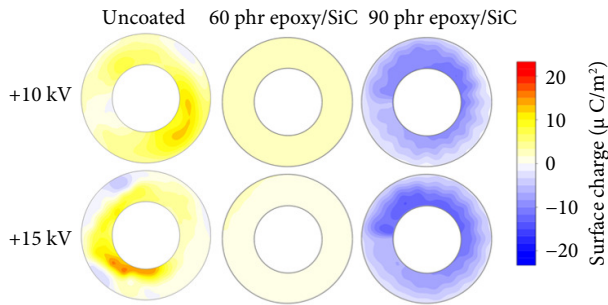
Fig. 24 Surface charge distributions on coated spacers with different SiC contents. Reproduced with permission from ref. [103], © 2022 IEEE.

Xue et al. and Dong et al.[104, 105] investigated the effectiveness of SiC/epoxy coating by using SiC particles in different sizes. The results showed that surface charges are significantly suppressed by SiC/epoxy coatings, especially using SiC particles in smaller size. Flashover voltage in 0.1 MPa 20% SF_6/N_2 mixtures increases gradually with decrease of SiC particle size. A surface conductivity graded coating (SCGC) scheme was further proposed to overcome the drawbacks of entire coating manner[63]. Four kinds of surface graded coating schemes are considered and the corresponding charge accumulation models are summarized, as shown in Figure 25.

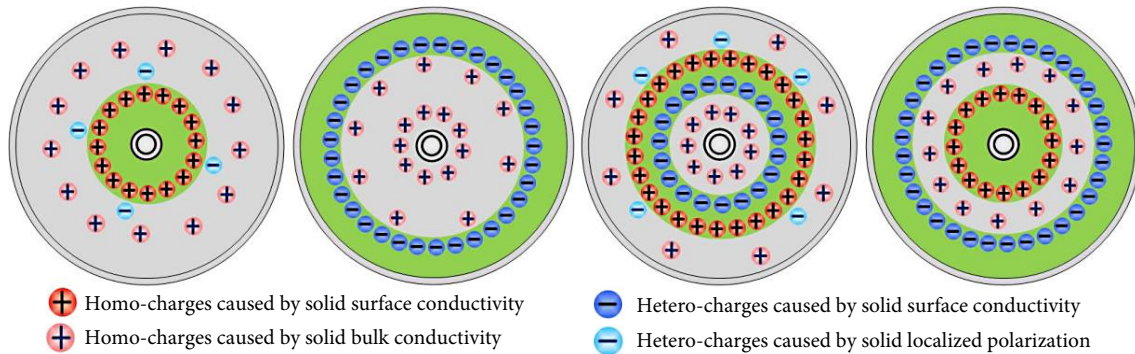Another surface coating method is depositing ZnO on epoxy

surface by a magnetron sputtering to prepare functional gradient surface layer[106], and the surface flashover voltage can be improved significantly. Further, Du et al.[107] developed a novel type of surface functionally graded materials (SFGM), for relaxing the electric field distortion of epoxy-based spacers by regulating the surface charge distribution. A thickness-graded layer of an epoxy/carbon black/BN component on the spacer surface was formed by electrospinning[108]. Experimental results showed that hetero-charges could accumulate on the conventional type of spacer, but huge number of homo-charges were introduced on the σ-SFGM spacer.

Figure 26 showed the typical surface charge distributions and the equivalent circuits of the conventional spacer and the σ-SFGM spacer, respectively. For the former, the hetero-charges come from the spacer-side injection by bulk conduction (J_b), enhancing the electric field strength around the HV triple junction.

For the latter, the homo-charge accumulation is dominated by surface conduction (J_S), relaxing the electric field distortion and improving the flashover voltage. Moreover, Du et al.[109] compared the insulation performances of the uniformly-fluorinated spacers and the gradient ones. The testing results proved that the flashover voltages of the latter were significantly higher than the former. Furthermore, the concept of the interfacial electric field self-regulating (IER) insulator was put forward and the tapered insulator with EP/SiC composite material was prepared as the IER insulator.

Fig. 25 Surface charge accumulation model on alumina/epoxy spacers with different SCGC schemes. (a) HV-coating. **(b)** GND-coating. **(c)** SPM-coating. **(d)** HV-GND-coating. Reprinted with permission from ref. [64], © 2020 IOP Publishing Ltd.
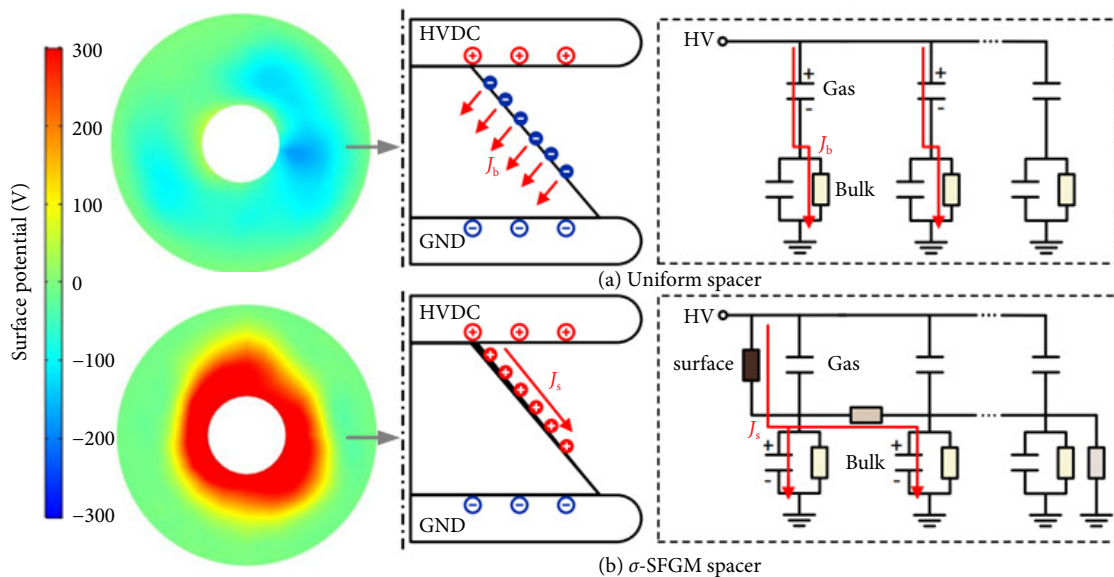

Fig. 26 Surface charge distributions and equivalent circuits of the uniform spacer and the σ-SFGM spacer.

Spacer shape modification

Generally, the DC-GIL/GIS spacer with optimized structure should be capable of minimizing the normal electric field for suppressing the charge accumulation from the insulation bulk, and smoothing the tangential electric field distribution for suppressing the charge accumulation from surface conduction. Based on this objective, Ma et al.[17] designed three types of spacers, i.e., disk-type, conical-type and obtuse conical type spacers for comparison. Numerical calculation results showed that the obtuse conical shape was the optimized geometric configuration for DC-GIL/GIS, due to its most evenly distributed electric field with minimum surface charge accumulation. Tu et al.[20] developed a ±100 kV spacer prototype considering the balance between tangential and normal electric fields along the spacer surface.

Figure 27 shows the physical image of that ±100 kV DC spacer and the electric field distribution. Neglectable normal electric fields with minus magnitude are found on bilateral spacer surfaces. Further, the suppression of normal electric field is even more significant on a ±200 kV DC spacer porotype following the same design, where the surface charge densities on the convex and the concave surfaces are reduced to 10 and 5 µC/m², respectively. As a conclusion, the optimization of spacer structure is an old and simple wayfor surface charge suppression, but it highly relies on the finite element simulation under ideal voltage energizations. This method cannot deal with the suppression of dynamic surface charge accumulation when subjected to complex testing conditions, e.g., variable temperature gradients and transient voltages by polarity reversal, switching and lightning over-voltages.
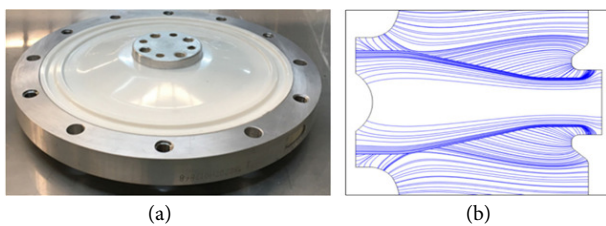

(a)   (b)

Fig. 27   (a) ±100 kV DC spacer and (b) the distribution of electric field lines. Reprinted with permission from ref. [20], © 2019 IEEE.

1.3.4   Comprehensive charging activity management

According to the Dam model, comprehensive charging activity management could be achieved by applying charge tailoring techniques which can initiatively control and decay charges. A common approach is designing charge adaptively controlling spacer by combining spacer shape optimization and non-linear conductive material techniques. Li et al.[18,110] designed a surface charge adaptively controlled spacer (CACS), which consisted of an "insulation region" around the central conductor and a "charge adaptive region" near the GND electrode, as shown in Figure 28(a). The "insulation region" of the spacer was made of an epoxy/Al₂O₃ composite, the "charge adaptive region" was made of an epoxy/SiC composite. When the surface charge accumulation in the "charge adaptive region" reached a certain degree, excess surface charges would be released. The surface charge density of CACS is significantly lower than that of the regular spacer (RS), as shown in Figure 28(b).

By combining surface treatment and nonlinear conductive materials, the σ-SFGM spacer proposed by Du et al. and Yao et al.[107,108] as introduced in Section 1.3.3 may also be considered as a comprehensive charging activity management.

1.4   Flashover

Surface flashover is a penetrating discharge along the gas-solid interface through electrodes accompanied by huge energy loss through voice, heat, and luminescence, which has great potential to generate large currents and degrade the surface insulation properties of insulators inside gas-insulated equipment[106,111]. Owing to the surface flashover voltage being lower than the discharge voltage of either gas or solid with the same discharge gap, it is crucial to clarify the microscopic DC surface flashover mechanism of gas-insulated equipment and explore methods to improve surface flashover performances[112]. In the last decade, lots of research works from China are focusing on the influence of surface charges on surface flashover and surface flashover microscopic mechanisms.

1.4.1   Influences of surface charge on DC flashover

Influenced by collaborative contributions from gas, solid, and interface states, flashover is triggered from triple point and usually propagates along the gas-solid interface. The trigger of flashover in compressed gas under DC voltage involves complex competitions of charge transport in the multiphase. A comparison between surface flashover and gas breakdown voltages in various environments has indicated that the final form of surface flashover in compressed gas is a plasma streamer discharge along the gas phase, while the effects of the solid is an "induced" factor to trigger the subsequent discharge[113]. Hence, finding the underlying inducing factor is essential to clarify the surface flashover mechanism.

In 2021, Li et al.[3] used the dust figure to present the charge clusters on the spacers subjected to DC voltage, showing that as
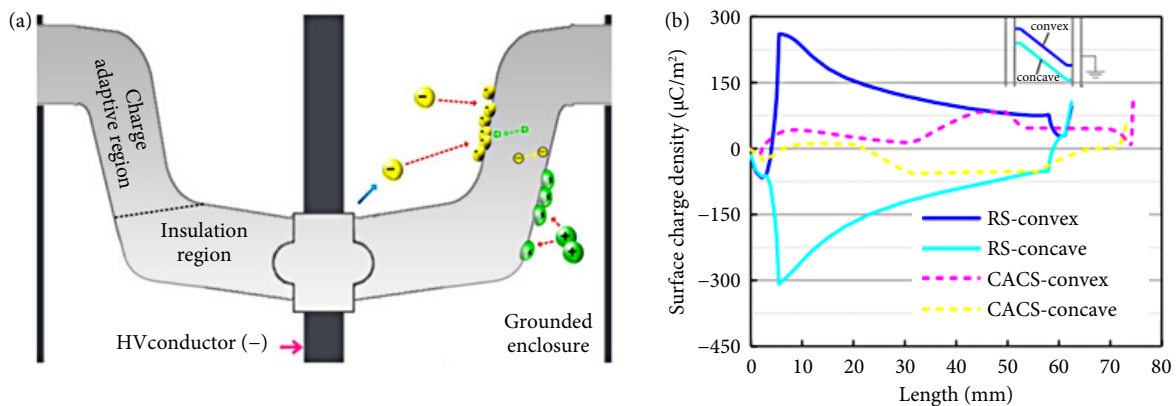

Fig. 28   (a) Structure and (b) surface charge distribution of the CACS spacer[18]. Reprinted with permission from ref. [110], © 2018 IEEE.
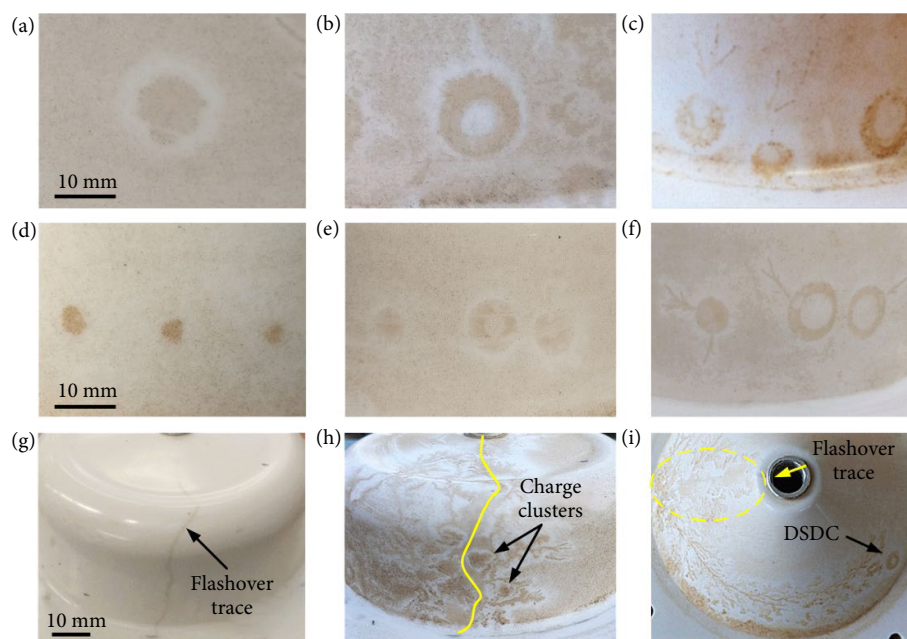
Fig. 29   Images of the dust clusters on the surface of the spacer, (a–c) without artificial defects at −150 kV, −165 kV, and −180 kV, and (d–f) with three needle tips parallel placed on the enclosure surface at −70 kV, −90 kV, and −100 kV. (g and h) Images of the same spacer with surface flashover trace before dust figure treatment and after dust figure treatment. (i) Image of a surface flashover trace connecting the DSDC to the grounded conductor. Reprinted with permission from ref. [3], © 2020 IOP Publishing Ltd.

applied voltage increases, the charge clusters transfer from dot-shaped cluster to donut-shaped cluster and finally to cluster with streamers. Charge clusters mainly concentrate in the vicinity of surface flashover trace, which is shown in Figure 29. The interesting experimental design and results indicate the accumulation of surface charges triggers streamer discharge over cluster edges in compressed SF_6 gas.

The polarity of surface charges greatly influences the DC surface flashover performance. Figure 30 shows the effects of pre-deposited surface charge on surface flashover voltage from research work in the last decade[71, 114–118]. Zhang et al.[114] deposited surface charges under −100 kV upon the 1100 kV insulator surface before surface flashover measurement and found the negative surface flashover is only 764 kV. Shao et al.[71] investigated the influence of surface charges with different polarity on surface flashover, the results indicated both flashover voltage decrease no matter whether pre-charged homo- or hetero-charges upon the surface of the sample, the surface flashover with homo-space charges decreases ~15%, while that with hetero-charges decreases ~25%. Li et al.[115] treated epoxy/Al_2O_3 spacer with ±8 kV corona discharge and found surface flashover voltage of the pretreated fluorinated sample nearly unchanged with the homo-charged surface, but slightly decreased with the hetero-surface charges. Wang et al.[116] found the surface flashover of crosslinked polyethylene (XLPE) and XLPE coated epoxy resin/copper dropped 27% and 18% when preset homo-surface charges and the percentage of dropped flashover voltage is associated with the surface conductivity. Liu et al.[117] also established a relation between surface flashover and surface charges, the results show that surface flashover voltage increases with the surface charge density when the polarities of them are the same, while it will decrease with the surface charge density with hetero-space charges. Ma et al.[118] found that hetero-surface charges distort the local electric field in the gas phase and sufficiently reduce surface flashover voltage, while homo-surface charges may impede the local electric field distortion and slightly improve flashover voltage. In Figure 30, it can be concluded that

the hetero-surface charges obviously reduce surface flashover voltage, while homo-surface charges may elevate or decline surface flashover voltage, and the influence degree of hetero-space charges on surface flashover is much server than that of homo-surface charge.

The position of surface charges also greatly affects the surface flashover. Recently, Dong et al.[105] coated epoxy/SiC on different positions of the insulator surface and investigated the effects of surface charges on flashover voltage. The results indicate high conductivity region near the high-voltage electrode accelerates the surface charge dissipation, while the region near the grounded electrode and in the middle part of the samples results in the polarity reversal phenomena upon the insulator surface, which further distorts the electric field and reduces surface flashover voltage.

1.4.2   *Flashover theories*

In the 1980s, some classic surface flashover models were proposed to describe the discharge along the gas-solid interface in the compressed gas, i.e., the diffusion-limited charge accumulation model established by Pai and Marton[120], the critical field model established by Cooke[121], and the comprehensive analytical model established by Sudarshan and Dougal[122]. Although the aforementioned theories sufficiently demonstrate some flashover phenomena in compressed gas, the models fail to describe the surface charge dynamics and their effects on flashover. From 1990 to 2010, most research works concentrate on the simulation of electric fields and surface charge distributions, and the flashover theory standstill with time. Notably, in recent 10 years, some new flashover models are proposed by researchers from China.

Analogous ineffective region expansion theory

In 2017, Li et al.[13] proposed an analogous ineffective region expansion model to clarify the effects of surface charge migration on surface flashover when a gradient temperature distribute upon the insulator surface, as shown in Figure 31. As temperature
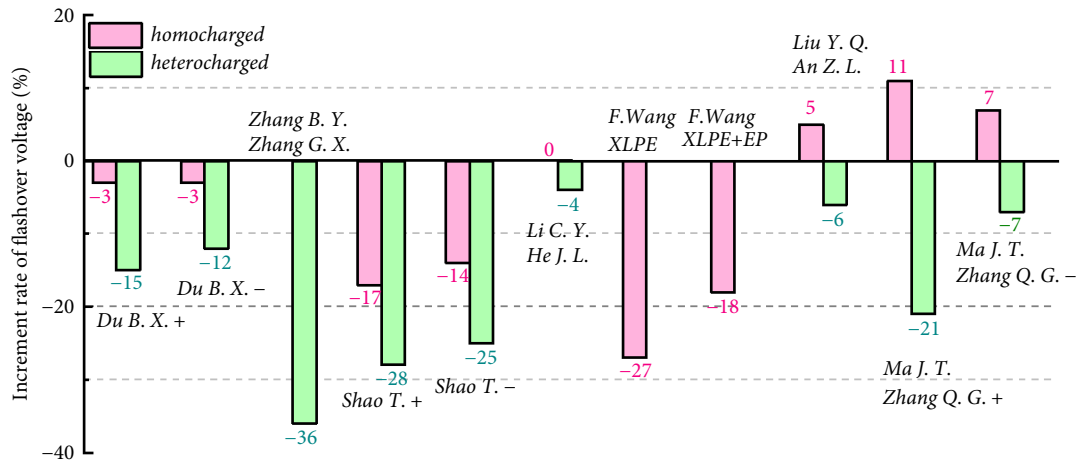
Fig. 30 Influence of surface charges on DC surface flashover[7, 114–119].

increases, the charge injected from the high-voltage electrode migrates to the grounded electrode with improved surface and volume conductivity, which lifts the potential of the high-temperature region. The region that reaches 60% surface potential of the high-voltage electrode is defined as "the analogous ineffective region" (AIR). When the AIR expands to the grounded electrode, the extremely distorted electric field between the ground electrode and analogous ineffective region triggers gas collision ionization at the triple junction near the grounded electrode, and then the plasma sheath extends to the HV electrodes, which finally induces surface flashover. This model emphasizes the influence of surface charge migration on surface flashover with a temperature gradient through the insulator, and indicates that a modified surface conductivity affects surface charge moves, which further influences flashover property.

Based on this finding, Li et al.[123] developed a method to mitigate surface partial discharge based on tailoring the surface conductivity of the insulation near triple junction area. The theory is verified by
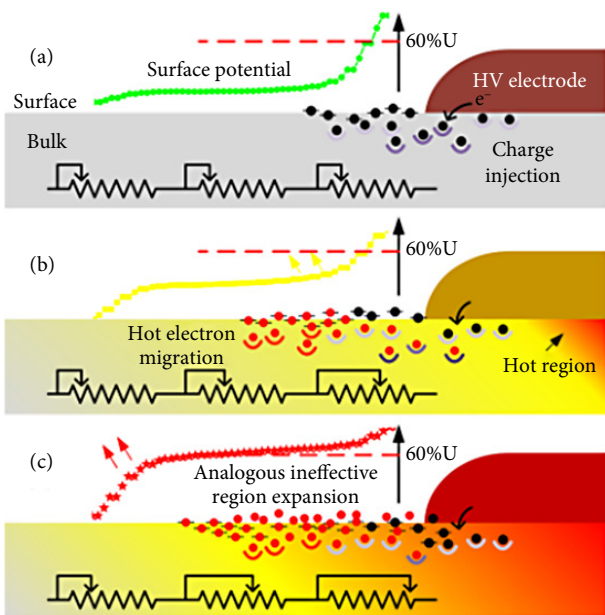
many researchers and provides routes to reduce the thermal conductivity or introduce deep traps into the spacer to suppress the migration of surface charge to improve surface flashover voltage[124].

Synergetic effects of gas adsorption and surface charging[125]

Surface flashover is a complex phenomenon concerning the properties of solid, gas, and gas-solid interaction. Although gas desorption is a triggering factor for flashover in a vacuum, it still lacks the physical process which can unravel the gas–solid coupling mechanism in compressed gas. To address the underlying mechanisms, a surface flashover model that involves synergetic effects of gas adsorption and surface charging is proposed by Li et al.[125], which is shown in Figure 32.
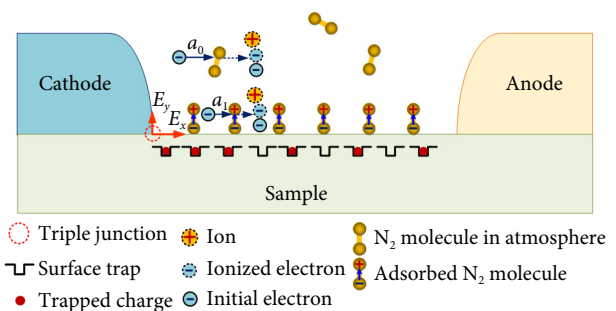

Fig. 32 Scheme of gas-solid coupling surface flashover model in compressed gas. Reprinted with permission from ref. [125], © 2019 The Author(s).

Three essential charge transport processes in multiphase are emphasized in the present model: (1) the electric field is highly distorted near the cathode triple junction (CTJ), electrons in the solid emit into the gas phase and leave large amounts of positive charges in the solid surface layer; (2) surface charge determines the vertical electric field, which greatly affects the collision ionization and electron emission processes in the gas phase; (3) large amounts of gas are absorbed upon insulator surface, the gas density in the gas surface layer gradient decreases with the distance to the surface, the improved gas density impede the collision ionization processes in the gas phase, which further determines surface flashover in compressed gas.

In the model, gas adsorption impedes collision ionization, while surface charge distorts the electric field and induces the discharge in gas, the synergetic of gas adsorption and surface charging greatly influence surface flashover in compressed gas. The model first ever introduces the concept of gas adsorption into the surface

Fig. 31 (a) Surface potential increase due to charge accumulation on the insulation surface. (b) Hot electron migration with the increase of temperature in the insulation near the HV electrode. (c) Expansion of "analogous ineffective region" due to hot electron migration. Reprinted with permission from ref. [13], © 2017 The Author(s).

flashover, and the relative adsorption ability is crucial for the difference between surface flashover and gas breakdown voltages in compressed gas with various pressures and temperatures[126]. In 2021, Li et al.[127] further established a numerical simulation model based on the synergetic effects of gas adsorption and surface charging and found the simulation results are consistent with experimental flashover voltage in nitrogen.

To date, the acknowledgment of the physical flashover process in GIS/GIL is greatly improved by a large number of significant Chinese research works in the past 10 years. Nonetheless, there are still two essential questions of surface flashover that need to be focused on in future work. One is the complex competing mechanism of surface charge accumulation, surface charging is a final form of the competition among gas ionization, surface conduction, and bulk conduction, it is important to unravel the synergetic and competing mechanisms of several charge transport modes in surface charge accumulation. The field-dependent theory[4] shows overall laws of charge behaviors with electric fields, however, effects of environmental factors shall also be considered carefully. The other is the inducing mechanism of surface flashover, especially how surface charging induces flashover in the pre-flashover stage. Since the surface flashover presents as a randomness discharge phenomenon which is triggered and completed within nano seconds, there is still no solution to directly detect the surface charge distribution in the pre-flashover stage. The presented models and theory only show charge transporting laws before flashover to correspondingly judge the charge-triggered flashover mechanism. Some solid experimental work is still needed.

1.5 Metal particle

In the DC gas-insulated equipment, a prominent problem that needs to be paid attention to is the metal particulate pollution. As metal particles are easy to obtain relatively large kinetic energy under the DC electric field, they have a high probability of moving to the vicinity of insulators, causing insulator surface charge accumulation. As has already been discussed in Section 2.4, randomly distributed surface charge clusters can significantly distort the electric field distribution and reduce the insulation strength[128–130].

In addition, because the DC gas-insulated equipment mostly has sliding plug-in structures and bolt fixing structures, etc., the friction and vibration during production, transportation, installation and maintenance may produce particles, making it difficult to cut off the influence of metal particle from the source. Therefore, the treatment of metal particle in DC gas-insulated equipment has received extensive attention from many scholars over the years[131, 132]. The current research mainly focuses on the motion characteristics of metal particle under DC field and the induced capture of particle, as is shown in Figure 33. The ultimate goal is to minimize the impact of metal particle on insulation and ensure the safety and reliability of equipment operation.
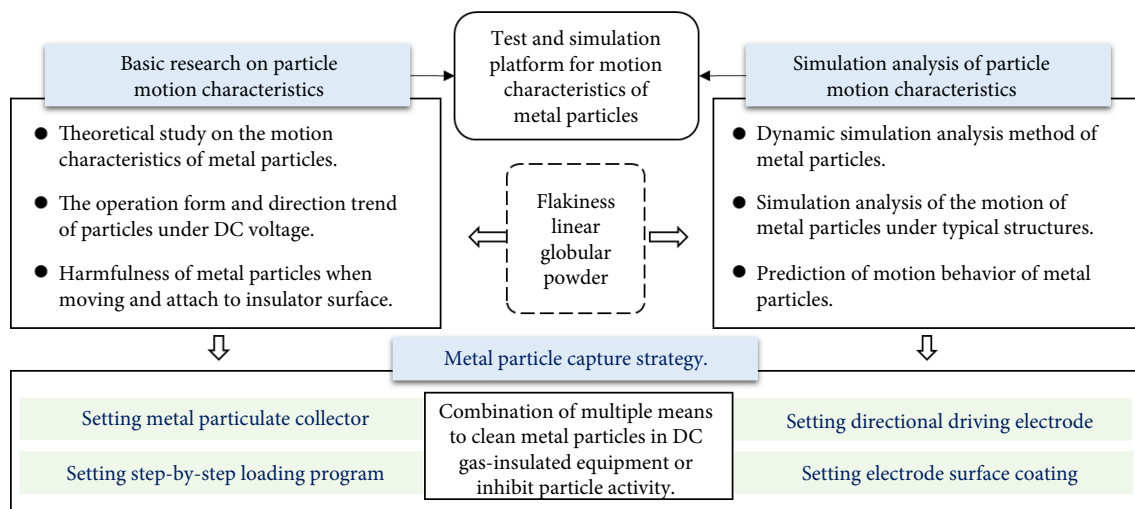

Fig. 33   The main research work on the motion behavior mode and inhibition measures of metal particle.

It will take a lot of cost and time to carry out the full-scale experiment for the motion characteristic of particle, including the reduction of GIL/GIS bus, the addition of observation equipment and higher test voltage level. Therefore, the experimental study of motion characteristics is usually based on the principle of field strength equivalence, using a scaled model or other devices that can simulate the electric field in the GIL/GIS cavity. Many researches have fully completed the calculation charging theory for flakiness, linear and globular particles and given dynamic parameters such as collision rebound and fluid resistance[133–135]. The motion behavior of metal particle with different shapes is well analyzed. In particular, in most cases the metal particle shows reciprocating motion between the two electrodes. However, when the coaxial electrode is arranged and the negative DC voltage is applied, the linear and flaking particles present the phenomenon of "flying firefly", which not only bump around the high-voltage electrode, but also do not contact the ground electrode[136, 137], as is shown in Figure 34. In addition, for the movement characteristics of metal powder under DC voltage, there is a phenomenon similar to sand storm[138, 139]. These special circumstances bring great difficulties to the capture and removal of metal particles in DC gas-insulated equipment.

The surface coating of electrode and the addition of particle collector are important means to limit the impact of metal particles on insulation. Many studies have shown that the surface coating has no contribution in moving the particle to the low electric field area, however, it prevents the particle from lift-off by limiting the charge of particle, thus avoiding the disorderly movement of particles in the equipment[139–141]. The particle collector is designed with a suitable structure to set a low field area, which can induce the metal particle move into it and limit their motion activity. After years of development, the particle collector used in AC gas-insulated equipment has been relatively mature with its structure including grid type, strip type, hole type, etc. However, under DC voltage,
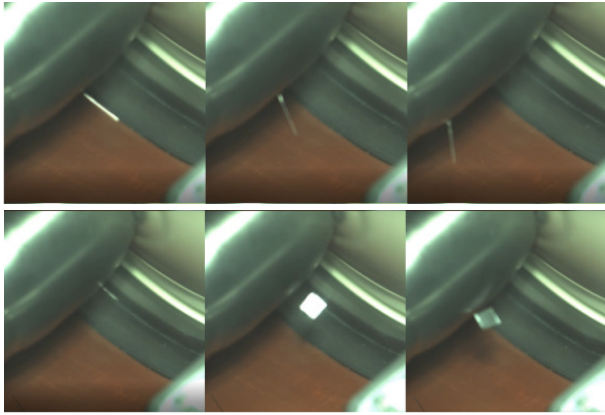
Fig. 34 The "flying firefly" phenomenon of particles under negative DC voltage.

the particle moves faster and has stronger disorder, which makes the particle collector used in AC gas-insulated equipment less effective. How to induce the metal particle trapped and limit its escape probability is an important issue in recent years.

In order to further develop the DC particle collector, the combination of simulation and experiment has been widely used. At present, many scholars have built simulation models under multiple types of coulomb force, viscous resistance, gravity, etc. based on the dynamics theory of particle motion[133]. Typical force is shown in Table 3.

Table 3   Expressions of the force acting on the metal particle

Force	Symbol	Expression
Coulomb force	F_q	Eq
Gravity	G	$(4/3)\pi r^3 g\rho$
Electric field gradient force	F_{grad}	$2\pi r^3 \varepsilon_0 \varepsilon_r |\nabla E^2|$
Viscous resistance	F_v	$6\pi\eta r|v|$
Buoyancy	F_f	$(4/3)\pi r^3 g\rho_a$

The van der Waals force is also analyzed considering the interaction between dust[142]. Previous studies have shown that these theories can be consistent with experiments under specific circumstances. Therefore, Zhan et al.[143], Liu et al.[144, 145], and Li et al.[146] have conducted some research on the structural optimization design of the particle collector. They analyzed the capture efficiency of different structure under DC voltage, and appropriately improved the corresponding size parameters. The improvement of parameters can improve the capture rate, enhance the number of trapping and prevent escape, but the efficiency is not as good as that under AC voltage, and relevant research is still under way.

A recently published work led by Xing et al.[147] shows that a slight decrease in spacer surface conductivity is effective in reducing the activity of particle motion near the spacer.

Although the surface coating of electrode can limit the movement of metal particle, it cannot completely eliminate the influence of particles on local electric field distortion. The particle collector might be a promising approach. However, the efficiency of the collector used under AC is relatively low, which cannot completely limit the particles from reaching the insulator. The design of trap and drive electrode with new structure still needs to be further developed. For the dust and other special cases, further analysis and research are also essential.

1.6 Conductor roughness

The conductor surface of GIS/GILs cannot be perfectly smooth,

which will inevitably lead to local non-uniformity of the electric field on the conductor surface. With the improvement of voltage level and gas pressure, the gas discharge voltage drop caused by the micro irregularities of the conductor surface has become an urgent problem to be solved[148]. At present, there is no special standard for the conductor surface roughness of DC GIS/GILs, it still mainly referred to the standard of AC GIS/GILs. The arithmetic average height R_a is used to characterize the inhomogeneity of conductor surface in the standard. The surface R_a of high voltage conductor is not greater than 6.3 μm. The internal surface R_a of the enclosure is not greater than 50 μm[149]. After finishing turning, grinding and other processes, the roughness of the conductors can be controlled within 1 μm. Excessive roughness of conductor surface will significantly reduce the insulation performance, while too small surface roughness will increase the cost of equipment manufacturing. It is of great significance to study the influence of conductor surface roughness on the insulation performance and formulate a more reasonable surface roughness evaluation standard. At present, for a DC GIL, the research on conductor surface roughness mainly focuses on two aspects. One is the effect of conductor surface roughness on gas breakdown. The other is the influence of conductor surface roughness or morphology on the charge accumulation on insulator surface.

1.6.1   Effect of surface roughness on gas breakdown

It can be seen that the gas breakdown voltage of SF_6 is negatively related to the conductor surface roughness under AC voltage stress. Besides, results show that the breakdown voltage of SF_6, 0.4 MPa decreases slightly linearly with the increase of the conductor surface roughness[148, 149]. The drop is more obvious than that of lower gas pressure. It can be inferred that the sensitivity of SF_6 gas to conductor surface roughness goes up with the increase of gas pressure.

Under DC voltage stress, the polarity effect should also be considered in addition to the above rules. Because of the difference in the movement of positive and negative space charges, the electrode is more prone to corona under negative voltage, and the negative breakdown voltage is lower than the positive breakdown voltage. The higher value of the conductor surface roughness results in a larger non-uniformity of the electric field. And this leads to a more obvious polarity effect. The DC breakdown voltage of the gas gap changes similarly with the surface roughness of the enclosure and the central conductor. However, the influence of the conductor surface roughness of the enclosure on the breakdown voltage is different with different gas pressures. When the gas pressure is lower than 0.2 MPa, there is no obvious effect on the negative DC breakdown voltage of the surface roughness of the enclosure which is among 0.5 μm and 4.6 μm[150]. While the negative DC breakdown voltage of gas gap is obviously affected by the surface roughness of the enclosure, which is among 0.5 μm and 0.94 μm, when the gas pressure is higher than 0.2 MPa.

In recent years, eco-friendly GIS/GILs are required in order to reduce environmental impacts and reach the net-zero carbon dioxide emissions. Due to the physical and electrical characteristics of different insulation gases, the sensitivity to the distorted high electric field is also different. The standard of conductor surface roughness in gas insulated electrical equipment should match with the insulating gas. The tolerance of the insulating gas to the non-uniform electric field can be evaluated by the merit. The greater the merit, the higher the allowable electric field distortion. Scholars used the merit only related to the tolerance to uneven electric field to evaluate the breakdown performance of C_3F_7CN/CO_2 gas mixtures refer to that of SF_6[151]. By improving the conductor surface

roughness and reducing the local electric field distortion, the gas shows good insulation performance. Buffer gases including N_2 and CO_2 can reduce the sensitivity of the mixtures to the distorted electric field at the expense of their insulation strength. Generally, the eco-friendly gas mixtures need to improve their electrical strength by increasing the gas pressure, and the applied gas pressure is higher than SF_6. Therefore, the maximum acceptable conductor surface roughness should be determined by comprehensive consideration.

Experience gained with AC GIS has shown that electrode surface dielectric coatings are effective in suppressing ionization phenomena in adjacent gas gap and increasing the overall insulation strength. However, coatings are not widely applied in GIS/GIL for some doubt regarding their long-term reliability.

1.6.2 Gas conduction and surface charge

As is known with DC GIS/GILs, it is subject to unipolar high electric field stress. Even if no gas gap breakdown occurs, the solid insulation system is still facing the problem of charge accumulation on the insulator surface. It is generally believed that the micro discharge caused by the protrusions and defects on the electrode surface and the field emission of the electrode under high electric field intensity are two key sources of the surface charge accumulation of DC GIS/GIL insulators[4,152]. Recently, the weak gas conduction current reflecting this process has been measured by researchers[98,153,154]. This kind of current is closely related to the surface roughness of the conductor. The main physical mechanism of such phenomenon is that, the surface roughness of the conductor has a significant impact on the micro discharge and field emission of the conductor surface. The design field strength of the conductor is usually calculated according to the ideal smoothness of the conductor. However, when we magnify the local morphology of the conductor, the effects of surface micro discharge and field emission mechanisms cannot be ignored, and the local area has approached or even exceeded the critical field strength. In addition, under the average field strength of more than 2.5 kV/mm, the increase of relative humidity has a significant positive correlation with the gas conduction current. This may be related to the emission of charged water clusters under local high field[153,154]. Figure 35 shows the micro-morphology of the finished conductor surface taken by the white light interferometer. It can be seen that although the average roughness R_a is as low as 0.35 μm, the influence of local burrs cannot be ignored.

To sum up, the conductor surface roughness of AC GIL is too large for DC GIL and cannot be directly applied. For DC GIL, it seems that the surface roughness of the conductor should be reduced to achieve satisfactory performance.

Furthermore, parameters suitable for DC conductor surface evaluation are expected to be found. The arithmetic average height R_a provides an evaluation method based on average roughness for the conductor surface in the conductor design of AC GIL. However, according to the recent results, it can be found that R_a is not sensitive to the surface structure with small local protrusions, and the influence of the surface structure with local protrusions generated by processing on the conduction current cannot be reflected. There is no linear relationship between the conducted current and the average roughness. The surface morphology of the conductor and its influence on the gas conduction current were studied. It is found that the proportion of high surface local field strength plays the major role in the gas conduction current, rather than the average roughness R_a. Figure 36 shows the local field strength statistical distribution of conductor surfaces with different average roughness. The researchers put forward a more reasonable method to
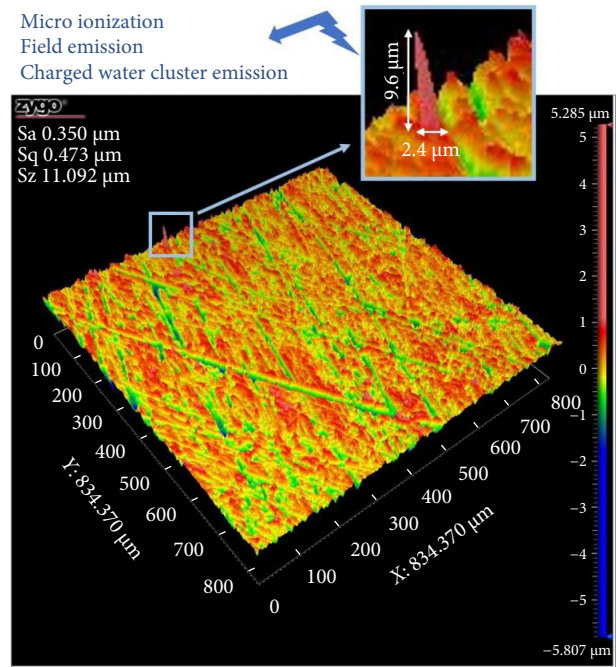

Fig. 35 Surface micro morphology of finished conductor.

characterize the surface morphology of DC GIS/GIL conductor by integrating S_{pa} and S_{pku}[154]. The results provide a basis for the design of conductor surface in DC gas insulated equipment.

The existing conductor processing and roughness evaluation methods of AC GIS/GIL cannot be directly applied to DC GIS/GILs. Problem remains on how to formulate conductor evaluation methods and roughness level for DC equipment. Meanwhile, there is a lack of corresponding conductor processing methods.

2 Industrial perspective

2.1 Background and challenges in China

As the "carbon peaking and carbon neutrality" goal was proposed, the capacity of China's installed renewable energy facilities has exceeded 1 billion kilowatts up to 2021, ranking first in the world and showing a rapid growth trend. However, the geographical distribution of China's new energy resources and load demand doesn't match its economic hub. The "West-East Power Transmission" has been extended from the eastern plain area to the western plateau, snow-capped mountains, Gobi Desert, far-reaching areas. With the further expansion of new energy, the reduction of wind generation and PV generation is becoming more and more prominent. As shown in Table 4, the consumption of new energy has become a bottleneck restricting the development of energy and power transformation in China. Therefore, the large-scale power transmission channel becomes one of the major problems that restricts the electric power development in China.

Since the construction of the world's first Yunnan–Guangdong UHV DC Project (Chusui DC), the high voltage direct current (HVDC) equipment has been constantly updated and iterated to address the needs of long-distance and large-capacity transmission of clean energy. To support current and future high-capacity power transmission, there are three major and urgent challenges to be addressed:

(1) How to transmit large-scale offshore wind power to isolated islands and offshore platforms?

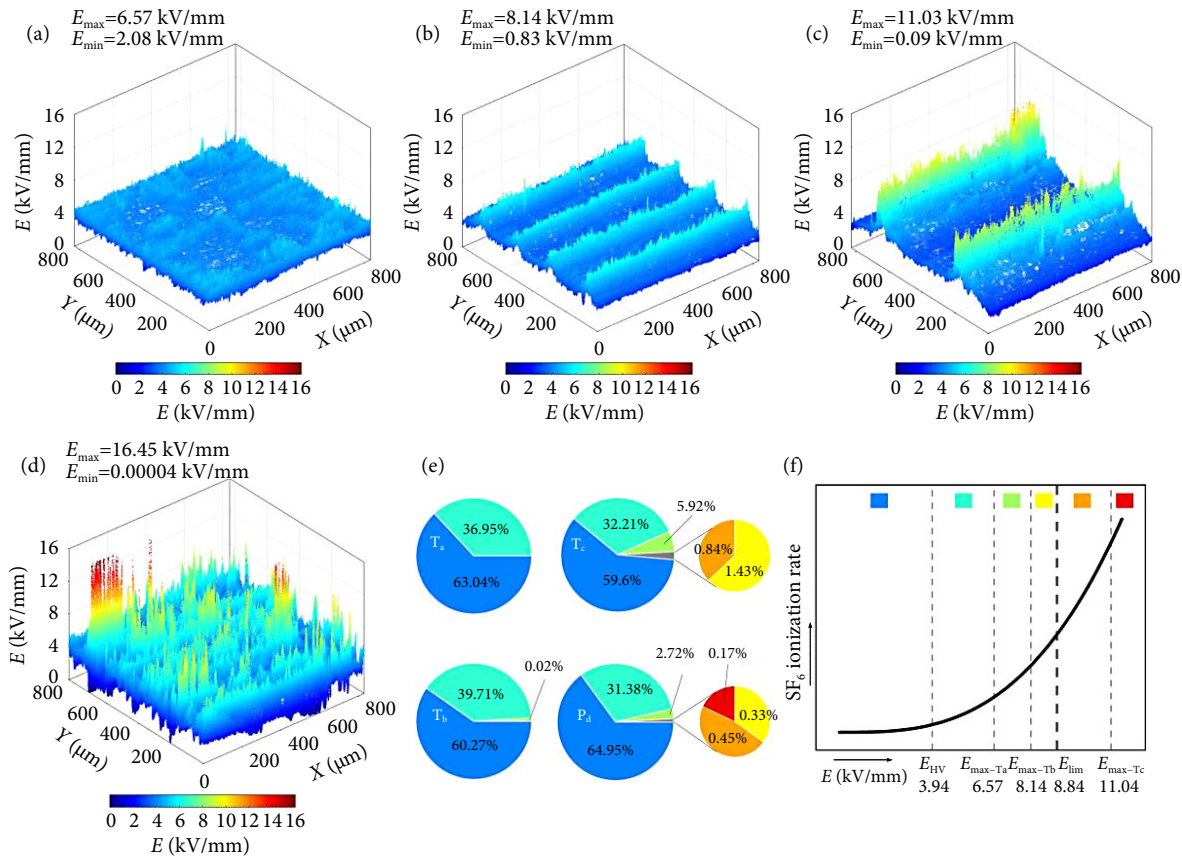Compact and lightweight offshore converter platform is a key

Fig. 36 The distribution and statistical law of electrode surface electric field strength. (a–d) The distribution of surface electric field. **(f)** The legend of pie chart **(e)**, and the relation among the five electric field strength intervals and the ionization coefficient of SF_6 (0.1 MPa). Reprinted with permission from ref. [158], © 2022 IOP Publishing Ltd.

Table 4 Distribution of wind and PV generation curtailment in China (2017).

Type	Province/Autonomous region
Wind generation curtailment ratio>20%	Xinjiang, Gansu, Jilin;
Wind generation curtailment ratio 10%–20%	Heilongjiang, Inner Mongolia;
Wind generation curtailment ratio<10%	Ningxia, Shaanxi, Shanxi, Hebei, Liaoning, Yunnan
PV generation curtailment ratio>5%	Xinjiang, Gansu, Qinghai, Ningxia, Shaanxi

constraint. At present, Rudong Offshore Wind Power Transmission Project, the first offshore wind power flexible DC transmission project that has been put into operation in China, adopts the symmetrical unipolar wiring mode, incorporating both positive and negative DC submarine cables. The grade of DC voltage is ±400 kV, and the rated transmission capacity is 1100 MW. However, the offshore wind power is developing towards a large-scale and long-distance direction, so the symmetrical bipolar flexible DC mode is employed to facilitate the large-scale networked transmission of wind energy. DC GIS/GIL is the key development direction of the large-scale utilization of offshore wind energy.

(2) How to solve the problem of insufficient UHVDC transmission corridors?

DC line plays an important role in planning China's power grid. In 2022, the constructions of nine UHVDC transmission projects have been scheduled, with DC lines built up to 14,000 km. Taking the Guangdong–Hong Kong–Macao Greater Bay Area for example, where the Southeast Tibet UHV multi-terminal DC power

transmission is carried out, there are dense line channels, crossing snow mountains, and depopulated zone. The development of DC GIL technology built under ground or on the surface is urgently needed to solve the problem of insufficient transmission capacity.

(3) How to reduce the impact of the terrain and environmental conditions on the converting equipment, and build power transmission lines with high capacity, high reliability and sustainability with the environment in the future?

Replacing DC outdoor equipment of converting plant with DC GIS can support the design and engineering applications of the full indoor compact converter station, perfectly solve the construction, operation and maintenance problems caused by the harsh natural environment of clean energy transmission in the west, and greatly reduce the cost of land in the populated areas in the eastern energy consumption center. The future power grid has the advantages of low loss, high reliability and little impact on environment. With conquering the challenges in long-distance, large-capacity, low-loss, and environmental-friendly DC GIL technology, the transmission-distribution all-DC super grid can be realized.

Therefore, the development of DC GIS/GIL technology is a major demand for national economic growth and social development, which will effectively solve the conflicts among power, natural environment and urbanization.

2.2 Progresses in China

At the end of 2021, CIGRE joint working group D1/B3.57 issued the report TB 842 - Insulation Test of High-Voltage DC Gas Insulation System, providing an important guidance for the

development and performance assessment of DC GIL. In September 2022, Siemens and other companies reported the latest progress of eco-friendly air-insulated DC GIS/GIL equipment and high-voltage switchgear for clean air insulated offshore wind power at the CIGRE Paris Conference 2022. Under the upcoming major demand and development trend, this section focuses on the application of DC gas-insulated equipment in the future projects of UHVDC transmission, and introduces the critical technical issues, major research achievements and progress of the implementation of DC GIS / DC GIL equipment in China in the past decade.

Compared with the research and development progress in Europe, China has no engineering application of DC GIS and DC GIL, and even not developed mature ±500 kV DC GIS/GIL. Different from the independent system design of Siemens and ABB, Chinese manufacturers are only a link in the industry chain, with the product research and development (R&D) power from the project promotion and profit accounting. Therefore, the R&D speed of DC gas-insulated equipment lags behind the engineering demand in China. Engineering application requirements depends on the existing mature and operational experience. This forms an enclosed loop with the R&D of new DC equipment. However, form the future perspective of DC power network development, several main manufacturers (XD, Pinggao, Shandong Taikai) are also attempting to make a breakthrough. Through the collaboration with universities in developing DC gas-insulated equipment, they strive to make the performance breakthroughs in the overseas projects and in turn contribute to the construction of domestic projects.

2.2.1 Progress in DC GIS

Pinggao Group has made some breakthroughs in the basic epoxy resin insulation materials design, compact equipment, equipment preparation, and assessment.

Solid insulation materials

Pinggao has developed a formula for DC epoxy materials composed of a double crosslinked solidified network structure, featured by high volume resistivity (10^{17} Ω·cm) and high mechanical strength (bending strength of 130~135 MPa). Formula comparison with the AC material is listed in the Table 5.

Table 5 Comparison of DC epoxy formula and AC materials

Test project	Unit	DC materials	AC materials
Density	g/cm³	2.21~2.33	2.0~2.3
Tensile strength	MPa	81~87	≥70
Tensile elastic modulus	MPa	$(12.8~13.5)\times10^3$	$≥12.7\times10^3$
Bending strength	MPa	137~141	≥125(131)
Volume resistivity	Ωcm	$(1.2~2.1)\times10^{17}$	$≥1\times10^{15}(7.2\times10^{15})$
Dielectric constant	—	5.32~5.41	≤6.3
Electrical strength	kV/mm	32~37	28~29
Glass transition temperature	°C	143~147	≥115

Equipment

Pinggao's research and development work in the compact DC GIS equipment includes:

(1) The multi-column parallel structure of the lightning arrester and shunt control technology are adopted to realize the core design of arrester resistor.

(2) DC GIS voltage transducer

The design technology of dry resistance-capacitance core has been overcome, and the oil-free and lightweight design of the primary voltage divider was also realized; Based on the error matrix, frequency characteristics and thermal field analysis technology, the GIS of the voltage divider embedded in the metal cylinder has been realized.

(3) DC GIS isolation grounding switch

Particle traps are set at the inner wall of enclosure near the insulators and are set below the switch break. The end of high-voltage mobile contact is in a semi-enclosed by a shielding structure. Transmission insulation rod is placed on the upper side of the contact, and the switches are arranged in a line, with no horizontal insulators.

(4) All external optical fiber structured current transducer

It is placed outside the casing grounding flange and working on the ground, providing a reliable insulation. As is shown in Figure 37.

Equipment manufacture and assessment

In 2021, the first ±210 kV DC GIS in China was developed, and the three-month assessment test was completed, as shown in Figure 38. In November 2022, it passed the product technology evaluation organized by the China Machinery Industry Federation. In 2022, a full set of performance verification tests of ±320 kV DC GIS was completed. At present, the insulation performance test verification of ±525 kV DC GIS is being carried out. It is expected that all relevant development work will be completed in 2023. In the future, Pinggao will also launch the research and development of metal closed DC converter switches, to realize the metal closure of DC middle-line switchgear and further promote the compact design of the converter station.

In terms of performance assessment, the DC GIS test circuit with DC voltage and impact voltage superposition, no-load and heavy-load flexible switching, and transformer and lightning arrester flexible cutting are constructed. The comprehensive assessment method of all DC GS components under the multi-physics influence of electric, magnetic, thermal, and mechanical stresses is proposed for the first time.

China XD Group Co., Ltd. has completed the research and development of ±500 kV DC GIS prototype. Performance validation tests are ongoing. The dielectric constant, dielectric loss tangent value, and resistivity of the three epoxy resin formulations at different temperatures were measured, as plotted in Figure 39. The surface charge accumulation at different time and locations subject to DC voltage was also studied.

Based on the conventional components of DC GIS, China XD Group Co., Ltd. has also developed ±500 kV DC high-speed switch (HSS) module to rapid isolating of DC line faults and the fast online switching, as is shown in Figure 40.

With the R&D strength of ±200 kV DC basin-type insulator, Shandong Taikai proposed for the first-time fluorinated insulator without changing the optimized formula and production process of epoxy insulator. The sample test results show that the DC flashover voltage can increase by more than 10% and the surface conductivity by more than three orders of magnitude. Currently, the company is cooperating with Tsinghua University to investigate and develop the enclosed busbar for ±500 kV DC GIS, with related work focusing on the cone spacer and particle capture technology for DC. The research and development are expected to be completed by the end of 2023, and the grid connection test will be completed by 2024.
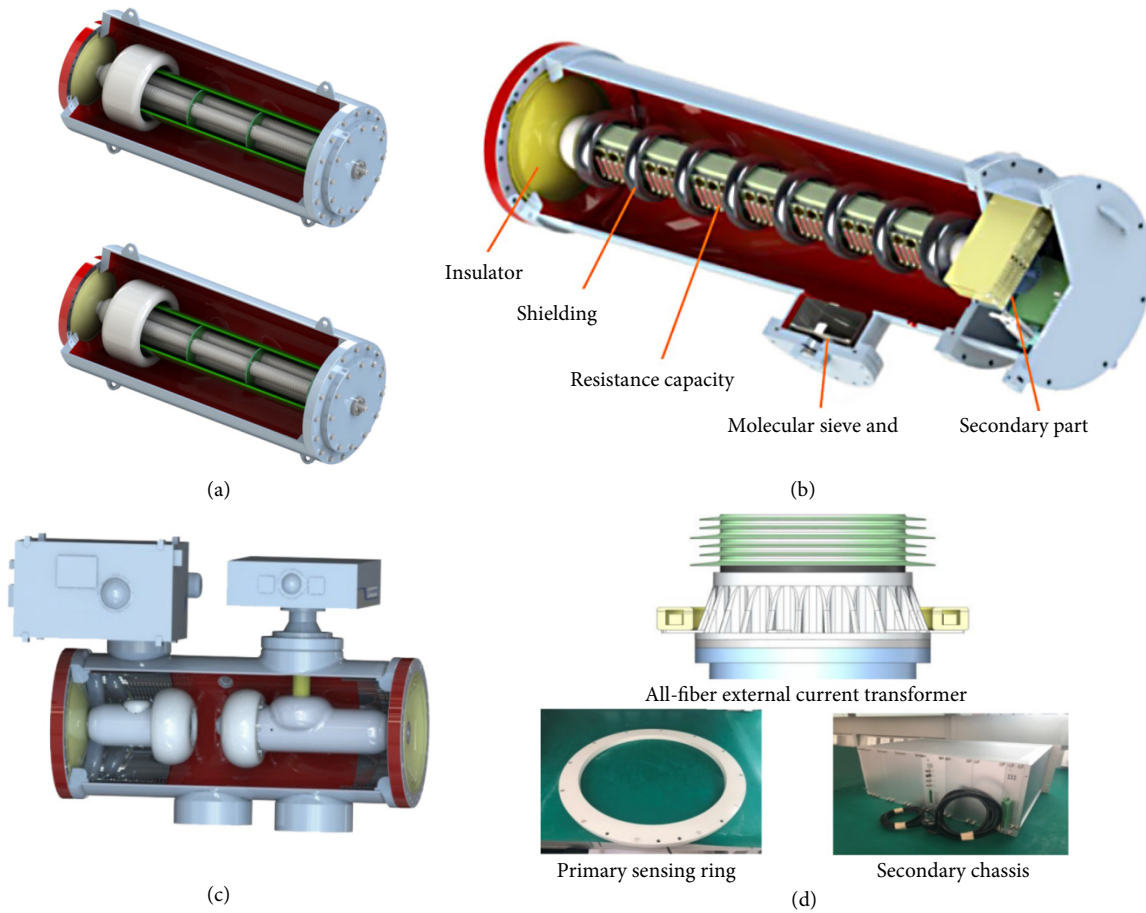
Fig. 37   (a) DC GIS surge arrester, (b) DC GIS voltage transducer, (c) a combined disconnector and earthing switch, (d) All-fiber external current transducer.
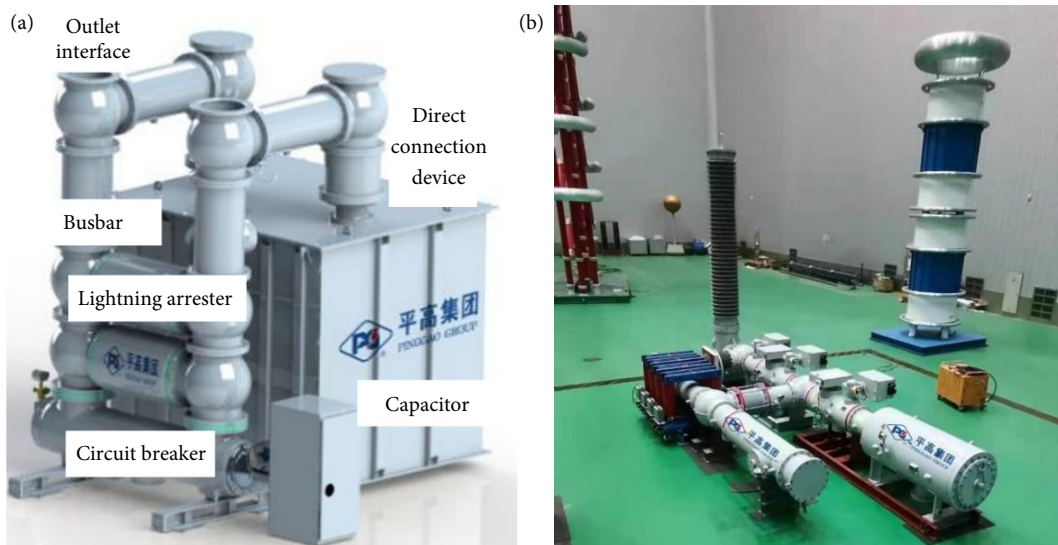

Fig. 38   (a) Metal-enclosed gas-insulated DC transfer switch. (b) Long-term test of ±210 kV DC GIS.

2.2.2   Progress in DC GIL

Tu et al.[20] designed and manufactured ±100 kV DC GIL and carried out hydraulic tests, gas tightness tests, lightning impact tests, operation impact tests, and other typical tests. All tests have successfully passed.

An environmentally friendly ±320 kV GIL, as shown in Figure 41(a), was developed by Tsinghua University, cooperating with Jiangsu Jinxin Electric Appliance Co., Ltd., which breaks

through four major technical bottlenecks, which are the evaluation of environmentally friendly insulating gas in ±320 kV GIL, the spacer to suppress surface charge, post-insulator design and its allowable electric field range, and metal particle suppression[①]. This ±320 kV GIL has passed multiple assessment tests, such as the polarity-reversal, short-term withstanding pressure PD, long-term pressure resistance, pressure resistance under the temperature

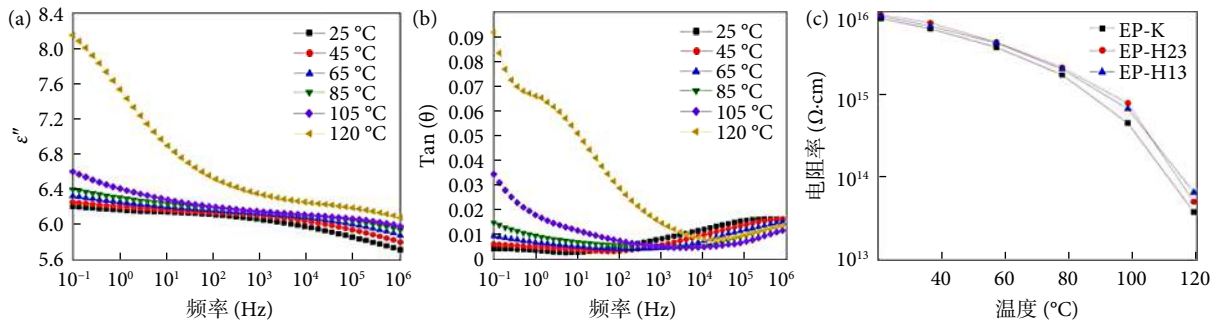[①]Private communication with Jinliang He and Chuanyang Li

Fig. 39 (a) Relative dielectric constant of samples at different temperatures. (b) Dielectric loss of samples at different temperatures. (c) Resistivity of samples at different temperatures.
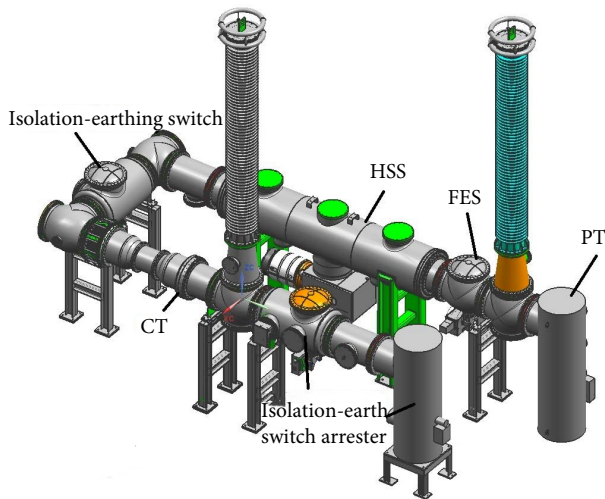

Fig. 40 Prototype Illustration of ±500 kV DC GIS from Xian Switchgear Electric.

gradient, etc. Figure 41(b) shows the surface potential distribution of the DC basin-type insulator after withstanding 7 hours applied voltage. The potential of the spacer is close to 2 kV after the saturation at the negative polar voltage. The potential is of only 600 V at the positive polarity, indicating a good effect of charge suppression.

2.3 Remaining issues

2.3.1 Industrial chain coordination and integration

In order to economize the clean energy development, especially the construction of the offshore wind power platform, the development of DC gas-insulated equipment gains great attentions. Offshore wind power started early and developed widespread in several countries. ABB and Siemens have developed a series of DC GIS products with different voltage levels and applied engineering products. In contrast, China has successively built ±400 kV Rudong, ±500 kV Qingzhou No. 5 and No. 7 offshore wind power projects, at a high weight (twice of foreign countries) and cost. It is more urgent to reduce the platform size and cost, but unfortunately it has not provided an opportunity to promote the research and development of novel DC GIS products in China.

Reviewing the development of China's West–East Power Transmission from the fully imported "Tianguang DC" to the semi-localized "Northwest Yunnan", and then to the fully localization of "Wudongde", the power equipment manufacturing factory in China has made great contributions to the localization of power equipment. But Chinese manufacturers are the unique link
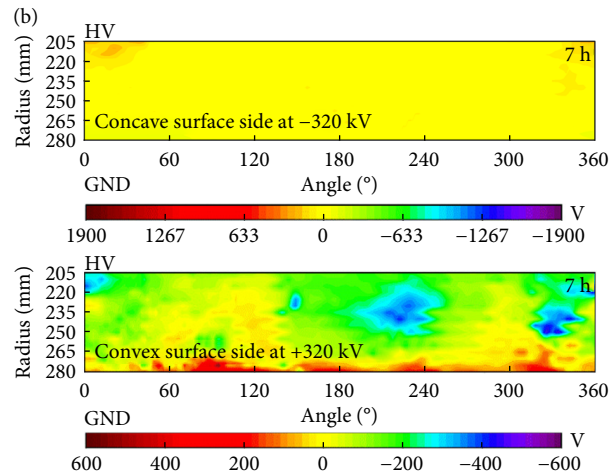

Fig. 41 (a) A photo of the environmentally friendly ±320 kV GIL prototype, and (b) surface potential distribution contour of the spacer after withstanding voltage of 320 kV with different polarity for 7 hours.

in the industry chain, with the product R&D power from the project promotion and profit accounting, resulting in the lagging in the new power equipment R&D. In front of the long-term strategic goal of national new power system construction, it is urgent to set up a long industrial chain, integrate resources through "industry–learning–research–user", build the research chain integrating technology, basic theory, complete machine R&D and application research, develop DC transmission equipment, and accelerate the construction of a new power system.

2.3.2 Other issues

With the rapid transformation of the consumption energy to green and low-carbon form, it becomes increasingly urgent to

build the UHVDC long-distance delivery project for clean energy in western China. The UHV multi terminal DC project in the Greater Bay area of "Guangdong–Hong Kong–Macao" for the transmission of clean energy from southeast Tibet is constrained by the complex factors such as high altitude, high seismic intensity, complex high drop terrain, compact installation of converter stations, and severe weather conditions, as well as the corridor of traditional overhead transmission lines. The research and development of ±800 kV DC GIS and ±800 kV AC GIL will be on the agenda. Due to the randomness of the gas discharge during the actual operation condition, the specificity of the solid insulation material surface properties, and the complexity of the operating conditions, the following technical problems still exist at the equipment level.

DC GIS/GIL performance assessment lacks standards

ABB stated that the design tests of DC GIS/GIL type should include the following: (1) Insulation performance assessment of materials, including resistivity test, breakdown experiment, space and surface charge test. (2) Electric field distribution characteristics in typical load cases. (3) Study on the long-term operation stability of DC GIS/GIL, considering the influence of electrical stress, temperature, and environmental factor. (4) Study on the sensitivity of electric field distribution subject to equipment size, material type and operating condition. According to IEC 62271 and the insulation system tests proposed by CIGRE, Siemens has carried out the insulation experiment, temperature rise test, mechanical life tests, high and low temperature tests, dynamic and thermal stability tests, insulation parts test sand insulation system tests on ±550 kV DC GIS. The insulation system experiments for ±550 kV DC GIS mainly includes AC withstand voltage test and local discharge measurement, withstand voltage test under lightning impulse, withstand voltage test under switching impulse, DC superimposed lightning impulse withstand voltage test and DC superimposed operation impulse withstand voltage test. In addition to the typical insulation experiment, there are other necessary test such as temperature rise, mechanical life cycling, dynamic and thermal stability experiment, etc. The GIS/GIL prototype is suggested to conduct one-year live test with the local discharge monitor to test its operation reliability referring to CIGRE test methods. However, there is a lack of experimental standard for DC gas-insulated equipment in China.

Multi-influence factor test of real size prototype

Under the conditions of practical application scenarios, the prototype experimental platform of DC gas-insulated equipment with high fit with the real insulator service scenarios is built, and the performance of the prototype under the comprehensive action of multiple factors including temperature, humidity, electric field, pressure, vibration, etc. is studied. China should try to test the flashover resistance performance of the control variable method on the prototype using different techniques and find out the advantages and disadvantages of each factor by comparing the test results.

Application of environmental gas in DC gas-insulated equipment

As the "carbon peaking and carbon neutrality" goal was set, the new power system was proposed and the large-scale clean energy are under development, power grid users are increasingly concerned about environmentally friendly equipment. It is necessary to develop DC equipment with environmental-friendly insulating gas. We should further study the application feasibility of envi-

ronment-friendly insulating gas such as C_4F_7N in DC GIL and DC GIS, study the high-throughput design theory and performance evaluation method and understand their characteristics of gap breakdown, surface flashover and gas-solid interface charge accumulation under DC voltage to effectively guide the product R&D and engineering application.

2.4 Worldwide (Europe, Japan, and America)

2.4.1 Progress in equipment

The potential of gas-insulated HVDC systems was recognized and studied in the 1960s following the first installation in 1983[155,156]. The first generation of HVDC GIS is shown in Figure 42. Nevertheless, the commercial application of HVDC GIS was limited to only few applications. The further use of gas-insulated systems was hampered by a tendency for the insulating materials to fail during polarity reversal tests. This was generally attributed to the presence of space charges trapped within the insulation[157]. The first commercial HVDC-GIS was installed in the year 2000 in Japan for the Kii channel link. The ±500 kV HVDC-GIS Anan Converter station and the Yura switching station of Shikoku Electric Power consists of disconnectors and one bus bar. Both GIS were installed because of the heavy salt contamination in coastal area. Because the charging on the insulating spacers would also bring about reduction of the insulation level, semi-conductive type insulating spacers were developed to mitigate surface and space charges. Since commissioning, the operating voltage is only ±250 kV[158]. A DC busbar with superimposed DC voltage of ±150 kV is in operation since 1983/1987 in Gotland (Sweden)[159]. In 1986 ABB and BPA have performed together a development of ±500 kV HVDC-GIS. From 1990 until 1995, long-term tests at BPA's test center were carried out. The project involved energizing a test pole containing the elements of an SF_6 insulated station for duration of approximately 2 years. The elements of the test pole consisted of GIS spacers, SF_6 air bushings, air insulated arrester, SF_6 insulated arrester, and SF_6 oil bushing. The primary concern was the dielectric performance of the components. This project was performed using a combination of 550 kV AC equipment and 800 kV AC equipment. All equipment was modified for DC application by installing special GIS insulators. The long-term tests were successfully completed in 1996[160].

With the growing demand of transporting higher power ratings over very long distances, the HVDC technology is technically superior over conventional HVAC technology. One worldwide driver of HVDC technology is the integration of renewable electric energy resources, resulting in a change of the existing electric power transmission system. Based on an increasing demand for space-saving and reliable HVDC solutions for both submarine and land applications, the 2nd generation of even more compact gas-insulated systems for HVDC applications are under development worldwide. The high level of quality of the GIS technology provides security of supply and high availability of electricity (Figure 43)[161].

Using of modern multi-physics simulation tools, the analysis of temperature and electrical field distribution is today possible with high accuracy, taking the following parameters into consideration: temperature and electrical field dependent characteristics of the insulating materials, accumulation of space and surface charges and the superposition of DC and impulse voltages. New DC insulators for HVDC gas insulated systems were designed by geometrical optimization and insertion of a current collector. With additional modifications at interface components, like cable termina-
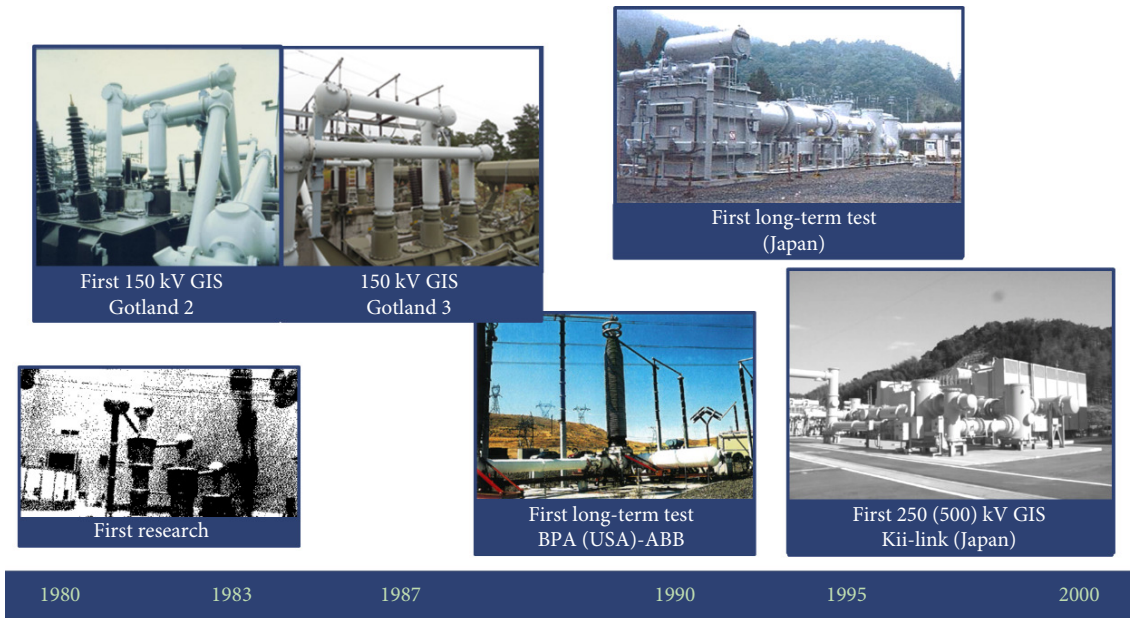
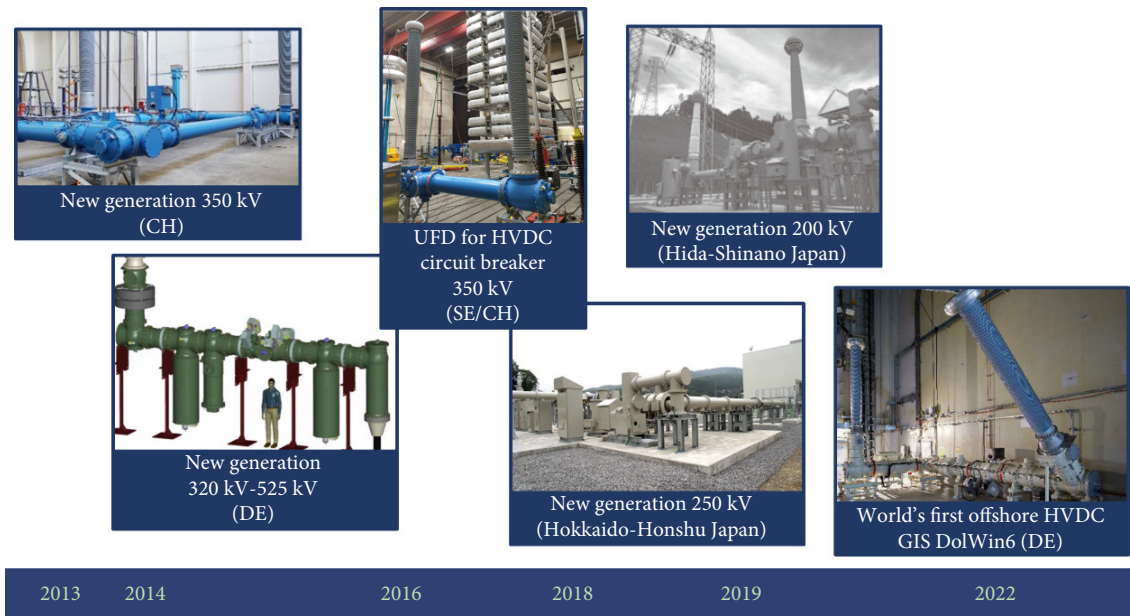Fig. 42   HVDC GIS development (1ˢᵗ generation).

Fig. 43   HVDC GIS development (2ⁿᵈ generation).

tion, and with the development of special current and voltage transformers, it is now possible to use gas-insulated HVDC systems for both onshore and offshore applications[162]. Gas-insulated components can also be used for other HVDC applications e.g., for HVDC circuit breaker. The hybrid HVDC circuit-breaker (HHB) was introduced by ABB in 2011. The HHB consists of three major units: Load commutation switch (LCS), ultra-fast disconnector (UFD) and main circuit-breaker (MB). Load current is conducted through the LCS and UFD path during normal operation and whenever the current interruption is triggered, the current will be commutated to the parallel main circuit-breaker path for interruption. In series to the LCS, a mechanical gas-insulated UFD is available to realize the high voltage insulation strength during the current interruption. The current rating of the UFD is similar to the LCS's to ensure reliable current conduction[163].

In Japan, two 2ⁿᵈ generation GIS were developed in the 2010s.

In 2019, a ±250 kV HVDC GIS was put into operation for the New Hokkaido-Honshu HVDC Link. The items relating to DC the specifications of the existing DC GIS, which are used for Kii Channel HVDC Link, were applied. The GIS with a rated voltage of ±250 kV and a rated current of 1200 A is in operation since 2019[164]. 2020 another HVDC was installed in Japan[165]. Hida converter station is located at an altitude of 1085 m where it is subject to snowfalls of 200 cm and ambient air temperatures of −30 ℃ to + 35 ℃. To allow for these environmental conditions, the system uses HVDC GIS (main circuit rated voltage: DC ±200 kV, rated current: DC 2250 A) that is equipped to deal with the external environment, with live parts being encased in a metal enclosure. It is noteworthy that a medium-voltage DC GIS was also used here for the first time (return circuit rated voltage: DC ±10 kV). Date for commencing operation was March 2021.

Within the German offshore grid connection system DolWin6,

the world's first offshore HVDC GIS was successfully installed and tested during commissioning in the dockyard in year 2021[166]. DolWin6 is a 900 MW offshore grid connection system utilizing HVDC technology for the transport of wind energy generated off-shore to the onshore grid. The offshore HVDC GIS is utilized for both DC voltage poles and connected to the HVDC export cables. Hence, the two HVDC GIS are installed in two different rooms within two different levels of the offshore platform. Following this first-time installation, further grid connection systems, BorWin5, Kontek, DolWin4, BorWin4 (Germany), Sunrise Wind (USA), EastAnglia, and Norfol Boreas (United Kingdom) will be utilizing HVDC GIS reducing the offshore converter platform in size and weight significantly.

The development of HVDC GIS is based on the technology used for HVAC GIS with, in principle, the same components and a newly designed HVDC insulator to meet the requirements of the electric field distribution under DC voltage stress[167]. The modular structure of HVAC GIS has been proven in many applications worldwide with high reliability and has been optimized over the last 50 years since the first HVAC GIS has been installed in Germany in 1968. Just as in AC power systems, all HVDC GIS technology spans a number of switchgear components as shown in Figure 44, for example bus-ducts and high voltage DC conductors (A), disconnect- and earthing switches (B), bushings (C), cable terminations (D), current (E), voltage (F) transformer, and surge arresters (G). Encapsulated surge arresters ensure the protection from overvoltage. Their active parts consist of metal oxide varistors with a strongly nonlinear current–voltage characteristic. Gas-insulated RC voltage dividers map high-voltage linearly over a frequency range from DC up to 30 kHz. They are designed also for an optimal transient behavior[168]. Current detection relies on the zero-flux measurement principle for rated currents up to 5000 A[169]. The interface modules enable the transition from the gas-insulated switchgear assemblies to other equipment. At the core of the switchgear assemblies is the disconnector. Together with the earthing switches on either side of the isolating gap, the disconnector ensures the safe insulation and earthing of de-energized circuits. These components can be applied in various HVDC applications such as DC pole equipment in HVDC converter stations including the DC switchyard, gas-insulated transmission lines, and cable to overhead line transition stations.

2.4.2 Standardization

The testing requirements for gas insulated HVDC systems are currently not standardized. The physical basis for HVDC applications was described by CIGRE already in 2010[170]. Based on these findings, together with new experiences of the manufacturers, recommendations have been elaborated in CIGRE JWG D1/B3.57[171].

According to these, the electrical and mechanical requirements of IEC 62271 series, that are independent of the type of operating

Fig. 44　HVDC GIS components (left) and example for a gas-insulated cable to overhead line transition station (right).

voltage, should be fulfilled also[172]. Beside DC withstand voltage tests, composite voltage tests with lightning impulse and switching impulse voltage, superimposed to DC voltage, have to be conducted after a defined period of DC pre-stress. The isolating distance of the disconnectors has to be stressed with combined voltage tests, consisting of DC voltage at one terminal and lightning or switching impulse voltage at the other.

Additional electric and thermo-electric tests must be performed to consider the special aspect of DC voltage in terms of electric field distribution of insulators, influenced by the accumulation of electrical charge carriers and the operation-related inhomogeneous temperature distribution. Electro-thermal tests are of high importance for HVDC GIS, due to the temperature-dependent field transition. The transition of a gas-solid insulation system from a capacitive field distribution at the moment of energization with DC voltage to a resistive field distribution, results in interface charging, particularly of the solid-gas surface and space charge accumulation in the solid insulation until the resistive steady state is reached. The design of solid insulating components as well the right testing procedure to verify the electrical insulation behavior are therefore of high importance.

The time duration of the long duration continuous DC voltage test depends on the transition time from capacitive to resistive field conditions and has to be determined before starting the tests. If a degree of charging of 90% has been passed at each location of the insulator, the transition time is reached. The transition itself depends on the local temperature distribution and on the lowest temperature. The transition to a DC field distribution could lead to a long test duration of hours to months. The accurate definition of the transition time and the verification of the transition behavior is essential to derive a reliable testing procedure of HVDC gas-insulated systems and must be measured before starting the test.

The newly developed insulation system test has similarity in the test procedure to the pre-qualification test for polymeric insulated HVDC cables. However, the prequalification test for HVDC extruded cable systems is intended to indicate the electrical long-term performance test on the voltage-time characteristic of the insulating material and to cover thermo-mechanical aspects. The transition itself depends on the local temperature distribution and on the lowest temperature. The temperature difference across the insulators is of high importance and must be defined and verified for testing. For superimposed voltage tests after long DC pre-stress to reach the defined DC steady state and worst-case temperature conditions with maximum temperature gradient across the insulators high load (HL) conditions must be used. High load consists of a continuous heating period at rated current up to the thermal steady state. As composite voltage test of DC voltage and impulse voltage, the rated lightning and switching impulse voltages shall be superimposed to the rated DC voltage. As insulation system test, a sufficient number of insulators assembled in realistic arrangements must be tested. A dielectric routine test or preconditioning could be considered before starting the insulation system test. The normal sequence of tests is described in Table 6. An example of a test set-up is given in Figures 44 and 45[162].

Based on service experience, gas-insulated HVAC systems feature a high degree of reliability and an excellent long-term performance. In comparison, HVDC GIS is a new technology with limited operational experience. The user who intends to apply gas insulated HVDC systems does expect the same reliability and long-term performance as in HVAC GIS. From a high-voltage engineering perspective the main differences between HVAC and HVDC GIS are the long periods required to reach steady state DC electric fields and charge accumulation phenomena. Thus, HVDC GIS
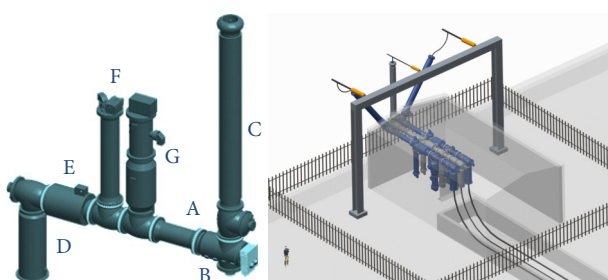
Table 6 The normal sequence of tests

| Test	Conditions	Load
Thermal pre-test	Heating @ defined temperature ±5 K	HL
Dielectric pre-test	PD test with alternating or direct voltage	ZL
Long-duration continuous direct voltage test	Rated direct voltage Urd (one polarity, positive or negative)	HL
Superimposed lightning impulse voltage test (bipolar and unipolar)	Rated LIWV values, superimposed to the rated direct voltage Urd	HL
Superimposed switching impulse voltage test (bipolar and unipolar)	Rated SIWV values, superimposed to the rated direct voltage Urd	HL
Long-duration continuous direct voltage test	Rated direct voltage Urd (other polarity)	HL
Superimposed lightning impulse voltage test (bipolar and unipolar)	Rated LIWV values, superimposed to the rated direct voltage Urd	HL
Superimposed switching impulse voltage test (bipolar and unipolar)	Rated SIWV values, superimposed to the rated direct voltage Urd	HL
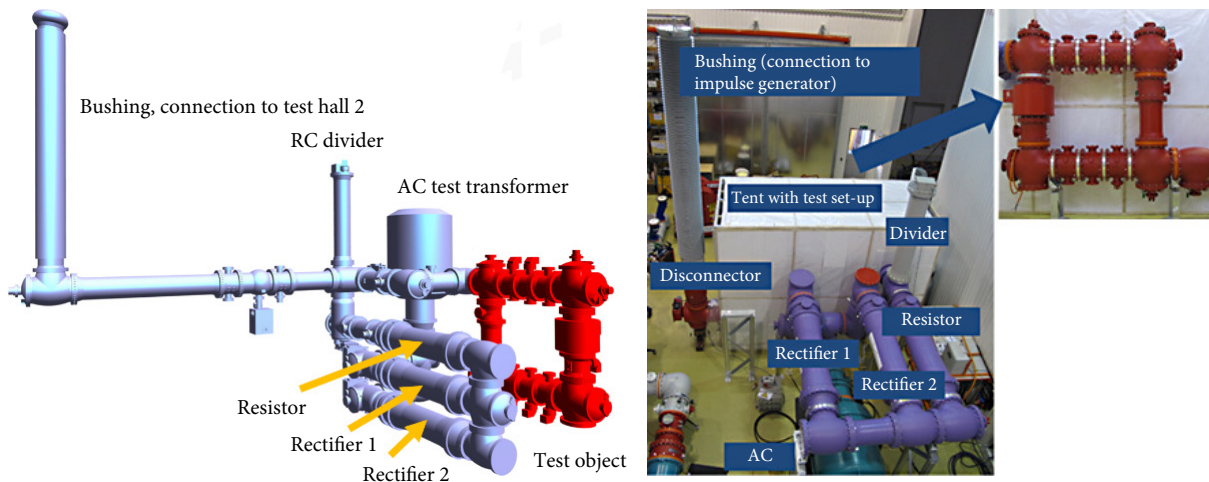
Fig. 45 Examples of test arrangements for insulation system tests, completely gas-insulated (left) and air-insulated (right).

requires adapted design and testing. CIGRE JWG D1/B3.57 has proposed a "prototype installation test" as a demonstration test[171]. The main intention of the prototype installation test for gas-insulated systems is to confirm the reliability of the system under real service conditions. Real service conditions refer to the components included in the test object, the installation and commissioning procedures, the dielectric, thermal and mechanical stresses applied in the test itself, testing with representative stresses for real life operation and inclusion of monitoring and diagnostics during the test[173].

Thus, the prototype installation test is not an additional type test, but rather a one-time, non-mandatory test performed after successfully completing the type tests to verify the effectiveness of the HVDC GIS specific type and routine test procedures.

The worldwide first prototype installation test for a HVDC GIS is shown in Figures 46 and 47[174]. The HVDC GIS test pole consists of a bus-duct ring that is connected to high-voltage via SF_6 to air bushings. To achieve a thermal regime typical for high load condition, an AC heating current can be induced in the ring using conventional current transformers. The dielectrically decisive quantity—temperature difference inner conductor to enclosure (at the insulator)—will be generated with at least the same magnitude compared to a DC current load[175].

At the same time, the test philosophy was also applied to a GIL for 550 kV. The test was completed after half a year. The test setup can be seen in Figure 48[176].

Currently, development of a dedicated IEC standard is ongoing within TC17 SC17C WG42 of IEC (CD status). Moreover, several cable connection assemblies have finished their qualification. Currently, recommendations for dielectric testing of HVDC cable
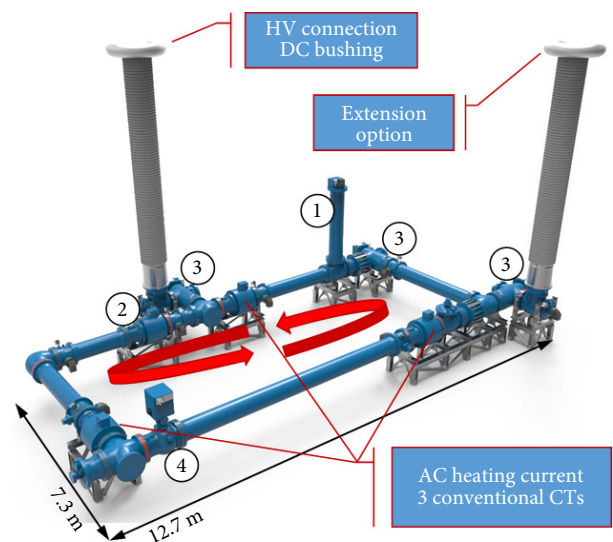
Fig. 46 Example of an HVDC GIS prototype installation: ①VT: RC-divider; ② CT: Zero-Flux Sensor; ③ Combined disconnector and earthing switches;④Fast-acting earthing switch.

connection assemblies are under development within CIGRE JWG B1/B3/D1.79.

3 Conclusions

China has made significant progress in DC gas-insulated equipment in the past ten years, from basic research to industrialization. At the basic research level, starting with focusing on surface charge

Fig. 47   Test set-up of a HVDC GIS prototype installation test.

Fig. 48   Test set-up of a HVDC GIL prototype installation test.

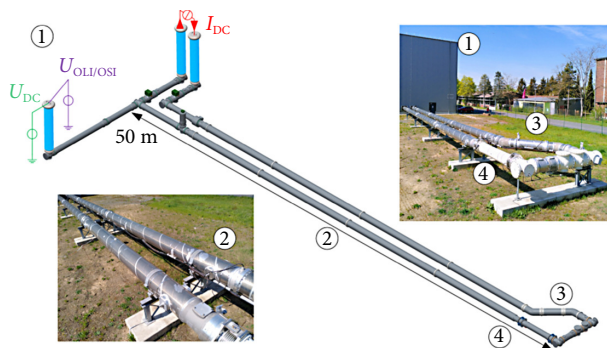measurement technology, various charge suppression methods based on material modification have been further extended, and some technologies have been tested and verified on real-size insulators. In recent years, many studies have been carried out in particle dynamics. Its progress has guided the research direction of the particle suppression approach in simulation and experiments. Initial research results have been published on conductor roughness in China since 2020. From an industrial point of view, ±500 kV GIS and ±320 kV GIL have been developed, and their type tests have been completed. However, compared with the progress in the world's leading HV companies, there is still a lack of research on long-term on-load assessment. In addition, some key technology needs to be further carried out, such as the online monitoring technology of DC systems and the development of DC GIS-cable terminals, etc.

Acknowledgement

Article history

Additional information

Declaration of competing interest

The authors have no competing interests to declare that are relevant to the content of this article.

References

[1] Li, C., Yang, Y., Xu, G., Zhou, Y., Jia, M., Zhong, S., Gao, Y., Park, C., Liu, Q., Wang, Y., Akram, S. (2022). Insulating materials for realising carbon neutrality: Opportunities, remaining issues and challenges. *High Voltage*, 7: 610–632.

[2] Zhang, L., Lin, C., Li, C., Suraci, S., Chen, G., Riechert, U., Shahsavarian, T., Hikita, M., Tu, Y., Zhang, Z., Fabiani, D., He, J. (2020). Gas–solid interface charge characterisation techniques for HVDC GIS/GIL insulators. *High Voltage*, 5: 95–109.

[3] Li, C., Zhu, Y., Hu, J., Li, Q., Zhang, B., He, J. (2020). Charge cluster triggers unpredictable insulation surface flashover in pressurized SF_6. *Journal of Physics D: Applied Physics*, 54: 015308.

[4] Li, C., Lin, C., Chen, G., Tu, Y. Zhou, Y., Li, Q., Zhang, B., He, J. (2019). Field-dependent charging phenomenon of HVDC spacers based on dominant charge behaviors. *Applied Physics Letters*, 114: 202904.

[5] Chen, X., Chen, S., Zhang, B., Li, G., Chang, Z., Zhang, G. (2020). Promotion of epoxy resin surface electrical insulation performance and its stability by atmospheric fluorocarbon dielectric barrier discharge. *IEEE Transactions on Dielectrics and Electrical Insulation*, 27: 1973–1981.

[6] Chen, J., Xue, J., Dong, J., Li, Y., Deng, J., Zhang, G. (2020). Effects of surface conductivity on surface charging behavior of DC-GIL spacers. *IEEE Transactions on Dielectrics and Electrical Insulation*, 27: 1038–1045.

[7] Qiang, D., He, M., Chen, G., Andritsch, T. (2015). Influence of nano-SiO_2 and BN on space charge and AC/DC performance of epoxy nanocomposites. In: Proceedings of the 2015 IEEE Electrical Insulation Conference (EIC), Seattle, WA, USA.

[8] Cai, Z., Li, M., Wang, W., Min, D., Li, S., Zhang, L., Yang, W., Chen, Y., Wang, K. (2020). Influence of surface trap parameters on AC/DC flashover of epoxy resin. In: Proceedings of the 2020 IEEE International Conference on High Voltage Engineering and Application (ICHVE), Beijing, China.

[9] Du, B., Tian, M., Su, J., Han, T. (2020). Temperature gradient dependence on electrical tree in epoxy resin with harmonic superimposed DC voltage. *IEEE Transactions on Dielectrics and Electrical Insulation*, 27: 270–278.

[10] Zhang, B., Zhong, J., Han, G., Yao, Y., Wang, Z., Zhong, L., Liu, Y., Zhang, H. (2020). Modification of HVDC GIS/GIL basin insulators based on electrical and mechanical collaborative design. In: Proceedings of the 2020 IEEE International Conference on High Voltage Engineering and Application (ICHVE), Beijing, China.

[11] Jia, Y., Gao, L., Ji, S., Li, X., Li, Z., Liu, Y. (2020). Electrical performance optimization for tri-post insulator on 1100 kV gas-insulated metal-enclosed transmission line. *Journal of Xi'an Jiaotong University*, 54(7): 168–179. (in Chinese)

[12] Hu, Q., Li, Q., Liu, Z., Liu, H. (2021). Impact analysis of charge accumulation on electric field distribution of DC GIL tri-post insulator under temperature gradients. *Advanced Technology of Electrical Engineering and Energy*, 40(7): 20–27. (in Chinese)

[13] Li, C., Hu, J., Lin, C., He, J. (2017). The potentially neglected culprit of DC surface flashover-electron migration under temperature gradients. *Scientific Reports*, 7: 3271.

[14] Yan, W., Zhang, Z., Deng, B., Zhang, Z. (2019). Influence of temperature and positive voltage on surface charge accumulation for the disc insulator of GIL under DC voltage. *High Voltage Engineering*, 45: 3889–3897.

[15] Jia, Z., Gan, D., Li, J. (2011). Design of insulation dimension for ± 500 kV DC gas insulated transmission line. *Power System Technology*, 35: 192–196.

[16] Liang, Z., Lin, C., Liang, F., Zhuang, W., Xu, Y., Tang, L., Zeng,

Y., Hu, J., Zhang, B., Li, C., He, J. (2022). Designing HVDC GIS/GIL spacer to suppress charge accumulation. *High Voltage*, 7: 645–651.

[17] Ma, G., Zhou, H., Li, C., Jiang, J. and Chen, X. (2015). Designing epoxy insulators in SF_6-filled DC-GIL with simulations of ionic conduction and surface charging. *IEEE Transactions on Dielectrics and Electrical Insulation*, 22: 3312–3320.

[18] Li, C., Lin, C., Yang, Y., Zhang, B., Liu, W., Li, Q., Hu, J., He, S., Liu, X., He, J. (2018). Novel HVDC spacers by adaptively controlling surface charges – part ii: Experiment. *IEEE Transactions on Dielectrics and Electrical Insulation*, 25: 1248–1258.

[19] Hu, Q., Li, Q., Liu, Z., Liu, H., Manu, H. (2022). Interfacial electric field optimization of DC tri-post insulator based on gradient surface conductance regulation. *Transactions of China Electrotechnical Society*, 37: 1856–1865.

[20] Tu, Y., Chen, G., Li, C., Wang, C., Ma, G., Zhou, H., Ai, X., Cheng, Y. (2020). ±100-kV HVDC SF_6/N_2 gas-insulated transmission line. *IEEE Transactions on Power Delivery*, 35: 735–744.

[21] Li, C., Zhu, Y., Zhu, Y., Zhi, Q., Song, S., Connelly, L., Li, Z., Chen, G., Lei, Z., Yang, Y., Mazzanti, G. (2021). Dust figures as a way for mapping surface charge distribution —A review. *IEEE Transactions on Dielectrics and Electrical Insulation*, 28: 853–863.

[22] Zhang, B., Xue, J., Chen, X., Chen, S., Mu, H., Xu, Y., Zhang, G. (2021). Review of surface transient charge measurement on solid insulating materials via the Pockels technique. *High Voltage*, 6: 608–624.

[23] Chen, J., Li, J., Dong, J., Sun, P., Deng, J., Li, Y., Zhang, G. J. (2022). Surface discharge propagation in C_4F_7N/CO_2 mixture under positive impulse voltages. *Applied Physics Letters*, 120: 061601.

[24] Chen, J., Sun, P., Li, J., Li, W., Li, Y., Deng, J., Ji, S., Zhang, G. J. (2022). Surface discharge pattern of C_4F_7N/CO_2 mixture under negative impulse voltages. *Applied Physics Letters*, 121: 171602.

[25] Zhang, Y., Wang, F., Li, Z., Zhou, X., He, R. (2014). Development of surface charge detection device for DC composite insulator. *High Voltage Engineering*, 40: 1514–1519.

[26] Gao, C., Qi, B., Li, C., Huang, M., Lv, Y. (2020). The surface charge of Al_2O_3 ceramic insulator under nanosecond pulse voltage in high vacuum: characteristics and its impact on surface electric field. *Journal of Physics D: Applied Physics*, 53: 055501.

[27] Wang, F., Liang, F., Chen, S., Tan, Y., Zhong, L., Sun, Q. (2021). Surface charge inversion method on cylindrical insulators based on surface potentials measured online. *IEEE Transactions on Dielectrics and Electrical Insulation*, 28: 192–197.

[28] Fan, L., Yin, Y., Wang, Y. (2022). Surface potential dynamics of polyimide under DC corona based on noninvasive measurement. *IEEE Transactions on Dielectrics and Electrical Insulation*, 29: 1307–1315.

[29] Fan, L., Yin, Y., Wang, Y. (2022). Surface potential dynamics and flashover resistance evaluation of epoxy resin under DC flashover. *IEEE Transactions on Dielectrics and Electrical Insulation*, 29: 575–582.

[30] Davies, D. (1967). The examination of the electrical properties of insulators by surface charge measurement. *Journal of Scientific Instruments*, 44: 521–524.

[31] Takuma, T., Yashima, M., Kawamoto, T. (1998). Principle of surface charge measurement for thick insulating specimens. *IEEE Transactions on Dielectrics and Electrical Insulation*, 5: 497–504.

[32] Rerup, T., Crichton, G., McAllister, I. (1997). Using the λ function to evaluate probe measurements of charged dielectric surfaces. *IEEE Transactions on Dielectrics and Electrical Insulation*, 3: 770–777.

[33] Faircloth, D., Allen, N. (2003). High resolution measurements of surface charge densities on insulator surfaces. *IEEE Transactions on Dielectrics and Electrical Insulation*, 10: 285–290.

[34] Ootera, H., Nakanishi, K. (1988). Analytical method for evaluating surface charge distribution on a dielectric from capacitive probe measurement-application to a cone-type spacer in ±500 kV DC-GIS. *IEEE Transactions on Power Delivery*, 3: 165–172.

[35] Zhang, B., Gao, W., Qi, Z. Zhang, G. (2017). Inversion algorithm to calculate charge density on solid dielectric surface based on surface potential measurement. *IEEE Transactions on Instrumentation and Measurement*, 66: 3316–3326.

[36] Kumada, A., Okabe, S. (2004). Charge distribution measurement on a truncated cone spacer under DC voltage. *IEEE Transactions on Dielectrics and Electrical Insulation*, 11: 929–938.

[37] Luo, Y. (2022). Surface charge accumulation characteristics and shape optimization of insulator under DC voltage. PhD Thesis, Wuhan University, China.

[38] Lin, C., Li, C., He, J. Hu, J., Zhang, B. (2017). Surface charge inversion algorithm based on bilateral surface potential measurements of cone-type spacer. *IEEE Transactions on Dielectrics and Electrical Insulation*, 24: 1905–1912.

[39] Kumada, A., Okabe, S., Hidaka, K. (2004). Resolution and signal processing technique of surface charge density measurement with electrostatic probe. *IEEE Transactions on Dielectrics and Electrical Insulation*, 11: 122–129.

[40] Deng, J., Wang, H., Xue, J. (2018). Improved reverse algorithm of surface charge density distribution and electric field distribution based on electrostatic probe. *Proceedings of the CSEE*, 38(4): 1239–1247. (in Chinese)

[41] Pan, Z., Tang, J., Hu, B. Pan, C., Luo, Y., Mao, S. (2021). Inversion algorithm for surface charge distribution on insulator in shift-invariant system based on constrained least square filter. *IEEE Transactions on Instrumentation and Measurement*, 70: 1–12.

[42] Winter, A., Kindersberger, J. (2014). Transient field distribution in gas–solid insulation systems under DC voltages. *IEEE Transactions on Dielectrics and Electrical Insulation*, 21: 116–128.

[43] Winter, A., Kindersberger, J. (2012). Stationary resistive field distribution along epoxy resin insulators in air under DC voltage. *IEEE Transactions on Dielectrics and Electrical Insulation*, 19: 1732–1739.

[44] Yan, W., Li, C., Lei, Z., Han, T., Zhang, Z., Fabiani, D. (2019). Surface charging on HVDC spacers considering time-varying effect of temperature and electric fields. *IEEE Transactions on Dielectrics and Electrical Insulation*, 26: 1316–1324.

[45] Li, C., Deng, B., Zhang, Z., Yan, W., Li, Q., Zhang, Z., Lin, C., Zhou, Y., Han, T., Lei, Z., et al. (2019). Full life property of surface charge accumulation on HVDC spacers considering transient and steady states. *IEEE Transactions on Dielectrics and Electrical Insulation*, 26: 1686–1692.

[46] Ma, G. M., Zhou, H. Y., Lu, S. J., Wang, Y., Liu, S. P., Li, C. R., Tu, Y. P. (2018). Effect of material volume conductivity on surface charges accumulation on spacers under dc electro-thermal coupling stress. *IEEE Transactions on Dielectrics and Electrical Insulation*, 25: 1211–1220.

[47] Zhang, Z., Deng, B., Li, C., Li, Q., Zhang, Z., Yan, W. (2019). Multiphysics coupled modelling in HVDC GILs: Critical re-examination of ion mobility selection. *IEEE Transactions on Dielectrics and Electrical Insulation*, 26: 835–842.

[48] Xue, J. et al. (2022). A temperature dependent adaptive conductivity coating for surface charge release and electric field control under electro-thermal coupling field. *High Voltage*. https://doi.org/10.1049/hve2.12309

[49] Niu, H., Chen, Z., Zhang, H., Luo, X., Zhuang, X., Li, X., Yang, B. (2020). Multi-physical coupling field study of 500 kV GIL: Simulation, characteristics, and analysis. *IEEE Access*, 8: 131439–131448.

[50] Zhou, H. Y., Ma, G. M., Li, C. R., Shi, C., Qin, S. C. (2017). Impact of temperature on surface charges accumulation on insulators in SF_6-filled DC-GIL. *IEEE Transactions on Dielectrics and Electrical Insulation*, 24: 601–610.

[51] Du, B. X., Liang, H. C., Ran, Z. Y. (2018). Electrical field distribution along $SG6/N_2$ filled DC-GIS/GIL epoxy spacer. *IEEE Transactions on Dielectrics and Electrical Insulation*, 25: 1202–1210.

[52] Du, B. X., Dong, J. N., Li, J., Liang, H. C., Kong, X. X. (2021). Gas convection affecting surface charge and electric field distribution

around tri-post insulators in ±800 kV GIL. *IEEE Transactions on Dielectrics and Electrical Insulation*, 28: 1372–1379.

[53] Li, X., Wan, M., Zhang, G., Lin, X. (2022). Surface charge characteristics of DC-GIL insulator under multiphysics coupled field: Effects of ambient temperature, load current, and gas pressure. *IEEE Transactions on Dielectrics and Electrical Insulation*, 29: 1530–1539.

[54] Li, X., Zhang, G., Jia, J., Cao, C., Lin, X. (2022). Improved method in calculating the surface charge distribution of DC-GIL insulators with 3D geometry models. *IET Science, Measurement & Technology*, 16: 400–411.

[55] Wang, Q, Zhang, G., Wang, X. (2012). Characteristics and mechanisms of surface charge accumulation on a cone-type insulator under DC voltage. *IEEE Transactions on Dielectrics and Electrical Insulation*, 19: 150–155.

[56] Pan, C., Tîang, J., Wang, D., Zhuo, R., Yang, D., Ye, G., Fu, M. (2017). Influence of temperature on the characteristics of surface charge accumulation on PTFE model insulators. *IEEE Transactions on Dielectrics and Electrical Insulation*, 24: 1210–1219.

[57] Qi, B., Gao, C., Liu, S., Zhao, L., Li, C. (2017). Surface charge distribution on GIS insulator under DC/AC voltage. *IEEE Transactions on Dielectrics and Electrical Insulation*, 24: 3173–3181.

[58] Wang, T. Y., Zhang, B. Y., Li, D. Y., Hou, Y. C., Zhang, G. X. (2020). Metal nanoparticle-doped epoxy resin to suppress surface charge accumulation on insulators under DC voltage. *Nanotechnology*, 31: 324001.

[59] Xue, J., Chen, J., Dong, J., Sun, G., Deng, J., Zhang, G. J. (2020). A novel sight for understanding surface charging phenomena on downsized HVDC GIL spacers with non-uniform conductivity. *International Journal of Electrical Power & Energy Systems*, 120: 105979.

[60] Zhang, B., Qi, Z, Zhang, G. (2017). Charge accumulation patterns on spacer surface in HVDC gas-insulated system: Dominant uniform charging and random charge speckles. *IEEE Transactions on Dielectrics and Electrical Insulation*, 24: 1229–1238.

[61] Xue, J., Wang, H., Liu, Y., Li, K., Liu, X., Fan, X., Deng, J., Zhang, G., Guo, B. (2018). Surface charge distribution patterns of a truncated cone-type spacer for high-voltage direct current gas-insulated metal-enclosed transmission line/gas-insulated metal-enclosed switchgear. *IET Science, Measurement & Technology*, 12: 436–442.

[62] Zhou, H. Y., Ma, G. M., Wang, Y., Li, C. R., Tu, Y. P., Ye, S. P., Zhang, B., Guo, X. F., Yan, X. L. (2018). Surface charge accumulation on 500kV cone-type GIS spacer under residual DC voltage. *IEEE Transactions on Dielectrics and Electrical Insulation*, 25: 1230–1237.

[63] Xue, J., Chen, J., Dong, J., Deng, J., Zhang, G. J. (2020). Enhancing flashover performance of alumina/epoxy spacers by adaptive surface charge regulation using graded conductivity coating. *Nanotechnology*, 31: 364002.

[64] Luo, Y., Tang, J., Pan, C., Pan, Z., Meng, G. (2020). Transition of the dominant charge accumulation mechanism at a Gas–solid interface under DC voltage. *IET Generation Transmission & Distribution*, 14: 3078–3088.

[65] Zhang, B., Qi, Z., Gao, W., Zhang, G. (2018). Accumulation characteristics of surface charge on a cone-type model insulator under DC voltage. In: Proceedings of the 2018 IEEE International Conference on High Voltage Engineering and Application (ICHVE), Athens, Greece.

[66] Li, C., Fu, J., Zi, Y., Cao, Y. (2022). Insulator surface charge behaviors: From hazards to functionality. *IEEE Electrical Insulation Magazine*, 38: 6–14.

[67] Zhang, Z., Wang, Z., Teyssedre, G., Shahsavarian, T., Arab Baferani, M., Chen, G., Lin, C., Zhang, B., Riechert, U., Lei, Z., et al. (2021). Gas–solid interface charge tailoring techniques: What we grasped and where to go. *Nanotechnology*, 32: 122001.

[68] Du, B., Du, Q., Li, J., Liang, H. (2018). Carrier mobility and trap distribution dependent flashover characteristics of epoxy resin. *IET Generation, Transmission & Distribution*, 12: 466–471.

[69] Liu, Y., An, Z., Yin, Q., Zheng, F., Zhang, Y., Lei, Q. (2013). Rapid potential decay on surface fluorinated epoxy resin samples. *Journal of Applied Physics*, 113: 164105.

[70] An, Z., Yin, Q., Liu, Y., Zheng, F., Lei, Q., Zhang, Y. (2015). Modulation of surface electrical properties of epoxy resin insulator by changing fluorination temperature and time. *IEEE Transactions on Dielectrics and Electrical Insulation*, 22: 526–534.

[71] Shao, T., Kong, F., Lin, H., Ma, Y., Xie, Q., Zhang, C. (2018). Correlation between surface charge and DC surface flashover of plasma treated epoxy resin. *IEEE Transactions on Dielectrics and Electrical Insulation*, 25: 1267–1274.

[72] Gao, Y., Du, B. X., Cui, J. D., Wu, K. (2011). Effect of gamma-ray irradiation on lateral charge motion on surface of laminated polymer insulating materials. In: Proceedings of the 2011 Annual Report Conference on Electrical Insulation and Dielectric Phenomena, Cancun, Mexico.

[73] Wang, F., Liang, F., Zhong, L., Chen, S., Li, C., Xie, Y. (2021). Short-time X-ray irradiation as a non-contact charge dissipation solution for insulators in HVDC GIS/GIL. *IEEE Transactions on Dielectrics and Electrical Insulation*, 28: 704–709.

[74] Huang, Y., Min, D., Xie, D., Li, S., Wang, X., Lin, S. (2017). Surface flashover performance of epoxy resin microcomposites infulenced by ozone treatment. In: Proceedings of the 2017 International Symposium on Electrical Insulating Materials (ISEIM), Toyohashi, Japan.

[75] Tu, Y., Zhou, F., Cheng, Y., Jiang, H., Wang, C., Bai, F., Lin, J. (2018). The control mechanism of micron and nano SiO_2/epoxy composite coating on surface charge in epoxy resin. *IEEE Transactions on Dielectrics and Electrical Insulation*, 25: 1275–1284.

[76] Du, B. X., Li, Z. L. (2015). Hydrophobicity, surface charge and DC flashover characteristics of direct-fluorinated RTV silicone rubber. *IEEE Transactions on Dielectrics and Electrical Insulation*, 22: 934–940.

[77] Du, B., Huang, P., Xing, Y. (2017). Surface charge and flashover characteristics of fluorinated PP under pulse voltage. *IET Science, Measurement & Technology*, 11: 18–24.

[78] Du, B. X., Li, Z. L. (2014). Surface charge and dc flashover characteristics of direct-fluorinated SiR/SiO_2 nanocomposites. *IEEE Transactions on Dielectrics and Electrical Insulation*, 21: 2602–2610.

[79] Que, L., An, Z., Ma, Y., Xie, D., Zheng, F., Zhang, Y. (2017). Improved DC flashover performance of epoxy insulators in SF_6 gas by direct fluorination. *IEEE Transactions on Dielectrics and Electrical Insulation*, 24: 1153–1161.

[80] Zhang, B., Zhang, G., Wang, Q., Li, C., He, J., An, Z. (2015). Suppression of surface charge accumulation on Al_2O_3-filled epoxy resin insulator under dc voltage by direct fluorination. *AIP Advances*, 5: 127207.

[81] Li, C., He, J., Hu, J. (2016). Surface morphology and electrical characteristics of direct fluorinated epoxy-resin/alumina composite. *IEEE Transactions on Dielectrics and Electrical Insulation*, 23: 3071–3077.

[82] Shao, T., Yang, W., Zhang, C., Niu, Z., Yan, P., Schamiloglu, E. (2014). Enhanced surface flashover strength in vacuum of polymethylmethacrylate by surface modification using atmospheric-pressure dielectric barrier discharge. *Applied Physics Letters*, 105: 071607.

[83] Zhang, C., Lin, H., Zhang, S., Xie, Q., Ren, C., Shao, T. (2017). Plasma surface treatment to improve surface charge accumulation and dissipation of epoxy resin exposed to DC and nanosecond-pulse voltages. *Journal of Physics D: Applied Physics*, 50: 405203.

[84] Shao, T., Liu, F., Hai, B., Ma, Y., Wang, R., Ren, C. (2017). Surface modification of epoxy using an atmospheric pressure dielectric barrier discharge to accelerate surface charge dissipation. *IEEE Transactions on Dielectrics and Electrical Insulation*, 24: 1557–1565.

[85] Yue, W., Min, D., Nie, Y., Li, S. (2018). Plasma treatment enhances surface flashover performance of EP/Al_2O_3 micro-composite in vacuum. In: Proceedings of the 2018 12th International

Conference on the Properties and Applications of Dielectric Materials, Xi'an, China.

[86] Tu, Y., Zhou, F., Jiang, H., Bai, F., Wang, C., Lin, J., Cheng, Y. (2018). Effect of nano-TiO_2/EP composite coating on dynamic characteristics of surface charge in epoxy resin. *IEEE Transactions on Dielectrics and Electrical Insulation*, 25: 1308–1317.

[87] Zhang, B., Wang, Q., Zhang, Y., Gao, W., Hou, Y., Zhang, G. (2019). A self-assembled, nacre-mimetic, nano-laminar structure as a superior charge dissipation coating on insulators for HVDC gas-insulated systems. *Nanoscale*, 11: 18046–18051.

[88] Xue, J., Wang, H., Chen, J., Li, K., Liu, Y., Song, B., Deng, J., Zhang, G. (2018). Effects of surface roughness on surface charge accumulation characteristics and surface flashover performance of alumina-filled epoxy resin spacers. *Journal of Applied Physics*, 124: 083302.

[89] Baytekin, H. T., Baytekin, B., Hermans, T. M., Kowalczyk, B., Grzybowski, B. A. (2013). Control of surface charges by radicals as a principle of antistatic polymers protecting electronic circuitry. *Science*, 341: 1368–1371.

[90] Li, C., Hu, J., Lin, C., He, J. (2016). The control mechanism of surface traps on surface charge behavior in alumina-filled epoxy composites. *Journal of Physics D: Applied Physics*, 49: 445304.

[91] Li, C., Hu, J., Lin, C., He, J. (2016). Hot electron injection regulation in Al_2O_3-filled epoxy resin composite using Cr_2O_3 coatings. In: Proceedings of the 2016 IEEE Conference on Electrical Insulation and Dielectric Phenomena, Toronto, Canada.

[92] He, S., Lin, C., Hu, J., Li, C., He, J. (2018). Tailoring charge transport in epoxy based composite under temperature gradient using $K_2Ti_6O_{13}$ and asbestine whiskers. *Journal of Physics D: Applied Physics*, 51: 215306.

[93] Li, S., Yin, G., Bai, S., Li, J. (2011). A new potential barrier model in epoxy resin nanodielectrics. *IEEE Transactions on Dielectrics and Electrical Insulation*, 18: 1535–1543.

[94] Chu, P., Zhang, H., Zhao, J., Gao, F., Guo, Y., Dang, B., Zhang, Z. (2017). On the volume resistivity of silica nanoparticle filled epoxy with different surface modifications. *Composites Part A: Applied Science and Manufacturing*, 99: 139–148.

[95] Du, B. X., Liang, H. C., Li, J. (2019). Surface coating affecting charge distribution and flashover voltage of cone-type insulator under DC stress. *IEEE Transactions on Dielectrics and Electrical Insulation*, 26: 706–713.

[96] Zhang, B., Gao, W., Hou, Y., Zhang, G. (2018). Surface charge accumulation and suppression on fullerene-filled epoxy-resin insulator under DC voltage. *IEEE Transactions on Dielectrics and Electrical Insulation*, 25: 2011–2019.

[97] Hanna, R., Lesaint, O., Zavattoni, L. (2016). Dark current measurements in humid SF_6 at high uniform electric field. In: Proceedings of the 2016 IEEE Conference on Electrical Insulation and Dielectric Phenomena, Toronto, Canada.

[98] Zavattoni, L., Hanna, R., Lesaint, O., Gallot-Lavallée, O. (2015). Dark current measurements in humid SF_6: Influence of electrode roughness, relative humidity and pressure. *Journal of Physics D: Applied Physics*, 48: 375501.

[99] Zavattoni, L., Lesaint, O., Gallot-Lavallée, O. (2013). Dark current measurements in pressurized air, N_2, and SF_6. In: Proceedings of the 2013 Annual Report Conference on Electrical Insulation and Dielectric Phenomena, Chenzhen, China.

[100] Liang, H., Du, B., Li, J., Li, Z., Li, A. (2018). Effects of non-linear conductivity on charge trapping and de-trapping behaviours in epoxy/SiC composites under DC stress. *IET Science Measurement & Technology*, 12: 83–89.

[101] Pan, Z., Tang, J., Pan, C., Luo Y., Liu Q., He H. (2020). Contribution of nano-SiC/epoxy coating with nonlinear conduction characteristics to surface charge accumulation under DC voltage. *Journal of Physics D: Applied Physics*, 53: 365303.

[102] Wang, T., Liu, C., Li, D., Hou, Y., Zhang, G., Zhang, B. (2020) Nano ZnO/epoxy coating to promote surface charge dissipation on insulators in DC gas-insulated systems. *IEEE Transactions on*

[103] Liang, H., Du, B., Kong, X. (2022). Basin-type spacer for DC-GIL —part II: Surface charge and electric field regulation. *IEEE Transactions on Dielectrics and Electrical Insulation*, 29: 1119–1126.

[104] Xue, J., Li, Y., Dong, J., Chen, J., Li, W., Deng, J., Zhang, G. (2020). Surface charge transport behavior and flashover mechanism on alumina/epoxy spacers coated by SiC/epoxy composites with varied SiC particle size. *Journal of Physics D: Applied Physics*, 53: 155503.

[105] Dong, J., Xue, J., Chen, J., Deng, J. (2020) Mechanism of SiC coating on surface charge behavior of epoxy/alumina spacers. In: Proceedings of the 2020 IEEE International Conference on High Voltage Engineering and Application, Beijing, China.

[106] Li, J., Liang, H. C., Du, B. X., Wang, Z. H. (2019). Surface functional graded spacer for compact HVDC gaseous insulated system. *IEEE Transactions on Dielectrics and Electrical Insulation*, 26: 664–667.

[107] Du, B., Yao, H., Liang, H., Dong, J. (2022). Multidimensional functionally graded materials (ε/σ-MFGM) for HVDC GIL/GIS spacers. *IEEE Transactions on Dielectrics and Electrical Insulation*, 29: 1966–1973.

[108] Yao, H., Du, B., Liang, H., Kong, X., Dong, J. (2022). Electric field relaxation of HVDC GIL spacer with surface conductivity gradient material (σ-SFGM) using electrospinning technology. *IEEE Transactions on Dielectrics and Electrical Insulation*, 29: 1167–1174.

[109] Du, B. X., Liang, H. C., Li, J. (2019). Interfacial E-field self-regulating insulator considered for DC GIL application. *IEEE Transactions on Dielectrics and Electrical Insulation*, 26: 801–809.

[110] Li, C., Lin, C., Hu, J., Liu, W., Li, Q., Zhang, B., He, S., Yang, Y., Liu, F., He, J. (2018). Novel HVDC spacers by adaptively controlling surface charges–part I: Charge transport and control strategy. *IEEE Transactions on Dielectrics and Electrical Insulation*, 25: 1238–1247.

[111] Qi, B., Gao, C., Li, C., Xiong, J. (2019). The influence of surface charge accumulation on flashover voltage of GIS/GIL basin insulator under various voltage stresses. *International Journal of Electrical Power & Energy Systems*, 105: 514–520.

[112] Li, Z., Xu, H., Zheng, X., Zhang, L., Li, S. (2020). Unraveling the transition from secondary electron emission dominated to surface charge trap dominated electronic avalanche process along the solid dielectric surface in vacuum. *Applied Physics Letters*, 116: 131601.

[113] Li, C., Lin, C., Zhang, B., Li, Q., Liu, W., Hu, J., He, J. (2018). Understanding surface charge accumulation and surface flashover on spacers in compressed gas insulation. *IEEE Transactions on Dielectrics and Electrical Insulation*, 25: 1152–1166.

[114] Zhang, B., Wang, Q., Zhang, G., Li, J. (2015). Surface charge accumulation on insulators in SF_6 and its effects on the flashover characteristics of HVDC GIL. *High Voltage Engineering*, 41(5), 1481–1487. (in Chinese)

[115] Li, C., Hu, J., Lin, C., Zhang, B., Zhang, G., He, J. (2017). Surface charge migration and dc surface flashover of surface-modified epoxy-based insulators. *Journal of Physics D: Applied Physics*, 50: 065301.

[116] Wang, F., Liang, F., Chen, S., Zhong, L., Sun, Q., Zhang, B., Xiao, P. (2021). Effect of surface charges on flashover voltage-an examination considering charge decay rates. *IEEE Transactions on Dielectrics and Electrical Insulation*, 28: 1053–1060.

[117] Liu, Y., Wu, G., Gao, G., Xue, J., Kang, Y., Shi, C. (2019). Surface charge accumulation behavior and its influence on surface flashover performance of Al_2O_3-filled epoxy resin insulators under DC voltages. *Plasma Science and Technology*, 21: 055501.

[118] Ma, J., Tao, F., Ma, Y., Zhao, K., Li, H., Wen, T., Zhang, Q. (2021). Quantitative analysis on the influence of surface charges on flashover of insulators in SF_6. *IEEE Transactions on Dielectrics and Electrical Insulation*, 28: 274–281.

[119] Du, B. X., Xiao, M. (2014). Influence of surface charge on DC flashover characteristics of epoxy/BN nanocomposites. *IEEE*

Transactions on Dielectrics and Electrical Insulation, 21: 529–536.

[120] Pai, S., Marton, J. (1982). Filamentary breakdown of gases in the presence of dielectric surfaces. *Journal of Applied Physics*, 53: 8583–8588.

[121] Cooke, C. M. (1982). Surface flashover of gas/solid interfaces. Gaseous Dielectrics III. In: Proceedings or the Third International Symposium on Gaseous Dielectrics, Knoxville, TN, USA.

[122] Sudarshan, T., Dougal. R. (1986). Mechanisms of surface flashover along solid dielectrics in compressed gases: A review. *IEEE Transactions on Electrical Insulation*, EI-21: 727–746.

[123] Li, C., Shahsavarian, T., Baferani, M., Cao, Y. (2021). Tailoring insulation surface conductivity for surface partial discharge mitigation. *Applied Physics Letters*, 119: 032903.

[124] Yuan, M., Zou, L. Li, Z., Pang, L., Zhao, T., Zhang, L., Zhou, J., Xiao, P., Akram, S., Wang, Z., He, S. (2021). A review on factors that affect surface charge accumulation and charge-induced surface flashover. *Nanotechnology*, 32: 262001.

[125] Li, S., Huang, Y., Min, D., Qu, G., Niu, H., Li, Z., Wang, W., Li, J., Liu, W. (2019). Synergic effect of adsorbed gas and charging on surface flashover. *Scientific Reports*, 9: 5464.

[126] Li, Z., Li, S., Xu, H., Qu, G., Niu, H., Huang, Y., Aslam, F. (2021). The mechanism of gas pressure and temperature dependent surface flashover in compressed gas involving gas adsorption. *Applied Surface Science*, 539: 148107.

[127] Li, Z., Min, D., Niu, H., Li, M., Li, S. (2021). Simulation of DC surface flashover of epoxy composites in compressed nitrogen. *Journal of Applied Physics*, 130: 053301.

[128] Xing, Y., Sun, X., Yang, Y., Mazzanti, G., Fabiani, D., He, J., Li, C. (2021). Metal particle induced spacer surface charging phenomena in direct current gas-insulated transmission lines. *Journal of Physics D: Applied Physics*, 54: 34LT03.

[129] You, H., Zhang, Q., Guo, C., Xu, P., Ma, J., Qin, Y., Wen, T., Li, Y. (2017). Motion and discharge characteristics of metal particles existing in GIS under DC voltage. *IEEE Transactions on Dielectrics and Electrical Insulation*, 24: 876–885.

[130] Wang, J., Wang, J., Hu, Q., Chang, Y., Liu, H., Liang, R. (2020). Mechanism analysis of particle-triggered flashover in different gas dielectrics under DC superposition lightning impulse voltage. *IEEE Access*, 8: 182888–182897.

[131] Xing, Y., Wang, Z., Liu, L., Xu, Y., Yang, Y., Liu, S., Zhou, F., He, S., Li, C. (2021). Defects and failure types of solid insulation in gas-insulated switchgear: *in situ* study and case analysis. *High Voltage*, 7: 158–164.

[132] Wang, J., Hu, Q., Chang, Y., Wang, J., Liang, R., Tu, Y., Li, C., Li, Q. (2021). Metal particle contamination in gas-insulated switchgears/gas-insulated transmission lines. *CSEE Journal of Power and Energy Systems*, 7: 1011–1025.

[133] Wu, Z., Li, Z., Liu, P., Peng, Z., Wang, H., Cui, B., Li, H. (2022). Simulation and analysis on motion behavior of metal particles in AC GIL. *IEEE Transactions on Dielectrics and Electrical Insulation*, 29: 567–574.

[134] Sun, J., Chen, W., Bian, K., Li, Z., Yan, X., Xu, Y. (2018). Movement characteristics of ball metallic particle between ball-plane electrodes under DC voltage. *IEEE Transactions on Dielectrics and Electrical Insulation*, 25: 1047–1055.

[135] Sun, J., Chen, W., Li, Z., Yan, X., Cui, B., Wang, H. (2016). Research on experiment and simulation of charged spherical metal particle collision characteristic under DC electric field. *IEEE Transactions on Dielectrics and Electrical Insulation*, 23: 3117–3125.

[136] Wang, J., Li, Q., Li, B., Liu, S., Wang, Z. (2016). Motion and discharge behavior of the free conducting wire type particle within DC GIL. *Proceedings of the CSEE*, 36(17): 4793–4800. (in Chinese)

[137] Liang, R., Hu, Q., Liu, H., Wang, J., Li, Q. (2020). Research on discharge phenomenon caused by cross—Adsorption of linear insulating fibre and metal dust under DC voltage. *High Voltage*, 7: 269–278.

[138] Liang, R., Hu, Q., Man, Y., Chang, Y., Wang, J. (2020). Study on

kinetic behavior and adsorption mechanism of the micron metal dust near the basin-type insulator in DC GIL. In: Proceedings of the 2019 IEEE Conference on Electrical Insulation and Dielectric Phenomena, Richland, WA, USA.

[139] Wang, R., Cui, C., Zhang, C., Ren, C., Chen, G., Shao, T. (2018). Deposition of SiO_x film on electrode surface by DBD to improve the lift-off voltage of metal particles. *IEEE Transactions on Dielectrics and Electrical Insulation*, 25: 1285–1292.

[140] Zhang, L., Cheng, H., Wei, W., Ayubi, B. I., Bretas, A. S. (2021). Suppression on particle movement and discharge by nanocomposite film coating on DC GIL electrode surface. *IEEE Access*, 9: 126095–126103.

[141] Huang, X., Ni, X., Wang, J., Li, Q., Lin, J., Wang, Z. (2018). Synthesis of phenyl-thioether polyimide as the electrode coating film and its suppression effect on motion behavior of the metal particles under DC stresses. *Transactions of China Electrotechnical Society*, 33(20): 4712–4721. (in Chinese)

[142] Liang, R., Liu, H., Hu, Q., Wang, J., Li, Q. (2020). Research advances in the kinetic behavior and induced discharge characteristics of micron metal duct within GIS/GIL. *Proceedings of the CSEE*, 40(22): 7153–7165. (in Chinese)

[143] Zhan, Z., Wang, D., Xie, J., Xin, W., Wang, W., Zhang, Z. (2021). Motion characteristics of metal powder particles in AC GIL and its trap design. *IEEE Access*, 9: 68619–68628.

[144] Liu, P., Li, Z., Tian, H., Wu, Z., Peng, Z., Tan, S., Li, J., Wen, Y. (2022). Research on motion characteristics of metal particle and capture efficiency of particle traps in gas insulated transmission lines under DC voltage. *Proceedings of the CSEE*, 42(15): 5740–5751. (in Chinese)

[145] Liu, P., Zhang, Y., Wu, Z., Li, Z., Tan, S., Peng, Z. (2022). Key parameter analysis and structure optimization of particle trap in ± 320kV DC GIL. *High voltage engineering*, https://doi.org/10.13336 /j.1003-6520.hve.20221207.

[146] Li, Q., Chang, Y., Wang, J., Hu, Q., Wang, J., Guo, R. (2020). Methodological advances of metal particle traps design in gas insulated transmission lines. *High voltage engineering*, 46(12): 4182–4193. (in Chinese)

[147] Xing, Y., Sun, X., Jiang, J., Liang, F., Liang, Z., Zhuang, W., Liu, B., Li, D., Cao, S., Li, M., He, J., Li, C. (2022). Significantly suppressing metal particle-induced surface charge accumulation of spacers in DC gas-insulated power transmission lines. *Journal of Physics D: Applied Physics*, 55: 504003.

[148] Qiu, Y., Chalmers, I. D. (1993). Effect of electrode surface roughness on breakdown in SF_6–N_2 and SF_6–CO_2 gas mixtures. *Journal of Physics D: Applied Physics*, 26: 1928–1932.

[149] Li, B. (2019). SF_6 High-Voltage Electrical Apparatus Design 5th edition. Beijing, China: China Machine Press.

[150] Ai, X., Tu, Y., Zhang, Y., Chen, G., Yuan, Z., Wang, C., Yan, X., Liu, W. (2020). The effect of electrode surface roughness on the breakdown characteristics of C_3F_7CN/CO_2 gas mixtures. *International Journal of Electrical Power & Energy Systems*, 118: 105751.

[151] Zheng, Y., Zhou, W., Li, H., Yan, X., Li, Z., Chen, W., Bian, K. (2019). Influence of conductor surface roughness on insulation performance of C_4F_7N/CO_2 mixed gas. *IEEE Transactions on Dielectrics and Electrical Insulation*, 26: 922–929.

[152] Zhang, L., Wang, Y., Yu, D., Pan, W., Zhang, Z., Tschentscher, M. (2021). Conductor surface roughness-dependent gas conduction process for HVDC GIL—part I: Simulation. *IEEE Transactions on Dielectrics and Electrical Insulation*, 28: 511–519.

[153] Li, C., Zhang, L., Wang, Y., Yu, D., Wang, Z., Zhang, Z., Connelly, L., Lin, C., Chen, G., Mazzanti, G., et al. (2021). Conductor surface roughness-dependent gas conduction process for HVDC GIL—part II: Experiment. *IEEE Transactions on Dielectrics and Electrical Insulation*, 28: 988–995.

[154] Chen, G., Xu, H., Xu, Y., Shao, Y., Wang, C., Li, C., Tu, Y. (2022). Standardizing conductor surface roughness for DC gas-insulated equipment-a careful analysis on local morphology. *Journal of Physics D: Applied Physics*, 55: 23LT01.

[155] Riechert, U., Hama, H., Endo; F., Juhre, K., Kindersberger, J., Meijer, S., Neumann, C., Okabe, S., Schichler, U. (2010). Gasisolierte Systeme für HGÜ. In: Isoliersysteme bei Gleich- und Mischfeldbeanspruchung. Köln, Germany: VDE Verlag GmbH. (in Germany)

[156] Hermann, J. K. (2022). Gas Insulated Substations, 2nd Edition. Hoboken, NJ, USA: Wiley-IEEE Press.

[157] Riechert, U. (2020). Compact high voltage direct current gas-insulated systems. In: Proceedings of the 2020 IEEE International Conference on High Voltage Engineering and Application (ICHVE), Beijing, China.

[158] Makino, Y., Hara, S., Hirose, M. (2001). Commissioning of the Kii-channel HVDC link. Application of new HVDC technology and operating experience. In: Proceedings of the Seventh International Conference on AC-DC Power Transmission, London, UK.

[159] Alvinsson, R., Borg, E., Hjortsberg, A., Höglund, T., Hörnfeldt, S. (1986). GIS for HVDC converter stations. CIGRE 1986, Report, No. 14-02.

[160] Mendik, M., Lowder, S. M., Elliott, F. (1999) Long term performance verification of high voltage DC GIS. In: Proceedings of the 1999 IEEE Transmission and Distribution Conference, New Orleans, LA, USA.

[161] Riechert, U., Kosse, M. (2020). HVDC gas-insulated systems for compact substation design. In: Proceedings of the 48th CIGRE Session, Paris, France.

[162] Hering, M., Koch, H., Jurhe, K. (2019). Direct current high-voltage gas insulated switchgear up to±550 kV. In: Proceedings of the CIGRE-IEC 2019 Conference on EHV and UHV (AC&DC), Hakodate, Hokkaido, Japan.

[163] Riechert, U., Gatzsche, M., Hassanpoor, A., Plet, C., Belda, N. (2019). Compact switchgear for meshed offshore HVDC networks – Between vision and reality. Available at https://www.promotion-offshore.net/fileadmin/PDFs/2019_WP15_HighVolt.pdf.

[164] Abe, Y., Yasuoka, T., Shiiki, M., Karube, T. (2019). Development of 250 kV DC gas insulated switchgear. In: Proceedings of the CIGRE-IEC 2019 Conference on EHV and UHV (AC&DC), Hakodate, Japan.

[165] Limura, M., Chiba, K., Kamoshida, S., Ogata, H., Utsumi, T., Nakano, Y. (2020). Key technologies used in Hida-Shinano HVDC link. Hitachi Review, 69: 490–491.

[166] Kosse, M., Tuczek, M., Klein, C., Claus, M. (2022). Experiences with on-site dielectric testing during commissioning tests of world's first offshore HVDC GIS ±320 kV. In VDE Hochspannungstechnik, Köln, Germany: VDE Verlag GmbH.

[167] Riechert, U., Straumann, U., Gremaud, R. (2016). Compact gas-insulated systems for high voltage direct current transmission: Basic design. In: Proceedings of the 2016 IEEE/PES Transmission and Distribution Conference and Exposition (T&D), Dallas, TX, USA.

[168] Sperling, E., Riechert, U. (2015). HVDC GIS RC-dividers in new GIS substations with increased dielectric requirements. In: Proceedings of the 2015 CIGRE Joint Colloquium, Nagoya, Japan.

[169] Appelo, H. C., Groenenboom, M., Lisser, J. (1977). The zero-flux DC current transformer a high precision bipolar wide-band measuring device. IEEE Transactions on Nuclear Science, 24: 1810–1811.

[170] Endo, F., Hama, H., Okabe, S., Juhre, K., Kindersberger, J., Meijer, S., & Schichler, U. (2012). Gas insulated systems for HVDC: DC stress at DC and AC systems. Report, Brochure No. 506, CIGRE.

[171] CIGRE Joint Working Group D1/B3.57 (2021). Dielectric testing of gas-insulated HVDC systems. Technical Brochure No. 842, CIGRE.

[172] Riechert, U., Blumenroth, F., Straumann, U., Kaufmann, B., Saltzer, M., Bergelin, P. (2018). Experiences in dielectric testing of gas-insulated HVDC systems. In: Proceedings of the 47th CIGRE Conference, Paris, France.

[173] Riechert, U., Gatzsche, M. (2019). Dielectric long-term behaviour and testing of gas-insulated HVDC systems. In: Proceedings of the CIGRE SC A2, B2 & D1 International Tutorials & Colloquium, New Delhi, India.

[174] Gatzsche, M., Riechert, U., He, H., Audichya, Y., Mor, A. R., Heredia, L. C., Muñoz, F. (2020). Prototype installation test of HVDC GIS for meshed offshore grids.In: Proceedings of the 48th CIGRE Session, Paris. France.

[175] PROMOTioN (2018). Work Package 15, Deliverable 15.4: Test report of prototype installation test on HVDC GIS. Available at https://www.promotion-offshore.net/results/deliverables/.

[176] Hallas, M., Tenzer, M., Neumann, C., Hinrichsen, V., Gross, D. (2022). Nachweis der Betriebstauglichkeit von gasisolierten HVDC Systemen unter betriebsnahen Bedingungen –Resümee einer Langzeituntersuchung in Griesheim. In: Proceedings of the Fachtagung Hochspannungsschaltanlagen: Anwendungen, Betrieb und Erfahrungen. GIS-Anwendungsforum, Darmstadt, Germany. (in Germany)